Eur. Phys. J. C (2012) 72:1926
DOI 10.1140/epjc/s10052-012-1926-0

THE EUROPEAN PHYSICAL JOURNAL C

Regular Article - Experimental Physics

Rapidity gap cross sections measured with the ATLAS detector in pp collisions at $\sqrt{s} = 7$ TeV

The ATLAS Collaboration[⋆]

CERN, 1211 Geneva 23, Switzerland

Received: 13 January 2012 / Revised: 16 February 2012 / Published online: 13 March 2012
© CERN for the benefit of the ATLAS Collaboration 2012. This article is published with open access at Springerlink.com

Abstract Pseudorapidity gap distributions in proton-proton collisions at $\sqrt{s} = 7$ TeV are studied using a minimum bias data sample with an integrated luminosity of 7.1 μb^{-1}. Cross sections are measured differentially in terms of $\Delta\eta^F$, the larger of the pseudorapidity regions extending to the limits of the ATLAS sensitivity, at $\eta = \pm 4.9$, in which no final state particles are produced above a transverse momentum threshold p_T^{cut}. The measurements span the region $0 < \Delta\eta^F < 8$ for 200 MeV $< p_T^{cut} <$ 800 MeV. At small $\Delta\eta^F$, the data test the reliability of hadronisation models in describing rapidity and transverse momentum fluctuations in final state particle production. The measurements at larger gap sizes are dominated by contributions from the single diffractive dissociation process ($pp \to Xp$), enhanced by double dissociation ($pp \to XY$) where the invariant mass of the lighter of the two dissociation systems satisfies $M_Y \lesssim 7$ GeV. The resulting cross section is $d\sigma/d\Delta\eta^F \approx 1$ mb for $\Delta\eta^F \gtrsim 3$. The large rapidity gap data are used to constrain the value of the Pomeron intercept appropriate to triple Regge models of soft diffraction. The cross section integrated over all gap sizes is compared with other LHC inelastic cross section measurements.

1 Introduction

When two protons collide inelastically at a centre-of-mass energy of 7 TeV in the Large Hadron Collider (LHC), typically around six charged particles are produced with transverse momentum[1] $p_T > 100$ MeV per unit of pseudorapidity in the central region [1–3]. On average, the rapidity difference between neighbouring particles is therefore around 0.15 units of rapidity, with larger gaps occurring due to statistical fluctuations in the hadronisation process. Such random processes lead to an exponential suppression with gap size [4], but very large gaps are produced where a t-channel colour singlet exchange takes place. This may be due to an electroweak exchange, but occurs much more frequently through the exchange of strongly interacting states. At high energies such processes are termed 'diffractive' and are associated with 'Pomeron' exchange [5, 6].

The total cross section in hadronic scattering experiments is commonly decomposed into four main components: elastic ($pp \to pp$ in the LHC context), single-diffractive dissociation (SD, $pp \to Xp$ or $pp \to pX$, Fig. 1a), double-diffractive dissociation (DD, $pp \to XY$, Fig. 1b) and non-diffractive (ND) contributions. The more complex central diffractive configuration (CD, $pp \to pXp$, Fig. 1c), in which final state particles are produced in the central region with intact protons on both sides, is suppressed relative to the SD process by a factor of around 10 at high energies [7]. Together, the diffractive channels contribute approximately 25–30 % of the total inelastic cross section at LHC energies [8]. Following measurements at the LHC of the elastic [9], total [10] and total inelastic [8, 10] cross sections, this article contains the first detailed exploration of diffractive dissociation processes.

Understanding diffractive processes is important in its own right, as they are the dominant contribution to high energy quasi-elastic scattering between hadrons and, via ideas derived from the optical theorem [11], are also related to the total cross section. They are often interpreted at the parton level in terms of the exchange of pairs of gluons [12, 13] and are thus sensitive to possible parton saturation effects in the low Bjorken-x regime of proton structure [14–16]. Diffractive cross sections also have relevance to cosmic ray physics [17] and may be related to the string theory of gravity [18]. At the LHC, diffractive dissociation must be well

⋆ e-mail: atlas.publications@cern.ch

[1] In the ATLAS coordinate system, the z-axis points in the direction of the anti-clockwise beam viewed from above. Polar angles θ and transverse momenta p_T are measured with respect to this axis. The pseudorapidity $\eta = -\ln\tan(\theta/2)$ is a good approximation to the rapidity of a particle whose mass is negligible compared with its energy and is used here, relative to the nominal $z = 0$ point at the centre of the apparatus, to describe regions of the detector.

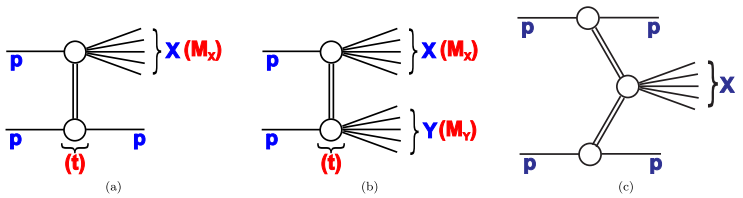

Fig. 1 Schematic illustrations of the single-diffractive dissociation (**a**), double-diffractive dissociation (**b**) and central diffractive (**c**) processes and the kinematic variables used to describe them. By convention, the mass M_Y is always smaller than M_X in the double dissociation case and $M_Y = M_p$ in the single dissociation case, M_p being the proton mass

understood for a good description of the additional inelastic proton-proton interactions (pile-up) which accompany most events. It also produces a significant uncertainty in approaches to luminosity monitoring which rely on measurements of the total, or total inelastic, cross section [19].

Diffractive dissociation cross sections have been measured previously over a wide range of centre-of-mass energies. Early measurements are reviewed in [20–24]. SD measurements have been made in $p\bar{p}$ scattering at the SPS [25, 26] and the Tevatron [27, 28], and also in photoproduction [29, 30] and deep inelastic scattering [31–33] at HERA. Limited high energy DD [26, 29, 34] and CD [7, 35, 36] data are also available. In most cases, the momentum transfer is too small to permit an interpretation in terms of partonic degrees of freedom [37]. Instead, phenomenological models such as those based on Regge theory have been developed [22, 38, 39], which underlie the Monte Carlo generators typically used to predict the properties of soft inelastic collisions [40–42]. Mixed approaches have also been developed which employ perturbative QCD where possible [43, 44]. Large theoretical uncertainties remain in the detailed dynamics expected at the LHC.

Direct measurements of the masses M_X and M_Y of the dissociated systems are difficult at ATLAS, since many of the final state particles are produced beyond the acceptance of the detector. However, the dissociation masses are closely correlated with the size of the rapidity region in which particle production is completely suppressed due to the net colour-singlet Pomeron exchange. This correlation is exploited in this paper, with cross sections reported as a function of the size of a pseudorapidity region which is devoid of final state particle production. These unpopulated pseudorapidity regions are referred to in the following as 'rapidity gaps', or simply 'gaps'.

To maximise the pseudorapidity coverage and sensitivity to charged and neutral particle production, rapidity gaps are identified using both the ATLAS calorimeters and tracking detectors. The specific observable studied is $\Delta\eta^F$, the larger of the two 'forward' pseudorapidity regions extending to at least $\eta = \pm 4.9$ in which no particles are produced with $p_{\mathrm{T}} > p_{\mathrm{T}}^{\mathrm{cut}}$, where $p_{\mathrm{T}}^{\mathrm{cut}}$ is varied between 200 MeV and 800 MeV. ND contributions appear at small gap sizes, with $p_{\mathrm{T}}^{\mathrm{cut}}$ and $\Delta\eta^F$ dependences which are sensitive to fluctuations in the hadronisation process. For small $p_{\mathrm{T}}^{\mathrm{cut}}$ choices, the large gap size region is dominated by SD events and DD events in which one of the dissociation masses is small.

2 Experimental method

2.1 The ATLAS detector

The ATLAS detector is described in detail elsewhere [45]. The beam-line is surrounded by the 'inner detector' tracking system, which covers the pseudorapidity range $|\eta| < 2.5$. This detector consists of silicon pixel, silicon strip and straw tube detectors and is enclosed within a uniform 2 T solenoidal magnetic field.

The calorimeters lie outside the tracking system. A highly segmented electromagnetic (EM) liquid argon sampling calorimeter covers the range $|\eta| < 3.2$. The EM calorimeter also includes a pre-sampler covering $|\eta| < 1.8$. The hadronic end-cap (HEC, $1.5 < |\eta| < 3.2$) and forward (FCal, $3.1 < |\eta| < 4.9$) calorimeters also use liquid argon technology, with granularity decreasing with increasing $|\eta|$. Hadronic energy in the central region ($|\eta| < 1.7$) is reconstructed in a steel/scintillator-tile calorimeter.

Minimum bias trigger scintillator (MBTS) detectors are mounted in front of the end-cap calorimeters on both sides of the interaction point and cover the pseudorapidity range $2.1 < |\eta| < 3.8$. The MBTS is divided into inner and outer rings, both of which have eight-fold segmentation. The MBTS is used to trigger the events analysed here.

In 2010, the luminosity was measured using a Čerenkov light detector which is located 17 m from the interaction point. The luminosity calibration is determined through van der Meer beam scans [19, 46].

2.2 Event selection and backgrounds

The data used in this analysis were collected during the first LHC run at $\sqrt{s} = 7$ TeV in March 2010, when the LHC was filled with two bunches per beam, one pair colliding at the

ATLAS interaction point. The peak instantaneous luminosity was 1.1×10^{27} cm^{-2} s^{-1}. Events were collected from colliding proton bunch crossings in which the MBTS trigger recorded one or more inner or outer segments above threshold on at least one side of ATLAS. After reconstruction, events are required to have hits in at least two of the MBTS segments above a threshold of 0.15 pC. This threshold cut suppresses contributions from noise, which are well modelled by a Gaussian with 0.02 pC width. No further event selection requirements are applied.

The data sample corresponds to an integrated luminosity of 7.1 ± 0.2 μb^{-1} and the number of recorded events is 422776. The mean number of interactions per bunch crossing is below 0.005, which is consistent with the approximately 400 events which have multiple reconstructed vertices. Pile-up contamination is thus negligible.

The data sample contains a contribution from beam-induced background, mainly due to scattering of beam protons from residual gas particles inside the detector region. This contamination is estimated using events collected in unpaired bunches and is subtracted statistically in each measurement interval. Averaged over the full measurement region, it amounts to 0.2 % of the sample. More complex backgrounds in which beam-induced background is overlaid on a physics event are negligible.

2.3 Reconstruction of rapidity gaps

The analysis of final state activity in the central region ($|\eta| < 2.5$) is based on combined information from inner detector tracks and calorimeter modules. In the region $2.5 < |\eta| < 4.9$, beyond the acceptance of the inner detector, calorimeter information alone is used. The track selection is as detailed in [1]. Energy deposits from final state particles in the calorimeters are identified using a topological clustering algorithm [47, 48], with a further requirement to improve the control over noise contributions, as described below.

The identification of rapidity gap signatures relies crucially on the suppression of calorimeter noise contributions. The root-mean-squared cell energies due to noise vary from around 20 MeV in the most central region to around 200 MeV for the most forward region [49]. The shapes of the cell noise distributions in each calorimeter are well described by Gaussian distributions of standard deviation σ_{noise}, with the exception of the tile calorimeter, which has extended tails. The default clustering algorithm [48] is seeded by cells for which the significance of the measured energy, E, is $S = E/\sigma_{\text{noise}} > 4$. However, with this threshold there are on average six clusters reconstructed per empty event due to fluctuations in the noise distributions. To suppress noise contributions to acceptable levels for gap finding, clusters of calorimeter energy deposits are thus considered only if they contain at least one cell outside the tile calorimeter with an energy significance above an η-dependent threshold, S_{th}. This threshold is determined separately in pseudorapidity slices of size 0.1 such that the probability of finding at least one noisy cell in each η-slice has a common value, 1.4×10^{-4}. This choice optimises the resolution of the reconstructed gap sizes with respect to the gaps in the generated final state particle distributions according to MC studies. Since the number of cells in an η-slice varies from about 4000 in the central region to 10 in the outer part of the FCal, the cell thresholds vary between $S_{\text{th}} = 5.8$ in the central region and $S_{\text{th}} = 4.8$ at the highest $|\eta|$ values in the FCal.

The level of understanding of the calorimeter noise is illustrated in Fig. 2, which shows the distributions of the cell significance S for each of the liquid argon modules. MBTS-triggered data from colliding bunch crossings are compared with a Monte Carlo simulation and with events which are required to exhibit no activity in the non-calorimeter components of the detector, triggered randomly on empty bunch crossings. The signal from pp collisions is clearly visible in the long positive tails, which are well described by the simulation. The data from the empty bunch crossings show the shape of the noise distribution with no influence from physics signals. The empty bunch crossing noise distributions are symmetric around zero and their negative sides closely match the negative parts of the MBTS-triggered data distributions. The noise distribution is well described over seven orders of magnitude by the MC simulation, the small residual differences at positive significances being attributable to deficiencies in the modelling of pp collision processes.

The measured energies of calorimeter clusters which pass the noise requirements are discriminated using a given value of $p_{\text{T}}^{\text{cut}}$, neglecting particle masses. The calorimeter energy scale for electromagnetic showers is determined from electron test-beam studies and $Z \to e^+e^-$ data [50], confirmed at the relatively small energies relevant to the gap finding algorithm through a dedicated study of $\pi^0 \to \gamma\gamma$ decays. The calorimeter response to hadronic showers is substantially lower than that to electromagnetic showers. In the central region, the scale of the hadronic energy measurements is determined relative to the electromagnetic scale through comparisons between the calorimeter and inner detector measurements of single isolated hadrons [51–53]. Beyond the acceptance region of the tracking detectors, the difference between the electromagnetic and the hadronic response is determined from test-beam results [54–56]. For the purposes of discriminating against thresholds in the gap finding algorithm, all cluster energy measurements are taken at this hadronic scale. An interval in η is deemed to contain final state particles if at least one cluster in that interval passes the noise suppression requirements and has a transverse momentum above $p_{\text{T}}^{\text{cut}}$, or if there is at least one good inner detector track with transverse momentum above $p_{\text{T}}^{\text{cut}}$.

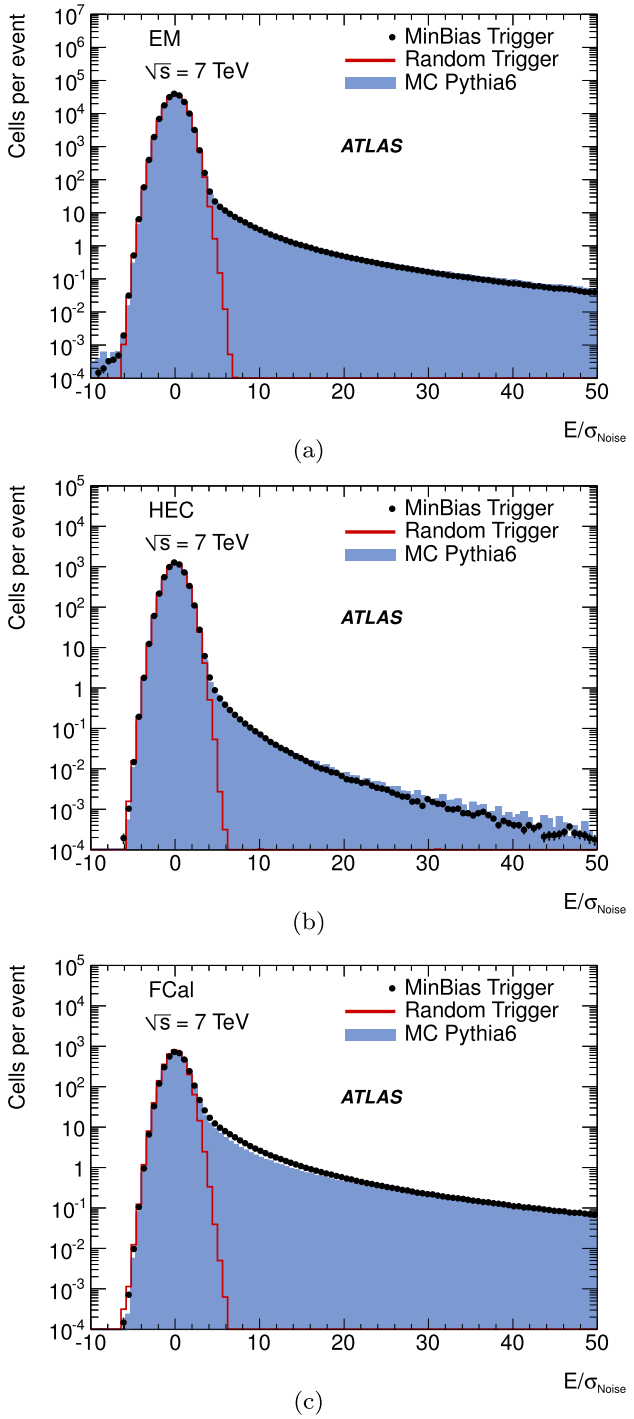

Fig. 2 Cell energy significance, $S = E/\sigma_{\text{noise}}$, distributions for the EM (**a**), HEC (**b**) and FCal (**c**) calorimeters. Each cell used in the analysis is included for every event, with the normalisation set to a single event. MBTS-triggered minimum bias data (*points*) are compared with events randomly triggered on empty bunch crossings (*histograms*) and with a Monte Carlo simulation (*shaded areas*)

2.4 Definition of forward rapidity gap observable

The reconstructed forward gap size $\Delta\eta^F$ is defined by the larger of the two empty pseudorapidity regions extending between the edges of the detector acceptance at $\eta = 4.9$ or $\eta = -4.9$ and the nearest track or calorimeter cluster passing the selection requirements at smaller $|\eta|$. No requirements are placed on particle production at $|\eta| > 4.9$ and no attempt is made to identify gaps in the central region of the detector. The rapidity gap size relative to $\eta = \pm 4.9$ lies in the range $0 < \Delta\eta^F < 8$, such that for example $\Delta\eta^F = 8$ implies that there is no reconstructed particle with $p_{\text{T}} > p_{\text{T}}^{\text{cut}}$ in one of the regions $-4.9 < \eta < 3.1$ or $-3.1 < \eta < 4.9$. The upper limit on the gap size is constrained via the requirement of a high trigger efficiency by the acceptance of the MBTS detector.

The measurement is performed in $\Delta\eta^F$ intervals of 0.2, except at the smallest values $\Delta\eta^F < 2.0$, where the differential cross section varies fastest with $\Delta\eta^F$ and the gap endpoint determination is most strongly dependent on the relatively coarse cell granularity of the FCal. The bin sizes in this region are increased to 0.4 pseudorapidity units, commensurate with the resolution.

The default value of the transverse momentum threshold is chosen to be $p_{\text{T}}^{\text{cut}} = 200$ MeV. This value lies within the acceptance of the track reconstruction for the inner detector and ensures that the efficiency of the calorimeter cluster selection is greater than 50 % throughout the η region which lies beyond the tracking acceptance.

As described in Sect. 3.4, the data are fully corrected for experimental effects using the Monte Carlo simulations introduced in Sect. 3.2. The rapidity gap observable defining the measured differential cross sections are thus specified in terms of stable (proper lifetime > 10 ps) final state particles (hereafter referred to as the 'hadron level'), with transverse momentum larger than the threshold, $p_{\text{T}}^{\text{cut}}$, used in the gap reconstruction algorithm.

3 Theoretical models and simulations

3.1 Kinematic variables and theory

As illustrated in Figs. 1a and b, diffractive dissociation kinematics can be described in terms of the invariant masses M_X and M_Y of the dissociation systems X and Y, respectively (with $M_Y = M_p$ in the SD case), and the squared four-momentum transfer t. In the following, the convention $M_Y < M_X$ is adopted. The cross section is vastly dominated by small values of $|t| \lesssim 1$ GeV^2, such that the intact proton in SD events is scattered through only a small angle, gaining transverse momentum $p_{\text{T}} \simeq \sqrt{|t|}$. Further commonly used kinematic variables are defined as

$$\xi_X = \frac{M_X^2}{s}, \qquad \xi_Y = \frac{M_Y^2}{s}, \tag{1}$$

where s is the square of the centre-of-mass energy.

Diffractive dissociation cross sections can be modelled using Regge phenomenology [38, 39, 57], with Pomeron exchange being the dominant process at small ξ_X values. For the SD case, the amplitude is factorised into a Pomeron flux associated with the proton which remains intact, and a total probability for the interaction of the Pomeron with the dissociating proton. The latter can be described in terms of a further Pomeron exchange using Muller's generalisation of the optical theorem [11], which is applicable for $s \gg M_X^2 \gg m_p^2$. The SD cross section can then be expressed as a triple Pomeron ($\mathbb{PPP}$) amplitude,

$$\frac{\mathrm{d}\sigma}{\mathrm{d}t\,\mathrm{d}M_X^2} = G_{3\mathbb{P}}(0)s^{2\alpha_{\mathbb{P}}(t)-2}\left(M_X^2\right)^{\alpha_{\mathbb{P}}(0)-2\alpha_{\mathbb{P}}(t)} f(t), \tag{2}$$

where $G_{3\mathbb{P}}(0)$ is a product of couplings and $\alpha_{\mathbb{P}}(t) = \alpha_{\mathbb{P}}(0) + \alpha'_{\mathbb{P}}t$ is the Pomeron trajectory. The term $f(t)$ is usually taken to be exponential such that $\mathrm{d}\sigma/\mathrm{d}t \propto e^{B(s,M_X^2)t}$ at fixed s and M_X, B being the slope parameter. With $\alpha_{\mathbb{P}}(0)$ close to unity and $|t|$ small, Eq. (2) leads to an approximately constant $\mathrm{d}\sigma/\mathrm{d}\ln\xi_X$ at fixed s. The DD cross section follows a similar dependence at fixed ξ_Y. The deviations from this behaviour are sensitive to the intercept $\alpha_{\mathbb{P}}(0)$ of the Pomeron trajectory [58, 59] and to absorptive corrections associated with unitarity constraints [43, 44].

The rapidity gap size and its location are closely correlated with the variables ξ_X and ξ_Y. For the SD process, the size $\Delta\eta$ of the rapidity gap between the final state proton and the X system satisfies

$$\Delta\eta \simeq -\ln\xi_X. \tag{3}$$

The $\Delta\eta^F$ observable studied here differs from $\Delta\eta$ in that $\Delta\eta^F$ takes no account of particle production at $|\eta| > 4.9$. For the SD process, where the intact proton has $\eta \simeq \pm\frac{1}{2}\ln(s/m_p^2) \simeq \pm 8.9$, the gap variables are related by $\Delta\eta^F \simeq \Delta\eta - 4$. Equations (2) and (3) thus lead to approximately constant predicted cross sections $\mathrm{d}\sigma/\mathrm{d}\Delta\eta^F$ for SD and low M_Y DD events. With the high centre-of-mass energy of the LHC and the extensive acceptance of the ATLAS detector, events with ξ_X between around 10^{-6} and 10^{-2} can be selected on the basis of their rapidity gap signatures, corresponding approximately to 7 GeV $< M_X <$ 700 GeV.

Previous proton-proton scattering [25] and photo-production [29, 30] experiments have observed enhancements relative to triple-Pomeron behaviour at the smallest M_X values in the triple Regge region. This effect has been interpreted in terms of a further triple Regge term ($\mathbb{PPR}$) in which the reaction still proceeds via Pomeron exchange, but where the total Pomeron–proton cross section is described by a sub-leading Reggeon ($\mathbb{R}$) with intercept $\alpha_{\mathbb{R}}(0) \simeq 0.5$ [58]. This leads by analogy with equation (2) to a contribution to the cross section which falls as $\mathrm{d}\sigma/\mathrm{d}M_X^2 \propto 1/M_X^3$. In the recent model of Ryskin, Martin and Khoze (RMK) [43], a modified triple-Pomeron approach to the large ξ_X region is combined with a dedicated treatment of low mass diffractive dissociation, motivated by the original s-channel picture of Good and Walker [60], in which proton and excited proton eigenstates scatter elastically from the target with different absorption coefficients. This leads to a considerable enhancement in the low ξ_X cross section which is compatible with that observed in the pre-LHC data [25].

3.2 Monte Carlo simulations

Triple Pomeron-based parameterisations are implemented in the commonly used Monte Carlo (MC) event generators, PYTHIA [40, 41] and PHOJET [42, 61]. These generators are used to correct the data for experimental effects and as a means of comparing the corrected data with theoretical models.

By default, the PYTHIA model of diffractive dissociation processes uses the Schuler and Sjöstrand parameterisation [62] of the Pomeron flux, which assumes a Pomeron intercept of unity and an exponential t dependence $e^{B(\xi_X,\xi_Y)t}$. Three alternative flux models are also implemented. The Bruni and Ingelman version [63] is similar to Schuler and Sjöstrand, except that its t dependence is given by the sum of two exponentials. In the Berger and Streng [64, 65] and Donnachie and Landshoff [66] models, the Pomeron trajectory is linear, with variable parameters, the default being $\alpha_{\mathbb{P}}(t) = 1.085 + 0.25t$ [67], consistent with results from fits to total [58, 59] and elastic [68] hadronic cross section data. Whilst the model attributed to Berger and Streng has an exponential t dependence, the Donnachie and Landshoff version is based on a dipole model of the proton elastic form factor. For all flux parameterisations in PYTHIA, additional factors are applied to modify the distributions in kinematic regions in which a triple-Pomeron approach is known to be inappropriate. Their main effects are to enhance the low mass components of the dissociation spectra, to suppress the production of very large masses and, in the DD case, to reduce the probability of the systems X and Y overlapping in rapidity space [41, 62].

Above the very low mass resonance region, dissociation systems are treated in the PYTHIA6 generator using the Lund string model [69], with final state hadrons distributed in a longitudinal phase space with limited transverse momentum. In PYTHIA8, diffractive parton distribution functions from HERA [31] are used to include diffractive final states which are characteristic of hard partonic collisions, whilst preserving the ξ_X, ξ_Y, s and t dependences of the diffractive cross sections from the PYTHIA6 model [70]. This approach yields a significantly harder final state particle transverse momentum spectrum in SD and DD processes in PYTHIA8 compared with PYTHIA6, in better agreement with the present data. The default PYTHIA multiple parton interaction model is applied to ND events and, in the case of

PYTHIA8, also within the dissociated systems in SD and DD events.

The specific versions used to correct the data are PYTHIA6.4.21 (with the AMBT1 tune performed by ATLAS [71]) and PYTHIA8.145 (with the 4C tune [72]). Updated versions, PYTHIA8.150 and PYTHIA6.4.25 (using the 4C and AMBT2B tunes, respectively), are used for comparisons with the corrected data (see Table 1). The 4C tune of PYTHIA8 takes account of the measurement of the diffractive fraction f_D of the inelastic cross section in [8], whilst keeping the total cross section fixed, resulting in a somewhat smaller diffractive cross section than in PYTHIA6.

The PHOJET model uses the two component dual parton model [73] to combine features of Regge phenomenology with AGK cutting rules [74] and leading order QCD. Diffractive dissociation is described in a two-channel eikonal model, combining a triple Regge approach to soft processes with lowest order QCD for processes with parton scattering transverse momenta above 3 GeV. The Pomeron intercept is taken to be $\alpha_{\mathbb{P}}(0) = 1.08$ and for hard diffraction, the diffractive parton densities are taken from [75, 76]. Hadronisation follows the Lund string model, as for PYTHIA. The CD process is included at the level of 1.7 % of the total inelastic cross section. The specific version used is PHOJET1.12.1.35, with fragmentation and hadronisation as in PYTHIA6.1.15.

After integration over t, ξ_X and ξ_Y, the cross sections for the diffractive processes vary considerably between the default MC models, as shown in Table 1. The DD variation is particularly large, due to the lack of experimental constraints. For use in the data correction procedure, the overall fractional non-diffractive (f_{ND}) and diffractive ($f_D = f_{\mathrm{SD}} + f_{\mathrm{DD}} + f_{\mathrm{CD}} = 1 - f_{\mathrm{ND}}$) contributions to the total inelastic cross section are modified to match the results obtained in the context of each model in a previous ATLAS analysis [8]. Despite the close agreement between the diffractive fractions $f_D \sim 30$ % determined for the three default models (see the 'Tuned' fractions in Table 1), the f_D parameter is rather sensitive to the choice of Pomeron flux model and to the value of $\alpha_{\mathbb{P}}(0)$, for example reaching $f_D \sim 25$ % for the Bruni and Ingelman flux in PYTHIA8 [8].

The default PHOJET and PYTHIA models do not take into account Tevatron data which are relevant to the decomposition of the diffractive cross section into SD, DD and CD components, so these fractions are also adjusted for the present analysis. Based on CDF SD [28] and DD [34] cross section data, extrapolated to the full diffractive kinematic ranges in each of the models, constraints of $0.29 < \sigma_{\mathrm{DD}}/\sigma_{\mathrm{SD}} < 0.68$ and $0.44 < \sigma_{\mathrm{DD}}/\sigma_{\mathrm{SD}} < 0.94$ are derived for the PYTHIA and PHOJET models of diffraction, respectively. The tuned ratios used in the correction procedure are taken at the centres of these bounds. The CD contribution in PHOJET is compatible with the measured Tevatron value of 9.3 % of the SD cross section [7] and $\sigma_{\mathrm{CD}}/\sigma_{\mathrm{SD}}$ is therefore kept fixed, with f_{CD} increasing in proportion to f_{SD}. Table 1 summarises the tuned decomposition of the inelastic cross section for each MC model.

Despite the substantial differences between the approaches to diffraction taken in PHOJET and PYTHIA, the two models both employ the Lund string model [69] of hadronisation. In order to investigate the sensitivity of the data at small gap sizes to the hadronisation model for ND processes, comparisons of the measured cross sections are also made with the HERWIG++ generator [77] (version 2.5.1 with the UE7-2 tune [78, 79]), which uses an alternative cluster-based model. The HERWIG++ minimum bias generator takes the total inelastic cross section to be 81 mb, based on a Donnachie–Landshoff model [80]. Perturbatively treated semi-hard processes are distinguished from soft processes according to whether they produce objects with transverse momentum above a fixed threshold which is taken to be 3.36 GeV. Partons produced from the parton shower are combined into colour singlet pairs called clusters, which can be interpreted as excited hadronic resonances. The clusters are then successively split into new clusters until they reach the required mass to form hadrons. The most recent HERWIG++ versions contain a mechanism to reconnect partons between cluster pairs via a colour reconnection (CR) algorithm, which improves the modelling of charged particle multiplicities in pp collisions [81]. Similarly to PYTHIA, HERWIG++ contains an eikonalised underlying event model, which assumes that separate scatterings in the same event

Table 1 Predicted ND, SD, DD and CD cross sections, together with the fractions of the total inelastic cross section f_{ND}, f_{SD}, f_{DD} and f_{CD} attributed to each process according to the default versions of the MC models (PYTHIA8.150, PYTHIA6.4.25 and PHOJET1.12.1.35), used for comparisons with the measured cross sections. The modified fractions used in the trigger efficiency and migration unfolding procedure, tuned as explained in the text, are also given

Cross section at $\sqrt{s} = 7$ TeV			
Process	PYTHIA6	PYTHIA8	PHOJET
σ_{ND} (mb)	48.5	50.9	61.6
σ_{SD} (mb)	13.7	12.4	10.7
σ_{DD} (mb)	9.2	8.1	3.9
σ_{CD} (mb)	0.0	0.0	1.3
Default f_{ND} (%)	67.9	71.3	79.4
Default f_{SD} (%)	19.2	17.3	13.8
Default f_{DD} (%)	12.9	11.4	5.1
Default f_{CD} (%)	0.0	0.0	1.7
Tuned f_{ND} (%)	70.0	70.2	70.2
Tuned f_{SD} (%)	20.7	20.6	16.1
Tuned f_{DD} (%)	9.3	9.2	11.2
Tuned f_{CD} (%)	0.0	0.0	2.5

are independent. At fixed impact parameter, this leads to Poisson distributions for both the number of soft scatters and the number of semi-hard processes per event. There is thus a small probability for 'empty' events to occur with no scatterings of either type. Under these circumstances, particle production occurs only in association with the dissociation of the beam protons, in a manner which is reminiscent of diffractive dissociation processes.

3.3 Comparisons between Monte Carlo simulations and uncorrected data

For use in the correction procedure, MC events are processed through the ATLAS detector simulation program [82], which is based on GEANT4 [83]. They are then subjected to the same reconstruction and analysis chain as is used for the data.

The quality of the MC description of the most important distributions for the correction procedure is tested through a set of control plots which compare the uncorrected data and MC distributions. These include energy flows, track and calorimeter cluster multiplicities and transverse momentum distributions, as well as leading cell energy significances in different pseudorapidity regions. All such distributions are reasonably well described. Examples are shown in Figs. 3a–d, where the total multiplicities of calorimeter clusters which pass the selection described in Sect. 2.3 are shown for events in four different regions of reconstructed forward rapidity gap size. Whilst none of the MC models gives a perfect description, particularly at small multiplicities, the three models tend to bracket the data, with PYTHIA6 showing an excess at low multiplicities and PYTHIA8 and PHOJET showing a deficiency in the same region.

A further example control distribution is shown in Fig. 3e. The probability of detecting at least one calorimeter cluster passing the noise requirements with $p_{\mathrm{T}} > p_{\mathrm{T}}^{\mathrm{cut}} = 200$ MeV in the most central region ($|\eta| < 0.1$) is shown as a function of the p_{T} of the leading track reconstructed in the same η region. In cases where this track has p_{T} below around 400 MeV, it spirals in the solenoidal field outside the acceptance of the EM calorimeter. The plotted quantity then corresponds to the detection probability for neutral particles in the vicinity of a track. Good agreement is observed between MC and data.

The shape of the uncorrected $\Delta\eta^F$ distribution for $p_{\mathrm{T}}^{\mathrm{cut}} = 200$ MeV is compared between the data and the MC models in Fig. 3f. The binning reflects that used in the final result (Sect. 2.4) except that contributions with $\Delta\eta^F > 8$, where the trigger efficiency becomes small, are also shown. None of the models considered are able to describe the data over the full $\Delta\eta^F$ range, with the largest deviations observed for small non-zero gaps in PHOJET. All of the models give an acceptable description of the shape of the distribution for large gaps up to the limit of the measurement at $\Delta\eta^F = 8$ and beyond.

Considering all control plots together, PYTHIA8 provides the best description of the shapes of the distributions. Hence this generator is chosen to correct the data. The deviations from PYTHIA8 of PYTHIA6 and PHOJET, which often lie in opposite directions and tend to enclose the data, are used to evaluate the systematic uncertainties on the unfolding procedure.

3.4 Corrections for experimental effects

After the statistical subtraction of the beam-induced background in each interval of $\Delta\eta^F$ (Sect. 2.2), the data are corrected for the influence of the limited acceptance and small particle detection inefficiencies of the MBTS using the MC simulation. For the ND, SD and DD processes, the trigger efficiency is close to 100 % for $\Delta\eta^F < 7$, dropping to around 80 % at $\Delta\eta^F = 8$. Since the topology of CD events sometimes involves hadronic activity in the central region of the detector, with gaps on either side, a larger fraction fail the trigger requirement, with efficiencies of close to 100 % for $\Delta\eta^F < 3$ and between 85 % and 95 % for $3 < \Delta\eta^F < 8$.

The data are corrected for migrations between the reconstructed and hadron level $\Delta\eta^F$ values, due to missed or spurious activity and cases where a final state particle is observed in a different η interval from that in which it is produced. The migration corrections are obtained using a Bayesian unfolding method [84] with a single iteration. The priors for the unfolding procedure with each MC model are taken after tuning the diffractive cross sections as described in Sect. 3.2. The migration matrix between the reconstructed and hadron level forward gap distributions according to the PYTHIA8 MC is shown for $p_{\mathrm{T}}^{\mathrm{cut}} = 200$ MeV in Fig. 4. An approximately diagonal matrix is obtained.

4 Systematic uncertainties

The sources of systematic uncertainty on the measurement are outlined below.

MC model and unfolding method dependence The trigger efficiency and migration correction procedure is carried out using each of the PYTHIA6, PYTHIA8 and PHOJET models. The deviation of the data unfolded with PHOJET from those obtained with PYTHIA8 is used to obtain a systematic uncertainty due to the assumed ξ_X, ξ_Y and t dependences in the unfolding procedure. The model dependence due to the details of the final state particle production is obtained from the difference between the results obtained with PYTHIA6 and PYTHIA8. Both of these model dependences are evaluated separately in each measurement interval and are applied symmetrically as upward and downward uncertainties.

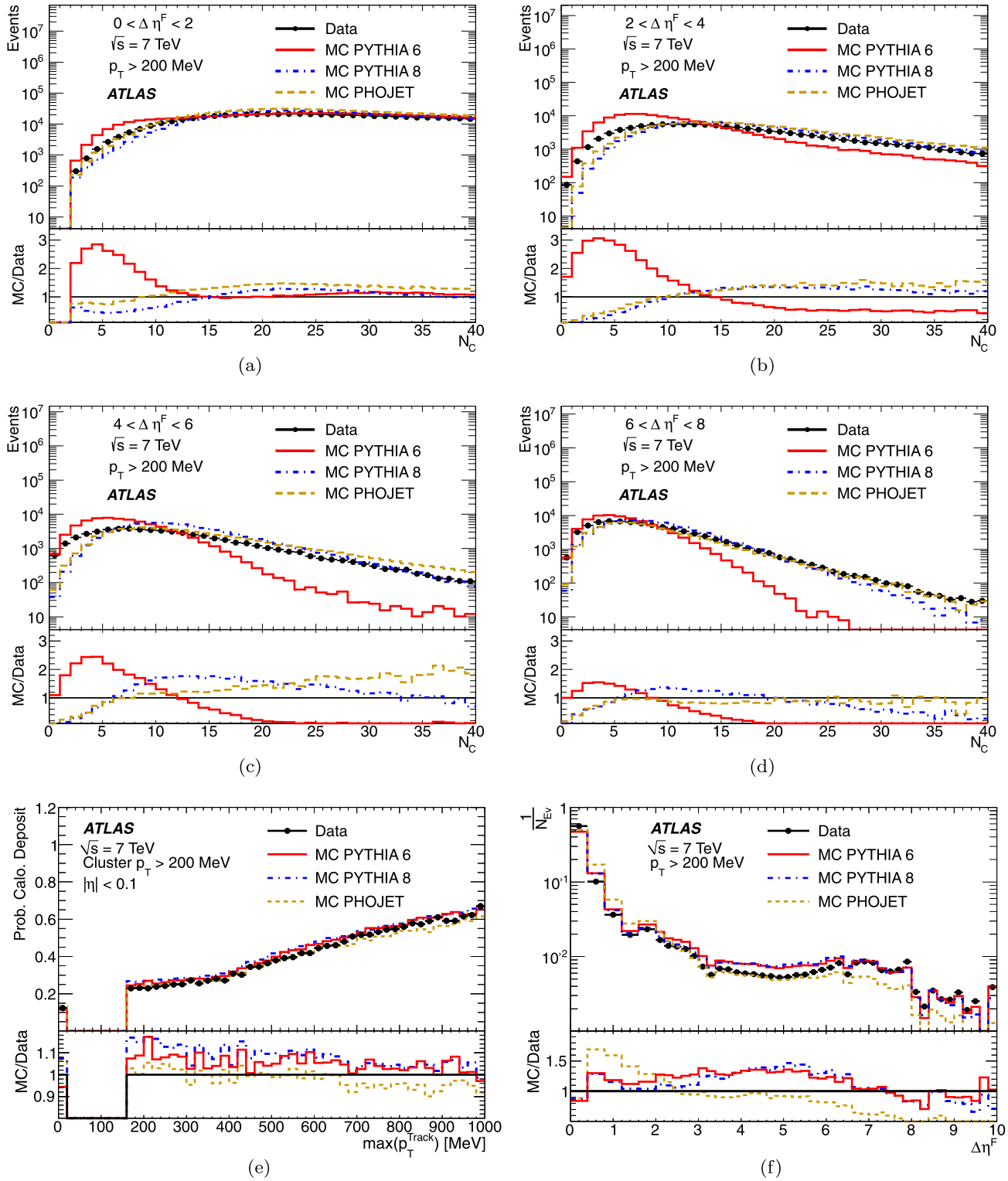

Fig. 3 Comparisons of uncorrected distributions between data and MC models. (**a**)–(**d**) Total calorimeter cluster multiplicities N_C for events reconstructed with (**a**) $0 < \Delta\eta^F < 2$, (**b**) $2 < \Delta\eta^F < 4$, (**c**) $4 < \Delta\eta^F < 6$ and (**d**) $6 < \Delta\eta^F < 8$. (**e**) Probability of detecting significant calorimeter energy in the most central region $|\eta| < 0.1$ as a function of the highest transverse momentum $\max(p_{\mathrm{T}}^{\mathrm{Track}})$ of the tracks reconstructed in the inner detector in the same $|\eta|$ range. The bin at zero corresponds to events where no charged track with $p_{\mathrm{T}} > 160$ MeV is reconstructed. (**f**) Forward rapidity gap distribution for $p_{\mathrm{T}}^{\mathrm{cut}} = 200$ MeV. The final bin at $\Delta\eta^F = 10$ corresponds to cases where no reconstructed particles have $p_{\mathrm{T}} > p_{\mathrm{T}}^{\mathrm{cut}}$

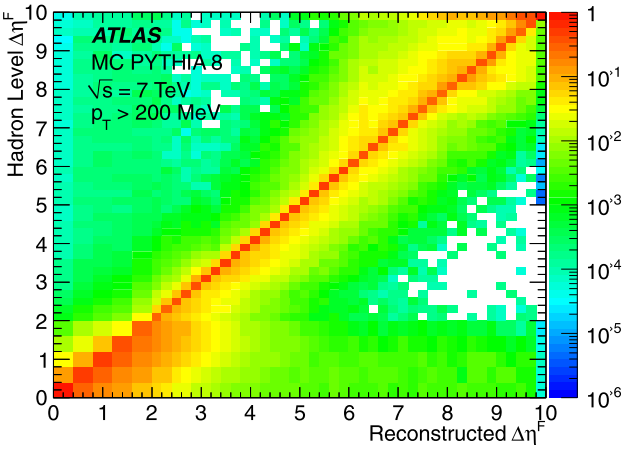

Fig. 4 Migration matrix between the reconstructed and hadron level values of $\Delta\eta^F$ for $p_{\mathrm{T}}^{\mathrm{cut}} = 200$ MeV, according to PYTHIA8. The distribution is normalised to unity in columns and is shown to beyond the limit of the measurement at $\Delta\eta^F = 8$

They produce the largest uncertainty on the measurement over most of the measured range. For $p_{\mathrm{T}}^{\mathrm{cut}} = 200$ MeV, the contributions from the PYTHIA6 and PHOJET variations are of similar size. Their combined effect is typically at the 6 % level for large $\Delta\eta^F$, growing to 20 % for gaps of around 1.5 pseudorapidity units. At larger $p_{\mathrm{T}}^{\mathrm{cut}}$ values, the PYTHIA6 source becomes dominant. The dependence on the unfolding technique has also been studied by switching between the default Bayesian method [84], a method using a Singular Value Decomposition of the unfolding matrix [85] and a simple bin-to-bin method. The resulting variations in the measured cross section are always within the systematic uncertainty defined by varying the MC model.

Modelling of diffractive contributions In addition to the differences between the Monte Carlo generators, additional systematic uncertainties are applied on the modelling of the fractional diffractive cross sections. The SD and DD cross sections in the PYTHIA8 model are each varied to the limits of the constraints from Tevatron data described in Sect. 3.2. The fraction f_{DD} is enhanced to 11.3 % of the total inelastic cross section, with f_{SD} reduced to 18.5 % to compensate. At the opposite extreme, f_{SD} is enhanced to 23.2 % of the cross section, with f_{DD} reduced to 6.6 %. These changes result in an uncertainty at the 1 % level for $\Delta\eta^F > 3$. A systematic uncertainty on the CD cross section is obtained by varying the CD and SD cross sections in PHOJET between the tuned values and $\sigma_{\mathrm{CD}}/\sigma_{\mathrm{SD}} = 0.093$, corresponding to the CDF measurement in [7]. This variation also results in a 1 % uncertainty in the large gap region.

Calorimeter energy scale The uncertainty on the calorimeter energy scale is constrained to be below the 5 % level down to energies of a few hundred MeV in the central region, $|\eta| < 2.3$, through comparisons between isolated calorimeter cluster energy measurements and momentum determinations of matched tracks in the inner detector [51–53]. This method is not available for larger $|\eta|$ values beyond the tracking acceptance. However, as $|\eta|$ grows, the default $p_{\mathrm{T}}^{\mathrm{cut}} = 200$ MeV threshold corresponds to increasingly large energies, reaching beyond 10 GeV at the outer limits of the FCal. The uncertainty on the response to electromagnetic showers in this energy range is determined as a function of $|\eta|$ from the maximum observed deviations between the data and the MC simulation in the peaks of $\pi^0 \to \gamma\gamma$ signals, under a variety of assumptions on background shapes and cluster energy resolutions. The relative response to charged pions compared with the electromagnetic scale has been studied in the relevant energy range for the FCal [55, 86] and HEC [54, 86] test-beam data, with systematic uncertainties of 8 % and 4 %, respectively, determined from the difference between data and MC. Adding the uncertainties in the electromagnetic scale and in the relative response to hadrons in quadrature, energy scale uncertainties of 5 % for $|\eta| < 1.37$, 21 % for $1.37 < |\eta| < 1.52$ (transition region between barrel and endcap), 5 % for $1.52 < |\eta| < 2.3$, 13 % for $2.3 < |\eta| < 3.2$ and 12 % for $3.2 < |\eta| < 4.9$ are ascribed. In addition to the absolute calorimeter response, these values account for systematic effects arising from dead material uncertainties and from the final state decomposition into different particle species. In the unfolding procedure, the corresponding systematic variation is applied to energy depositions from simulated final state particles in MC, with noise contributions left unchanged. The clustering algorithm is then re-run over the modified calorimeter cells. The scale uncertainty variation is thus considered both in the application of the $p_{\mathrm{T}}^{\mathrm{cut}}$ threshold to the clusters and in the discrimination of cells within selected clusters against the significance cut used to veto noise. The resulting fractional uncertainties on the differential cross sections at the default $p_{\mathrm{T}}^{\mathrm{cut}} = 200$ MeV are largest (reaching ∼12 %) in the region $\Delta\eta^F \lesssim 3$, where the gap identification relies most strongly on the calorimeter information. For larger gaps, the well measured tracks play an increasingly important role in defining the gap size and the cross section is dominated by low ξ_X diffractive events for which particle production in the gap region is completely suppressed. The sensitivity to the calorimeter scale is correspondingly reduced to a few percent.

MBTS efficiency The description of the MBTS efficiency in the MC models leads to a potential systematic effect on the trigger efficiency and on the off-line MBTS requirement. Following [8], the associated uncertainty is evaluated by increasing the thresholds of all MBTS counters in the simulation to match the maximum variation in the measured response in data according to studies with particles

extrapolated from the tracker or FCal. This systematic error amounts to typically 0.5–1 % for $\Delta\eta^F > 2$ and is negligible at the smallest $\Delta\eta^F$.

Tracking efficiency The dominant uncertainty in the charged particle track reconstruction efficiency arises due to possible inadequacies in the modelling of the material through which the charged particles pass [1]. This uncertainty is quantified by studying the influence on the data correction procedure of using an MC sample produced with a 10 % enhancement in the support material in the inner detector. The resulting uncertainty is smaller than 3.5 % throughout the measured distribution.

Luminosity Following the van der Meer scan results in [46], the normalisation uncertainty due to the uncertainty on the integrated luminosity is 3.4 %.

Each of the systematic uncertainties is determined with correlations between bins taken into account in the unfolding by repeating the full analysis using data or MC distributions after application of the relevant systematic shift. The final systematic error on the differential cross section is taken to be the sum in quadrature of all sources. Compared with the systematic uncertainties, the statistical errors are negligible at the smallest gap sizes, where the differential cross section is largest. For gap sizes $\Delta\eta^F \gtrsim 3$, the statistical errors are at the 1 % level and are typically smaller than the systematic errors by factors between five and ten.

5 Results

5.1 Differential cross section for forward rapidity gaps

In this section, measurements are presented of the inelastic cross section differential in forward rapidity gap size, $\Delta\eta^F$, as defined in Sect. 2.4. The data cover the range $0 < \Delta\eta^F < 8$. In the large gap region which is populated by diffractive processes, the cross section corresponds to a t-integrated sum of SD events in which either of the colliding protons dissociates and DD events with $\xi_Y \lesssim 10^{-6}$ ($M_Y \lesssim 7$ GeV). The data span the range $\xi_X \gtrsim 10^{-5}$. Diffractive events with smaller ξ_X values are subject to large MBTS trigger inefficiencies and thus lie beyond the kinematic range of the measurement.

As discussed in Sect. 2.4, the lowest transverse momentum requirement for the gap definition which is directly accessible experimentally is $p_{\mathrm{T}}^{\mathrm{cut}} = 200$ MeV. Figure 5a shows the differential gap cross section for this choice of $p_{\mathrm{T}}^{\mathrm{cut}}$, which is also given numerically in Table 2. The uncertainty on the measurement is typically less than 8 % for $\Delta\eta^F > 3$, growing to around 20 % at $\Delta\eta^F = 1.5$ before improving to around 10 % for events with little or no forward gap. The data are compared with the predictions of the default settings of the PYTHIA6 (labelled 'PYTHIA6 ATLAS AMBT2B') PYTHIA8 ('PYTHIA8 4C') and PHOJET models. In Figs. 5b–d, the results are compared with each of the MC models separately, with the default decomposition of the cross section into ND, SD, DD and CD contributions according to the models (Table 1) also indicated.

5.2 Small gap sizes and constraints on hadronisation models

At $\Delta\eta^F \lesssim 2$, all models agree that the ND process is dominant and the expected [4] exponential decrease of the cross section with increasing gap size, characteristic of hadronisation fluctuations, is the dominant feature of the data. According to the models, this region also contains DD events which have $\xi_Y \gtrsim 10^{-6}$, such that the Y system extends into the ATLAS detector acceptance, as well as both SD and DD events with very large ξ_X, such that no large rapidity gap is present within the region $|\eta| < 4.9$. The default MC models tend to lie above the data in this region, a result which is consistent with the overestimates of the total inelastic cross section observed for the same models in [8]. The PYTHIA8 model is closest in shape to the data, which is partly due to the modification of f_D in the most recent versions made in light of the previous ATLAS data [8]. Both PYTHIA models are closer to the small $\Delta\eta^F$ data than PHOJET, which exhibits an excess of almost a factor of two for $\Delta\eta^F \sim 1$.

As can be inferred from comparisons between the predicted shapes of the ND contributions in the different MC models (Figs. 5b–d), there are considerable uncertainties in the probability of obtaining large hadronisation fluctuations among low transverse momentum final state particles [87]. Studying the dependence of the measured differential cross section on $p_{\mathrm{T}}^{\mathrm{cut}}$ provides a detailed probe of fluctuations in the hadronisation process in soft scattering and of hadronisation models in general. The measurement is thus repeated with different choices of $p_{\mathrm{T}}^{\mathrm{cut}}$, applied both in the rapidity gap reconstruction and in the definition of the measured hadron level cross section. To avoid cases where the largest gap switches from one side of the detector to the other when low p_{T} particles are excluded by the increased $p_{\mathrm{T}}^{\mathrm{cut}}$ choice, the side of the detector on which the gap is located is fixed to that determined at $p_{\mathrm{T}}^{\mathrm{cut}} = 200$ MeV for all measured cross sections.

A comparison between the results with $p_{\mathrm{T}}^{\mathrm{cut}} = 200$ MeV, 400 MeV, 600 MeV and 800 MeV is shown in Fig. 6a. Figures 6b–d show the results for $p_{\mathrm{T}}^{\mathrm{cut}} = 400$ MeV, 600 MeV and 800 MeV, respectively, compared with the PYTHIA8, PYTHIA6 and PHOJET MC models. The ND contributions according to each of the models are also shown. As $p_{\mathrm{T}}^{\mathrm{cut}}$ increases, the exponential fall becomes less steep, so larger $\Delta\eta^F$ values become more heavily populated and the non-diffractive and diffractive contributions in the models be-

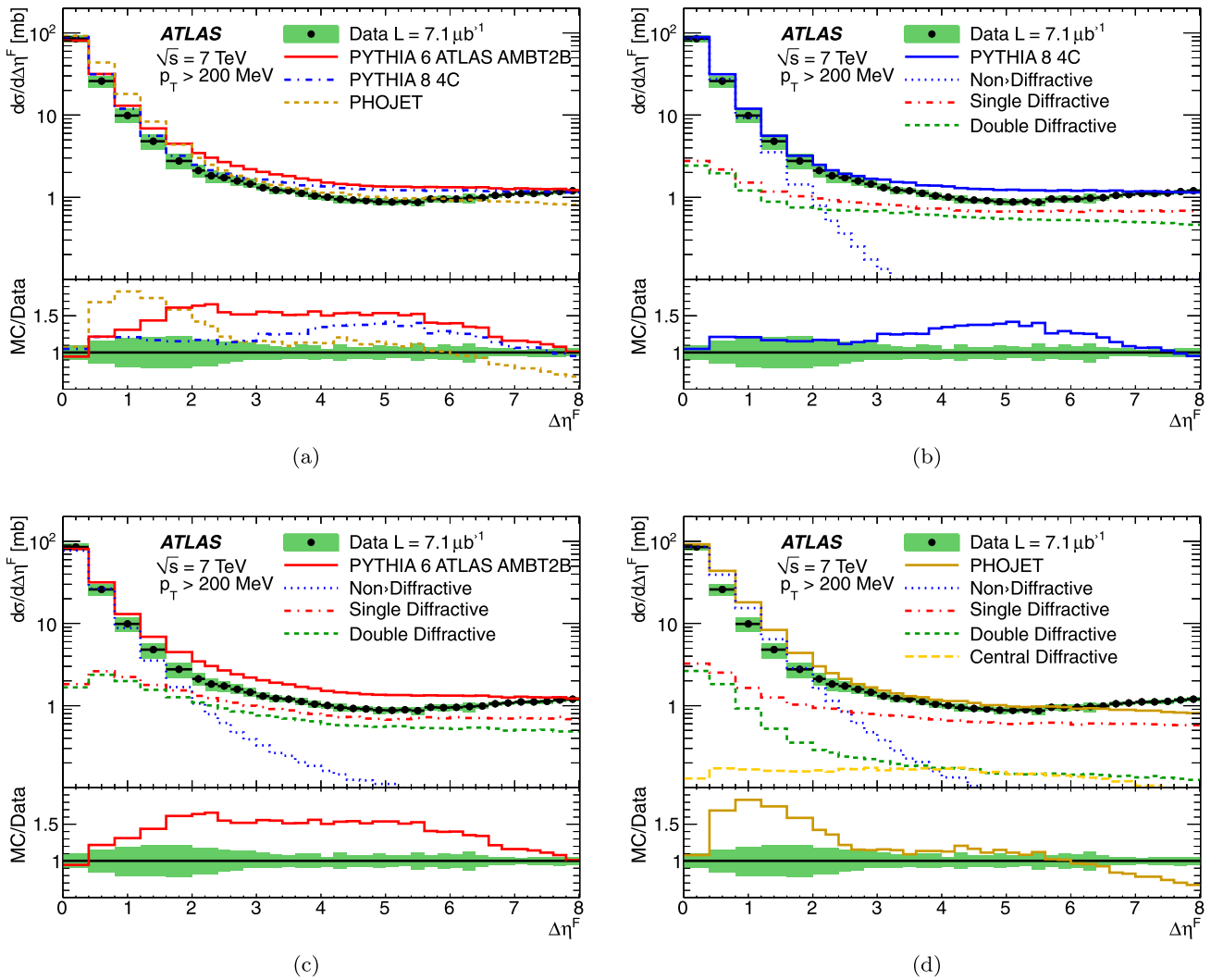

Fig. 5 Inelastic cross section differential in forward gap size $\Delta\eta^F$ for particles with $p_T > 200$ MeV. *The shaded bands* represent the total uncertainties. *The full lines* show the predictions of PHOJET and the default versions of PYTHIA6 and PYTHIA8. *The dashed lines* in (**b**–**d**) represent the contributions of the ND, SD and DD components according to the models. The CD contribution according to PHOJET is also shown in (**d**)

come similar. Also, the uncertainties due to the MC model dependence of the unfolding procedure grow.

The influence of changing from $p_T^{\rm cut} = 200$ MeV to $p_T^{\rm cut} = 400$ MeV is small at large $\Delta\eta^F$, where the cross section is dominated by small ξ_X diffractive events and particle production is kinematically forbidden over a wide range of pseudorapidity. For $\Delta\eta^F \lesssim 4$, where ND contributions become important, a significant fraction of events are assessed as having larger gaps for $p_T^{\rm cut} = 400$ MeV than for $p_T^{\rm cut} = 200$ MeV. As the value of $p_T^{\rm cut}$ increases to 600 MeV and 800 MeV, soft ND events migrate to larger $\Delta\eta^F$ values, giving significant contributions throughout most of the distribution and confirming [1] that the production of final state particles with more than a few hundred MeV is rare in minimum bias events, even at LHC energies. All MC models are able to reproduce the general trends of the data, though none provides a full description.

It is interesting to investigate the extent to which the alternative cluster-based approach to hadronisation in the non-diffractive HERWIG++ model is able to describe the data at small gap sizes, where the contribution from ND processes is dominant. A comparison of the data at each of the $p_T^{\rm cut}$ values with HERWIG++ is shown in Fig. 7. Four versions of the UE7-2 tune are shown, with variations in the details of the model which are expected to have the largest influence on rapidity gap distributions. These are the default version (UE7-2), a version in which the colour reconnection model is switched off (UE7-2, No CR) and similar versions which exclude events with no scatterings of either the soft or semi-hard types (UE7-2, No Empty Evts and UE7-2, No Empty

Table 2 The measured differential cross section data points for $p_{\mathrm{T}}^{\mathrm{cut}} = 200$ MeV, with each value corresponding to an average over the given $\Delta\eta^F$ range. Also quoted are the percentage statistical (δ_{stat}) uncertainty and the upward ($+\delta_{\mathrm{tot}}$) and downward ($-\delta_{\mathrm{tot}}$) total uncertainties, obtained by adding all uncertainties in quadrature. The remaining columns contain the percentage shifts due to each of the contributing systematic sources, which are correlated between data points. Those due to the modelling of final state particle production (δ_{py6}), the modelling of the ξ_X, ξ_Y and t dependences (δ_{pho}) and variation of the CD (δ_{cd}) cross section in the unfolding procedure are applied symmetrically as upward and downward uncertainties, as are those due to the dead material budget in the tracking region (δ_{mat}) and the MBTS response (δ_{mbts}). The uncertainties due to variations in the relative energy scale in data and MC are evaluated separately for upward (δ_{e+}) and downward (δ_{e-}) shifts, as are the modelling uncertainties due to enhancing (δ_{sd}) or reducing (δ_{dd}) the $\sigma_{\mathrm{SD}}/\sigma_{\mathrm{DD}}$ cross section ratio. Minus signs appear where the shift in a variable is anti-correlated rather than correlated with the shift in the differential cross section. The 3.4 % normalisation uncertainty due to the luminosity measurement is also included in the $\pm\delta_{\mathrm{tot}}$ values. These data points can be obtained from the HEPDATA database [90], along with their counterparts for $p_{\mathrm{T}}^{\mathrm{cut}} = 400$ MeV, 600 MeV and 800 MeV. A Rivet [91] routine is also available

$\Delta\eta^F$	$\mathrm{d}\sigma/\mathrm{d}\Delta\eta^F$ [mb]	δ_{stat} [%]	$+\delta_{\mathrm{tot}}$ [%]	$-\delta_{\mathrm{tot}}$ [%]	δ_{py6} [%]	δ_{pho} [%]	$\delta_{\mathrm{e+}}$ [%]	$\delta_{\mathrm{e-}}$ [%]	δ_{sd} [%]	δ_{dd} [%]	δ_{cd} [%]	δ_{mat} [%]	δ_{mbts} [%]
0.0–0.4	85	0.2	9.4	−9.5	−2.9	−7.6	3.0	−3.2	0.1	−0.1	0.0	−1.1	−0.1
0.4–0.8	26	0	15	−15	4	14	−3	3	−0	0	0	2	0
0.8–1.2	10	0	20	−20	5	18	−6	5	−0	0	0	3	0
1.2–1.6	5	0	21	−21	10	17	−6	7	0	−0	0	2	−0
1.6–2.0	2.8	0	22	−22	15	13	−7	9	0	−0	−0	3	0
2.0–2.2	2.1	1	18	−18	15	5	−9	8	−0	0	−0	1	0
2.2–2.4	1.8	1	18	−18	14	7	−8	8	−0	0	−0	1	0
2.4–2.6	1.7	1	15	−14	9	2	−9	10	−0	0	−0	−3	0
2.6–2.8	1.6	1	14	−13	5	1	−11	13	−0	0	−0	−0	0
2.8–3.0	1.4	1	14	−10	5	2	−8	12	−0	0	−1	−1	0
3.0–3.2	1.3	1	11	−9	4	2	−7	10	−1	0	−0	1	1
3.2–3.4	1.2	1.3	8.4	−9.9	3.5	3.7	−7.5	5.4	−0.6	0.4	−0.4	1.1	0.6
3.4–3.6	1.20	1.3	7.3	−8.2	4.4	0.4	−4.9	3.4	−0.7	0.6	−0.5	−2.6	0.9
3.6–3.8	1.1	1	11	−9	6	5	−4	7	−1	0	−1	−1	1
3.8–4.0	1.0	2	10	−10	7	4	−4	4	−0	0	−1	−2	1
4.0–4.2	1.01	1.6	5.7	−8.5	3.1	2.6	−6.2	0.2	−0.7	0.6	−1.0	−0.6	0.8
4.2–4.4	0.9	1	11	−11	5	8	−2	3	−1	1	−1	−3	1
4.4–4.6	0.92	1.8	7.8	−7.8	3.9	5.0	−2.1	2.1	−0.3	0.3	−1.0	−0.7	0.4
4.6–4.8	0.91	1.7	7.8	−8.4	4.5	4.8	−3.3	0.8	−0.9	0.7	−0.9	−0.3	1.1
4.8–5.0	0.88	2	10	−10	6	7	−0	3	−1	1	−1	−1	1
5.0–5.2	0.87	1.6	8.2	−7.8	5.3	4.0	0.5	2.5	−0.7	0.5	−0.9	−0.4	0.9
5.2–5.4	0.89	1.8	7.3	−7.5	5.5	2.5	−1.5	−1.6	−0.7	0.5	−0.8	−0.5	0.9
5.4–5.6	0.9	1	12	−12	8	7	1	1	−1	1	−1	2	1
5.6–5.8	0.95	1.2	7.5	−8.4	5.1	3.8	−2.2	−3.5	−1.0	0.8	−0.8	0.8	1.3
5.8–6.0	0.9	1	11	−10	7	6	3	0	−1	0	−1	1	1
6.0–6.2	0.95	1.4	8.6	−9.3	7.0	2.7	0.2	−3.5	−0.6	0.5	−1.1	1.5	1.0
6.2–6.4	1.0	1	12	−13	6	7	7	−8	−1	1	−1	4	1
6.4–6.6	0.99	1.3	7.8	−7.9	3.6	5.7	−0.2	−0.5	−0.6	0.5	−0.7	0.8	1.2
6.6–6.8	1.06	1.3	5.4	−5.4	2.0	3.0	−0.9	1.0	−0.5	0.4	−0.5	−0.4	1.0
6.8–7.0	1.08	1.3	5.4	−5.2	−0.0	3.3	−0.9	1.7	−0.1	0.1	−0.5	−1.3	0.6
7.0–7.2	1.11	1.2	4.4	−4.5	−1.9	−0.2	−1.2	1.0	−0.4	0.3	−0.1	−0.6	1.1
7.2–7.4	1.11	0.9	5.3	−5.7	−3.4	0.1	1.2	−2.5	−0.4	0.3	−0.2	−1.0	1.3
7.4–7.6	1.13	1.0	5.1	−6.1	−3.2	−0.6	−0.0	−3.3	−0.6	0.4	−0.2	0.5	1.6
7.6–7.8	1.17	1.0	5.9	−6.7	−4.0	−1.7	−0.0	−3.1	−0.3	0.2	−0.2	1.2	1.3
7.8–8.0	1.20	1.0	5.7	−5.4	−4.0	−0.5	1.0	1.8	−0.0	0.0	−0.1	−0.0	1.0

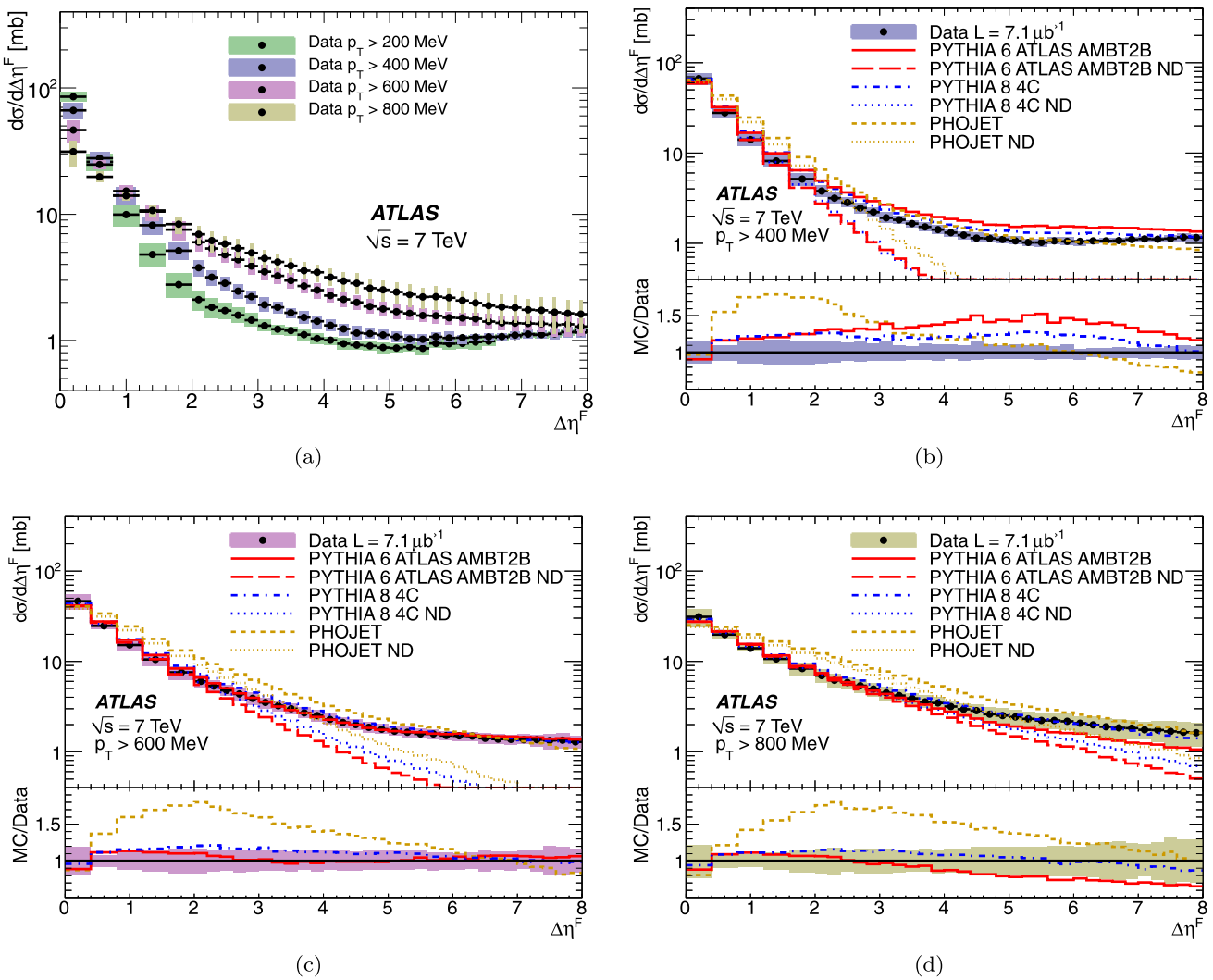

Fig. 6 Inelastic cross section differential in forward gap size $\Delta\eta^F$ for different $p_{\mathrm{T}}^{\mathrm{cut}}$ values. (**a**) Comparison between the measured cross sections. The full uncertainties are shown. They are correlated between the different $p_{\mathrm{T}}^{\mathrm{cut}}$ choices. (**b–d**) Comparison between the data and the MC models for $p_{\mathrm{T}}^{\mathrm{cut}} = 400$ MeV, 600 MeV and 800 MeV. The non-diffractive component in each MC model is also shown

Evts, No CR). At small gap sizes, all versions of the model produce an exponential fall with increasing gap size, though the dependence on $\Delta\eta^F$ is not steep enough in the default model and is too steep when colour recombination effects are switched off.

Despite not containing an explicit diffractive component, the default HERWIG++ minimum bias model produces a sizeable fraction of events with large gaps, overshooting the measured cross section by up to factor of four in the interval $2 < \Delta\eta^F < 7$ and producing an enhancement centred around $\Delta\eta^F = 6$. When colour reconnection is switched off, this large gap contribution is reduced considerably, but remains at a similar level to that measured in the range $3 < \Delta\eta^F < 5$. The enhancement near $\Delta\eta^F \approx 6$ is still present. The events with zero scatters in the HERWIG++ underlying event model provide a partial explanation for the large gap contribution. Removing this contribution reduces the predicted large gap cross section, but the non-exponential tail and large $\Delta\eta^F$ enhancement persist. For all scenarios considered, the alternative cluster based hadronisation model in HERWIG++ shows structure which is incompatible with the data.

5.3 Large gap sizes and sensitivity to diffractive dynamics

At large $\Delta\eta^F$, the differential cross section exhibits a plateau, which is attributed mainly to diffractive processes (SD events, together with DD events at $\xi_Y \lesssim 10^{-6}$) and is shown in detail in Fig. 8. According to the PHOJET MC model, the CD contribution is also distributed fairly uniformly across this region. Over a wide range of gap sizes with $\Delta\eta^F \gtrsim 3$, the differential cross section is roughly con-

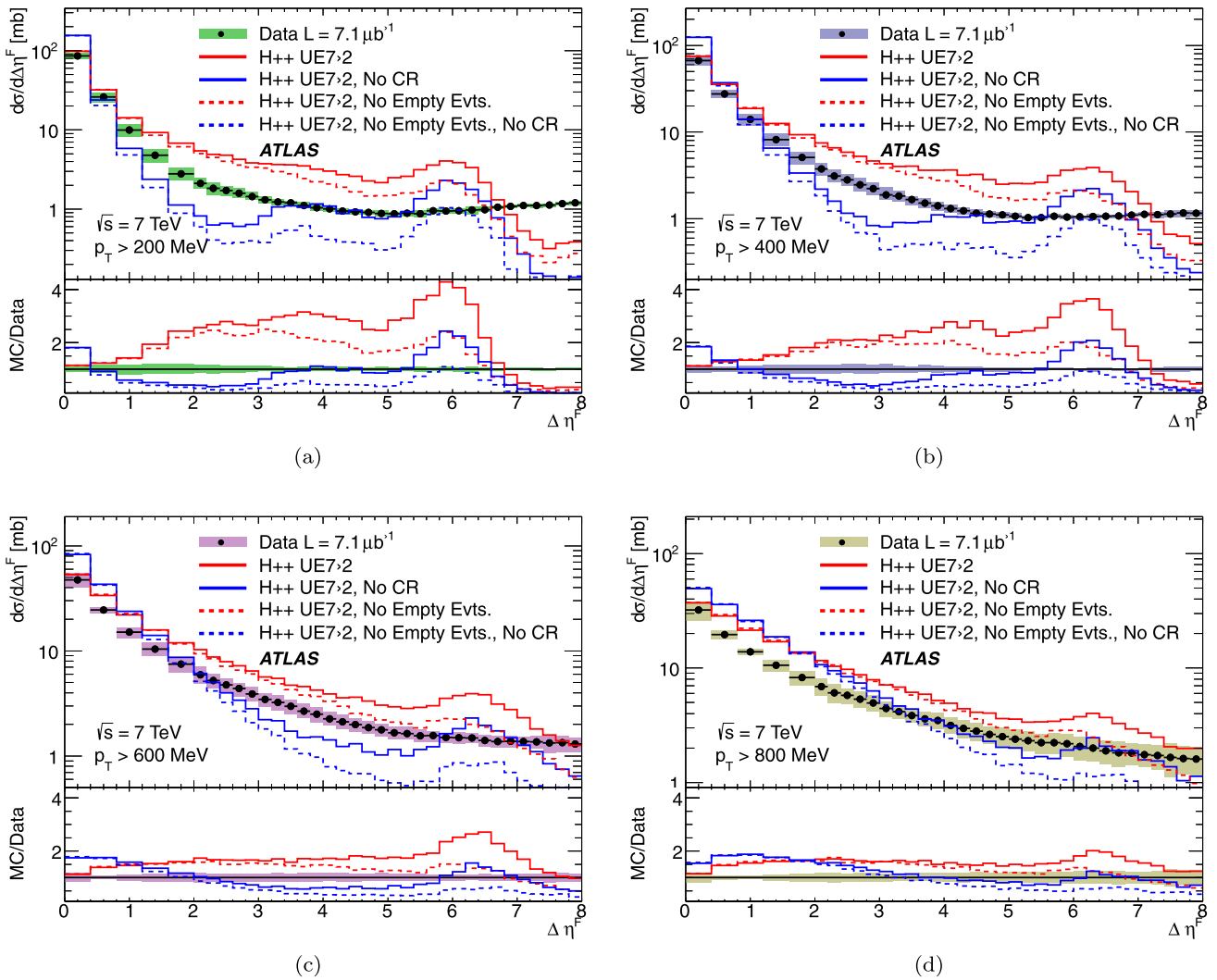

Fig. 7 Inelastic cross section differential in forward gap size $\Delta\eta^F$ for $p_{\mathrm{T}}^{\mathrm{cut}} =$ (**a**) 200 MeV, (**b**) 400 MeV, (**c**) 600 MeV and (**d**) 800 MeV. The data are compared with the UE7-2 tune of the HERWIG++ model. In addition to the default tune, versions are shown in which the colour reconnection model is switched off and in which events with zero scatters are excluded (see text for further details)

stant at around 1 mb per unit of rapidity gap size. Given the close correlation between $\Delta\eta^F$ and $-\ln\xi$ (Sect. 3.1), this behaviour is expected as a consequence of the dominance of soft diffractive processes. All MC models roughly reproduce the diffractive plateau, though none gives a detailed description of the shape as a function of $\Delta\eta^F$.

When absolutely normalised, the PYTHIA predictions overshoot the data throughout most of the diffractive region, despite the tuning of f_D to previous ATLAS data [8] in these models. The excess here is partially a reflection of the 10 % overestimate of the PYTHIA prediction in the total inelastic cross section and may also be associated with the large DD cross section in the measured region, which exceeds that expected based on Tevatron data [34] and gives rise to almost equal SD and DD contributions at large $\Delta\eta^F$. For PHOJET, the underestimate of the diffractive fraction f_D is largely compensated by the excess in the total inelastic cross section, such that the large gap cross section is in fair agreement with the measurement up to $\Delta\eta^F \approx 6$. The DD contribution to the cross section in PHOJET is heavily suppressed compared with that in the PYTHIA models.

Integrated over the diffractive-dominated region $5 < \Delta\eta^F < 8$, corresponding approximately to $-5.1 \lesssim \log_{10}(\xi_X) \lesssim -3.8$ according to the MC models, the measured cross section is 3.05 ± 0.23 mb, approximately 4 % of the total inelastic cross section. This can be compared with 3.58 mb, 3.89 mb and 2.71 mb for the default versions of PYTHIA8, PYTHIA6 and PHOJET, respectively.

As can be seen in Fig. 8, the differential cross section rises slowly with increasing $\Delta\eta^F$ for $\Delta\eta^F \gtrsim 5$. Non-diffractive contributions in this region are small and fall with increasing $\Delta\eta^F$ according to all models, so this rise

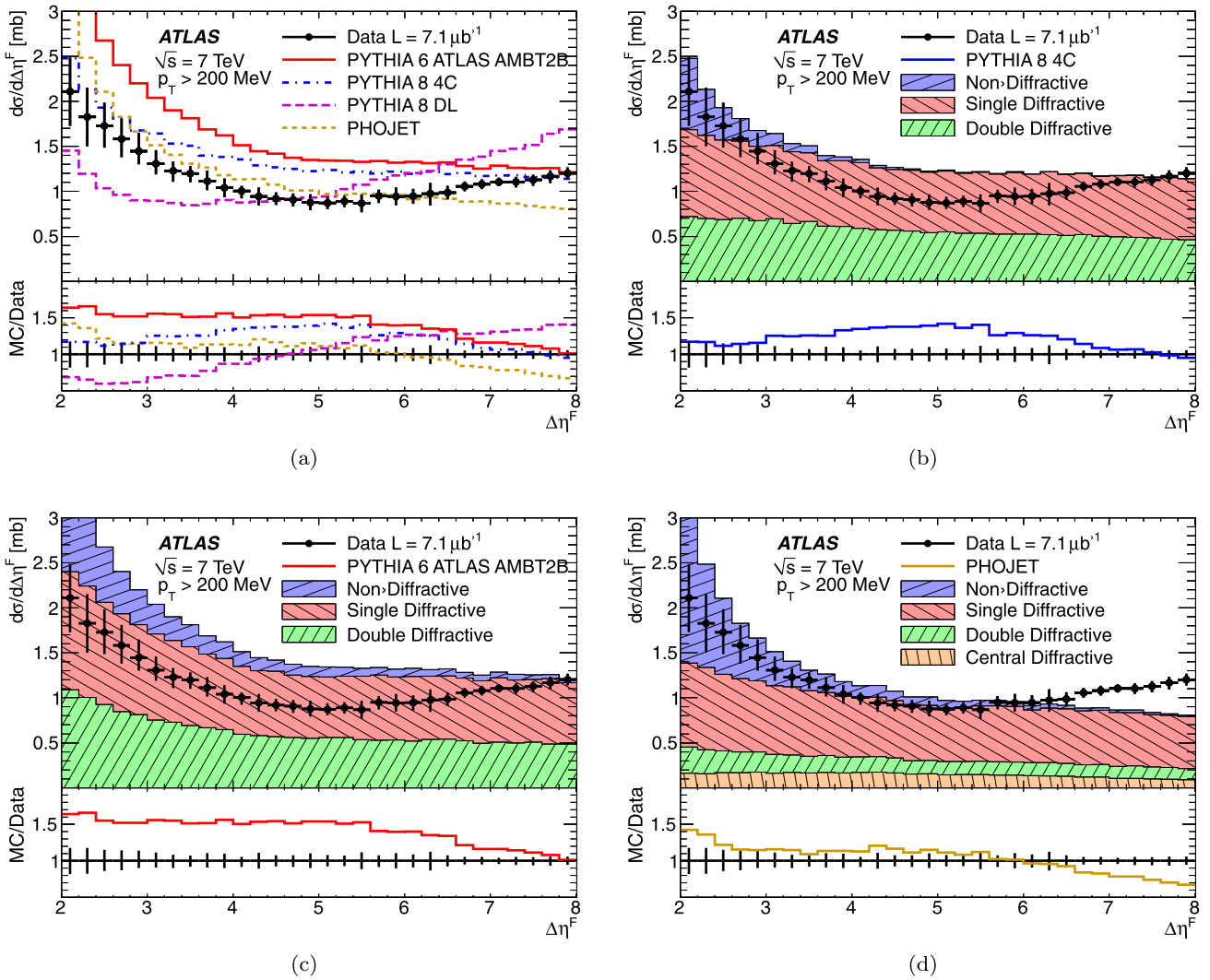

Fig. 8 Inelastic cross section differential in forward gap size $\Delta\eta^F$ for particles with $p_T > 200$ MeV and $\Delta\eta^F > 2$. The error bars indicate the total uncertainties. In (**a**), *the full lines* show the predictions of PHOJET, the default versions of PYTHIA6 and PYTHIA8, and PYTHIA8 with the Donnachie–Landshoff Pomeron flux. The remaining plots show the contributions of the SD, DD and ND components according to each generator. The CD contribution according to PHOJET is also shown in (**d**)

is attributable to the dynamics of the SD and DD processes. Specifically the rising cross section is as expected from the $\mathbb{PPP}$ term in triple Regge models with a Pomeron intercept in excess of unity (see (2)). In Fig. 8a, a comparison is made with the PYTHIA8 model, after replacing the default Schuler and Sjöstrand Pomeron flux with the Donnachie and Landshoff (DL) version using the default Pomeron trajectory, $\alpha_{\mathbb{P}}(t) = 1.085 + 0.25t$ ('PYTHIA8 DL'). It is clear that the data at large $\Delta\eta^F$ are not perfectly described with this choice.

Whilst the data are insensitive to the choice of $\alpha_{\mathbb{P}}\prime$, there is considerable sensitivity to the value of $\alpha_{\mathbb{P}}(0)$. The data in the cleanest diffractive region $\Delta\eta^F > 6$ are used to obtain a best estimate of the appropriate choice of the Pomeron intercept to describe the data. SD and DD PYTHIA8 samples are generated with the DL Pomeron flux for a range of $\alpha_{\mathbb{P}}(0)$ values. In each case, the default $\alpha_{\mathbb{P}}\prime$ value of 0.25 GeV^{-2} is taken and the tuned ratios of the SD and DD contributions appropriate to PYTHIA8 from Table 1 are used. The χ^2 value for the best fit to the data in the region $6 < \Delta\eta^F < 8$ is obtained for each of the samples with different $\alpha_{\mathbb{P}}(0)$ values, with the cross section integrated over the fitted region allowed to float as a free parameter. The optimum $\alpha_{\mathbb{P}}(0)$ is determined from the minimum of the resulting χ^2 parabola.

The full procedure is repeated for data points shifted according to each of the systematic effects described in Sect. 4, such that correlations between the uncertainties on the data points are taken into account in evaluating the uncertainties. The systematic uncertainty is dominated by the MC model dependence of the data correction procedure, in particular

the effect of unfolding using PYTHIA6 in place of PYTHIA8, which leads to a significantly flatter dependence of the data on $\Delta\eta^F$ at large gap sizes.

The result obtained in the context of the PYTHIA8 model with the DL flux parameterisation is

$$\alpha_{\mathbb{P}}(0) = 1.058 \pm 0.003(\text{stat.})^{+0.034}_{-0.039}(\text{syst.}). \quad (4)$$

The data are thus compatible with a value of $\alpha_{\mathbb{P}}(0)$ which matches that appropriate to the description of total hadronic cross sections [58, 59]. When the Berger–Streng Pomeron flux, which differs from the DL version in the modelling of the t dependence, is used in the fit procedure, the result is modified to $\alpha_{\mathbb{P}}(0) = 1.056$. The effects of varying $\alpha_{\mathbb{P}}{}'$ between 0.1 GeV^{-2} and 0.4 GeV^{-2} and of varying the f_{SD} and f_{DD} fractions assumed in the fit in the ranges given in Sect. 4 are also smaller than the statistical uncertainty. Compatible results are obtained by fitting the higher $p_{\text{T}}^{\text{cut}}$ data.

A comparison between the data and a modified version of PYTHIA8, with $\alpha_{\mathbb{P}}(0)$ as obtained from the fit, is shown in Fig. 9. Here, the diffractive contribution to the inelastic cross section $f_D = 25.6$ % is matched[2] to the fitted value of $\alpha_{\mathbb{P}}(0)$ using the results in [8]. Together with the cross section integrated over the region $6 < \Delta\eta^F < 8$ as obtained from the fit and the tuned ratio $f_{\text{DD}}/f_{\text{SD}}$ from Table 1, this fixes the normalisation of the full distribution. The description of the data at large $\Delta\eta^F$ is excellent and the exponential fall at small $\Delta\eta^F$ is also adequately described. There is a discrepancy in the region $2 < \Delta\eta^F < 4$, which may be a consequence of the uncertainty in modelling large hadronisation fluctuations in ND events (compare the ND tails to large $\Delta\eta^F$ in Figs. 8b, c and d). It may also be attributable to sub-leading trajectory exchanges [29, 31] or to the lack of a CD component in the PYTHIA model.

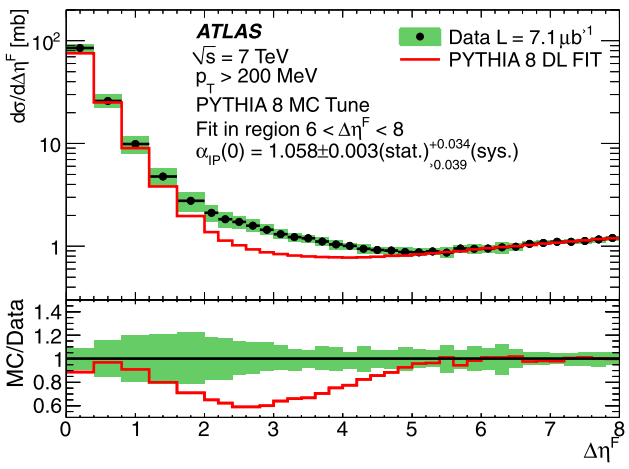

Fig. 9 Inelastic cross section differential in forward gap size $\Delta\eta^F$ for particles with $p_{\text{T}} > 200$ MeV. The data are compared with a modified version of the PYTHIA8 model with the DL flux, in which the Pomeron intercept $\alpha_{\mathbb{P}}(0)$ is determined from fits to the data in the region $6 < \Delta\eta^F < 8$. See text for further details

[2]Since only data at large $\Delta\eta^F$ are included in the fit, the result for $\alpha_{\mathbb{P}}(0)$ is insensitive to systematic variations in f_D.

5.4 The integrated inelastic cross section

By summing over the $\Delta\eta^F$ distribution from zero to a maximum gap size $\Delta\eta^F_{\text{Cut}}$, the integrated inelastic cross section can be obtained, excluding the contribution from events with very large gaps $\Delta\eta^F > \Delta\eta^F_{\text{Cut}}$. As discussed in Sect. 3.1, there is a strong correlation between the size of the gap and the kinematics of diffraction (see e.g. Eq. (3) for the SD process). The cross section integrated over a given range of gap size can thus be converted into an integral over the inelastic pp cross section down to some minimum value ξ_{Cut} of ξ_X. The variation in the integrated inelastic cross section with $\Delta\eta^F_{\text{Cut}}$ can then be used to compare inelastic cross section results with different lower limits, ξ_{Cut}.

The integral of the forward gap cross section

$$\int_0^{\Delta\eta^F_{\text{Cut}}} \frac{\mathrm{d}\sigma}{\mathrm{d}\Delta\eta^F}\,\mathrm{d}\Delta\eta^F$$

is obtained for $\Delta\eta^F_{\text{Cut}}$ values varying between 3 and 8 by cumulatively adding the cross section contributions from successive bins of the measured gap distribution. The correspondence between maximum gap size and minimum ξ_X used here is determined from the PYTHIA8 model to be $\log_{10}\xi_{\text{Cut}} = -0.45\Delta\eta^F_{\text{Cut}} - 1.52$. The uncertainty on this correlation is small; for example the PHOJET model results in the same slope of -0.45 with an intercept of -1.56. This correlation is applied to convert to an integral

$$\int_{\xi_{\text{Cut}}}^1 \frac{\mathrm{d}\sigma}{\mathrm{d}\xi_X}\,\mathrm{d}\xi_X.$$

A small correction is applied to account for the fact that the gap cross section neglects particles with[3] $p_{\text{T}} < p_{\text{T}}^{\text{cut}} = 200$ MeV and includes a contribution from ND processes. This correction factor is calculated using PYTHIA8 with the DL flux, and the optimised $\alpha_{\mathbb{P}}(0)$ and f_D values, as determined in Sect. 5.3. The integration range is chosen such that the correction is always smaller than ± 1.3 %. The systematic uncertainty on the correction factor, evaluated by comparison with results obtained using PHOJET or PYTHIA8 with the default Schuler and Sjöstrand flux, together with the systematic variations of the tuned fractions f_{SD} and f_{DD} as in Sect. 4, is also small.

[3]The finite $p_{\text{T}}^{\text{cut}}$ value in the measured gap cross sections tends to increase gap sizes slightly relative to $p_{\text{T}}^{\text{cut}} = 0$. However, MC studies indicate that this effect has the biggest influence on the exponentially falling distribution at small gap sizes, whereas the difference for the $\Delta\eta^F$ values which are relevant to the integrated cross section are relatively small. According to the MC models, the cross section integrated over $5 < \Delta\eta^F < 8$ decreases by 2 % when changing from $p_{\text{T}}^{\text{cut}} = 200$ MeV to $p_{\text{T}}^{\text{cut}} = 0$.

The integrated inelastic cross section is shown as a function of ξ_{Cut} in Fig. 10, where it is also compared with a previous ATLAS result [8] and with the TOTEM extraction of the full inelastic cross section [10], derived from a measurement of the elastic cross section via the optical theorem. The errors on all of the experimental data points are dominated by the luminosity uncertainties. The previous ATLAS result was also based on MBTS-triggered data, but is quoted at the ξ_X value corresponding to 50 % trigger efficiency, which is slightly beyond the range accessed here. Extrapolating according to the measured dependence on ξ_{Cut}, the new data are in good agreement with the previous result, the small apparent difference being well within the uncertainty due to run-to-run luminosity measurement variations.

It is instructive to compare the TOTEM result with the ATLAS measurements, since the latter omit the poorly understood lowest ξ_X region. By comparing the lowest ξ_{Cut} data point from the present analysis with the TOTEM measurement and neglecting any correlations between the ATLAS and TOTEM uncertainties, the inelastic cross section integrated over $\xi_X < 8 \times 10^{-6}$ is inferred to be $14.5^{+2.0}_{-1.5}$ mb. Significantly smaller contributions are predicted by the default versions of PYTHIA (∼6 mb) and PHOJET (∼3 mb). Figure 10 also shows two versions of the RMK model (see Sect. 3.1), corresponding to versions (i) (upper curve) and (ii) (lower curve) in [43]. These versions differ in the radii attributed to the elastically scattered eigenstates comprising the low ξ_X contribution which is added to the more standard triple Pomeron calculation in the model, (ii) being the favoured version and (i) being indicative of the flexibility in the model whilst preserving an acceptable description of pre-LHC data. The additional low ξ_X processes enhance the inelastic cross section by 5.5 mb and 6.7 mb in versions (i) and (ii), respectively. Although the RMK model lies below the data in general, the low ξ_X enhancement is compatible with that observed [88]. The shape of the distribution at low ξ_X is not predicted in the model, but is compatible with the data if, as shown here [89], it is assumed to have the steep ξ_X dependence associated with the $\mathbb{PPR}$, rather than the $\mathbb{PPP}$ triple Regge term. Similar conclusions have been reached previously from proton–proton [25] and photo-production [29, 30] data.

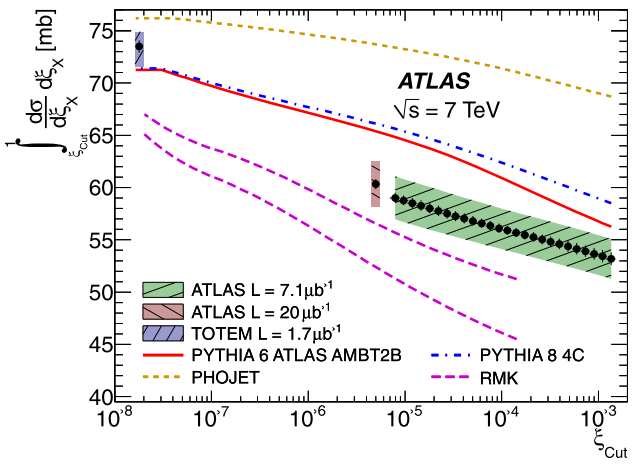

Fig. 10 Inelastic cross section excluding diffractive processes with $\xi_X < \xi_{\mathrm{Cut}}$, obtained by integration of the differential cross section from gap sizes of zero to a variable maximum. The results from the present analysis ('ATLAS L = 7.1 μb^{-1}') are compared with a previous ATLAS result [8] and a TOTEM measurement integrated over all kinematically accessible ξ_X values [10]. The predictions of the default versions of the PYTHIA6, PYTHIA8 and PHOJET models are also shown, along with two versions of the RMK model [43] (see text). The vertical error bars on the ATLAS measurements denote the systematic uncertainties excluding that on the luminosity measurement, whilst *the shaded area* represents the full systematic uncertainty. For the TOTEM point, the error bar represents the statistical uncertainty whilst *the shaded area* represents the full uncertainty. The uncertainties on the data points obtained in the present analysis are strongly correlated between neighbouring points

6 Summary

A novel algorithm has been devised for identifying rapidity gaps in the final state of minimum bias ATLAS data, leading to measurements in which particle production is considered down to transverse momentum thresholds $p_{\mathrm{T}}^{\mathrm{cut}}$ between 200 MeV and 800 MeV. The differential cross section $\mathrm{d}\sigma/\mathrm{d}\Delta\eta^F$ is measured for forward rapidity gaps of size $0 < \Delta\eta^F < 8$, corresponding to the larger of the two gaps extending to $\eta = \pm 4.9$, with no requirements on activity at $|\eta| > 4.9$. An exponentially falling non-diffractive contribution is observed at small gap sizes, which is also a feature of the PYTHIA, PHOJET and HERWIG++ Monte Carlo models. However, none of the models describes the $\Delta\eta^F$ or $p_{\mathrm{T}}^{\mathrm{cut}}$ dependence of this region in detail. At large gap sizes, the differential cross section exhibits a plateau, which corresponds to a mixture of the single-diffractive dissociation process and double dissociation with $\xi_Y \lesssim 10^{-6}$. This plateau amounts to a cross section close to 1 mb per unit of gap size and its magnitude is roughly described by the PYTHIA and PHOJET Monte Carlo models. None of the default models reproduce the rise of the differential cross section as a function of gap size at the largest $\Delta\eta^F$ values. This rise is interpreted within the triple Pomeron-based approach of the PYTHIA8 model with a Donnachie–Landshoff Pomeron flux in terms of a Pomeron intercept of $\alpha_{\mathbb{P}}(0) = 1.058 \pm 0.003(\mathrm{stat.})^{+0.034}_{-0.039}(\mathrm{syst.})$. Since the bulk of the inelastic pp cross section is contained within the measured range, integrated cross sections are also obtained and compared with previous measurements. The contribution to the total inelastic cross section from the region $\xi_X < 10^{-5}$ is determined to be around 20 %, which is considerably larger than is predicted by most models.

Acknowledgements We are grateful to the HERWIG++ collaboration for their assistance in investigating the low p_T rapidity gap spectrum produced by their generator and to M. Ryskin, A. Martin and V. Khoze for supplying their prediction for the behaviour of the inelastic cross section as a function of ξ_{Cut}.

We thank CERN for the very successful operation of the LHC, as well as the support staff from our institutions, without whom ATLAS could not be operated efficiently.

We acknowledge the support of ANPCyT, Argentina; YerPhI, Armenia; ARC, Australia; BMWF, Austria; ANAS, Azerbaijan; SSTC, Belarus; CNPq and FAPESP, Brazil; NSERC, NRC and CFI, Canada; CERN; CONICYT, Chile; CAS, MOST and NSFC, China; COLCIENCIAS, Colombia; MSMT CR, MPO CR and VSC CR, Czech Republic; DNRF, DNSRC and Lundbeck Foundation, Denmark; ARTEMIS and ERC, European Union; IN2P3-CNRS, CEA-DSM/IRFU, France; GNAS, Georgia; BMBF, DFG, HGF, MPG and AvH Foundation, Germany; GSRT, Greece; ISF, MINERVA, GIF, DIP and Benoziyo Center, Israel; INFN, Italy; MEXT and JSPS, Japan; CNRST, Morocco; FOM and NWO, Netherlands; RCN, Norway; MNiSW, Poland; GRICES and FCT, Portugal; MERYS (MECTS), Romania; MES of Russia and ROSATOM, Russian Federation; JINR; MSTD, Serbia; MSSR, Slovakia; ARRS and MVZT, Slovenia; DST/NRF, South Africa; MICINN, Spain; SRC and Wallenberg Foundation, Sweden; SER, SNSF and Cantons of Bern and Geneva, Switzerland; NSC, Taiwan; TAEK, Turkey; STFC, the Royal Society and Leverhulme Trust, United Kingdom; DOE and NSF, United States of America.

The crucial computing support from all WLCG partners is acknowledged gratefully, in particular from CERN and the ATLAS Tier-1 facilities at TRIUMF (Canada), NDGF (Denmark, Norway, Sweden), CC-IN2P3 (France), KIT/GridKA (Germany), INFN-CNAF (Italy), NL-T1 (Netherlands), PIC (Spain), ASGC (Taiwan), RAL (UK) and BNL (USA) and in the Tier-2 facilities worldwide.

Open Access This article is distributed under the terms of the Creative Commons Attribution License which permits any use, distribution, and reproduction in any medium, provided the original author(s) and the source are credited.

References

1. ATLAS Collaboration, New J. Phys. **13**, 053033 (2011). arXiv:1012.5104 [hep-ex]
2. CMS Collaboration, J. High Energy Phys. **1101**, 079 (2011). arXiv:1011.5531 [hep-ex]
3. ALICE Collaboration, Eur. Phys. J. C **68**, 345 (2010). arXiv:1004.3514 [hep-ex]
4. J. Bjorken, S. Brodsky, H.J. Lu, Phys. Lett. B **286**, 153 (1992)
5. E. Feinberg, I. Pomerančuk, Suppl. Nuovo Cim. **3**, 652 (1956)
6. G. Chew, S. Frautschi, Phys. Rev. Lett. **7**, 394 (1961)
7. CDF Collaboration, Phys. Rev. Lett. **93**, 141601 (2004). arXiv:hep-ex/0311023
8. ATLAS Collaboration, Nat. Commun. **2**, 463 (2011)
9. TOTEM Collaboration, Europhys. Lett. **95**, 41001 (2011). arXiv:1110.1385 [hep-ex]
10. TOTEM Collaboration, Europhys. Lett. **96**, 21002 (2011). arXiv:1110.1395 [hep-ex]
11. A. Mueller, Phys. Rev. D **2**, 2963 (1970)
12. F. Low, Phys. Rev. D **12**, 163 (1975)
13. S. Nussinov, Phys. Rev. Lett. **34**, 1286 (1975)
14. L. Gribov, E. Levin, M. Ryskin, Phys. Rep. **100**, 1 (1983)
15. K. Golec-Biernat, M. Wüsthoff, Phys. Rev. D **59**, 014017 (1998). arXiv:hep-ph/9807513
16. E. Iancu, A. Leonidov, L. McLerran, Nucl. Phys. A **692**, 583 (2001). arXiv:hep-ph/0011241
17. Z. Ajaltouni et al., in *Proceedings of the 'HERA and the LHC' Workshop Series, Chap. 5*. arXiv:0903.3861 [hep-ex]
18. R. Brower, J. Polchinski, M. Strassler, C. Tan, J. High Energy Phys. **0712**, 005 (2007). arXiv:hep-th/0603115
19. ATLAS Collaboration, Eur. Phys. J. C **71**, 1630 (2011). arXiv:1101.2185 [hep-ex]
20. K. Goulianos, Phys. Rep. **101**, 169 (1983)
21. G. Alberi, G. Goggi, Phys. Rep. **74**, 1 (1981)
22. N. Zotov, V. Tsarev, Sov. Phys. Usp. **31**, 119 (1988)
23. A. Kaidalov, Phys. Rep. **50**, 157 (1979)
24. M. Albrow, T. Coughlin, J. Forshaw, Prog. Part. Nucl. Phys. **65**, 149 (2010). arXiv:1006.1289 [hep-ph]
25. UA4 Collaboration, Phys. Lett. B **186**, 227 (1987)
26. UA5 Collaboration, Z. Phys. C **33**, 175 (1986)
27. E710 Collaboration, Phys. Lett. B **301**, 313 (1993)
28. CDF Collaboration, Phys. Rev. D **50**, 5535 (1994)
29. H1 Collaboration, Z. Phys. C **74**, 221 (1997). arXiv:hep-ex/9702003
30. ZEUS Collaboration, Z. Phys. C **75**, 421 (1997). arXiv:hep-ex/9704008
31. H1 Collaboration, Eur. Phys. J. C **48**, 715 (2006). arXiv:hep-ex/0606004
32. ZEUS Collaboration, Nucl. Phys. B **816**, 1 (2009). arXiv:0812.2003 [hep-ex]
33. H1 Collaboration, Eur. Phys. J. C **71**, 1578 (2011). arXiv:1010.1476 [hep-ex]
34. CDF Collaboration, Phys. Rev. Lett. **87**, 141802 (2001). arXiv:hep-ex/0107070
35. D. Joyce et al., Phys. Rev. D **48**, 1943 (1993)
36. UA8 Collaboration, Eur. Phys. J. C **25**, 361 (2002). arXiv:hep-ex/0205037
37. G. Ingelman, P. Schlein, Phys. Lett. B **152**, 256 (1985)
38. A. Kaidalov, V. Khoze, Y. Pirogov, N. Ter-Isaakyan, Phys. Lett. B **45**, 493 (1973)
39. R. Field, G. Fox, Nucl. Phys. B **80**, 367 (1974)
40. T. Sjöstrand, S. Mrenna, P. Skands, J. High Energy Phys. **0605**, 026 (2006). arXiv:hep-ph/0603175
41. T. Sjöstrand, S. Mrenna, P. Skands, Comput. Phys. Commun. **178**, 852 (2008). arXiv:0710.3820 [hep-ph]
42. R. Engel, Z. Phys. C **66**, 203 (1995)
43. M. Ryskin, A. Martin, V. Khoze, Eur. Phys. J. C **71**, 1617 (2011). arXiv:1102.2844 [hep-ph]
44. E. Gotsman, E. Levin, U. Maor, Eur. Phys. J. C **71**, 1553 (2011). arXiv:1010.5323 [hep-ph]
45. ATLAS Collaboration, JINST **3**, S08003 (2008)
46. ATLAS Collaboration, Updated luminosity determination in pp collisions at $\sqrt{s} = 7$ TeV using the ATLAS detector. ATLAS-CONF-2011-011 (2011)
47. ATLAS Collaboration, Eur. Phys. J. C **71**, 1512 (2011). arXiv:1009.5908 [hep-ex]
48. W. Lampl et al., Calorimeter clustering algorithms: description and performance. ATL-LARG-PUB-2008-002. ATL-COM-LARG-2008-003 (2008)
49. ATLAS Collaboration, Eur. Phys. J. C **70**, 723 (2010). arXiv:0912.2642 [physics.ins-det]
50. ATLAS Collaboration, J. High Energy Phys. **1012**, 060 (2010). arXiv:1010.2130 [hep-ex]
51. ATLAS Collaboration, Response of the ATLAS calorimeters to single isolated hadrons produced in proton-proton collisions at $\sqrt{s} = 900$ GeV. ATLAS-CONF-2010-017 (2010)
52. ATLAS Collaboration, ATLAS calorimeter response to single isolated hadrons and estimation of the calorimeter jet energy scale uncertainty. ATLAS-CONF-2010-052 (2010)
53. ATLAS Collaboration, ATLAS calorimeter response to single isolated hadrons and estimation of the calorimeter jet scale uncertainty. ATLAS-CONF-2011-028 (2011)
54. J. Pinfold et al., Nucl. Instrum. Methods A **593**, 324 (2008)
55. J. Archambault et al., JINST **3**, P02002 (2008)

56. B. Dowler et al., Nucl. Instrum. Methods A **482**, 94 (2002)
57. D. Roy, R. Roberts, Nucl. Phys. B **77**, 240 (1974)
58. A. Donnachie, P. Landshoff, Phys. Lett. B **296**, 227 (1992). arXiv:hep-ph/9209205
59. J. Cudell, K. Kang, S. Kim, Phys. Lett. B **395**, 311 (1997). arXiv:hep-ph/9601336
60. M. Good, W. Walker, Phys. Rev. **120**, 1857 (1960)
61. F. Bopp, R. Engel, J. Ranft, Rapidity gaps and the PHOJET Monte Carlo. arXiv:hep-ph/9803437
62. G. Schuler, T. Sjöstrand, Phys. Rev. D **49**, 2257 (1994)
63. P. Bruni, G. Ingelman, Phys. Lett. B **311**, 317 (1993)
64. E. Berger, J. Collins, D. Soper, G. Sterman, Nucl. Phys. B **286**, 704 (1987)
65. K. Streng, Hard QCD scatterings in diffractive reactions at HERA. CERN-TH-4949 (1988)
66. A. Donnachie, P. Landshoff, Nucl. Phys. B **244**, 322 (1984)
67. H. Jung, Comput. Phys. Commun. **86**, 147 (1995)
68. CDF Collaboration, Phys. Rev. D **50**, 5518 (1994)
69. B. Andersson, G. Gustafson, G. Ingelman, T. Sjöstrand, Phys. Rep. **97**, 31 (1983)
70. S. Navin, Diffraction in pythia. arXiv:1005.3894 [hep-ph]
71. ATLAS Collaboration, Charged particle multiplicities in pp interactions at $\sqrt{s} = 0.9$ and 7 TeV in a diffractive limited phase space measured with the ATLAS detector at the LHC and a new PYTHIA6 tune. ATLAS-CONF-2010-031 (2010)
72. ATLAS Collaboration, ATLAS tunes of PYTHIA 6 and PYTHIA 8 for MC11. ATL-PHYS-PUB-2011-009 (2009)
73. A. Capella, U. Sukhatme, C. Tan, J. Tran Thanh Van, Phys. Rep. **236**, 225 (1994)
74. V. Abramovsky, V. Gribov, O. Kancheli, Yad. Fiz. **18**, 595 (1973). [Sov. J. Nucl. Phys. **18**, 308 (1974)]
75. A. Capella, A. Kaidalov, C. Merino, J. Tran Thanh Van, Phys. Lett. B **343**, 403 (1995). arXiv:hep-ph/9407372
76. A. Capella et al., Phys. Rev. D **53**, 2309 (1996). arXiv:hep-ph/9506454
77. M. Bähr et al., Eur. Phys. J. C **58**, 639 (2008). arXiv:0803.0883 [hep-ph]
78. S. Gieseke, C.A. Röhr, A. Siódmok, Multiple partonic interaction developments in Herwig++. arXiv:1110.2675 [hep-ph]
79. HERWIG++ Collaboration, Minimum bias and underlying event tunes. URL: http://projects.hepforge.org/herwig/trac/wiki/MB_UE_tunes
80. A. Donnachie, P. Landshoff, Phys. Lett. B **595**, 393 (2004). arXiv:hep-ph/0402081
81. S. Gieseke et al., Herwig++ 2.5 release note. arXiv:1102.1672 [hep-ph]
82. ATLAS Collaboration, Eur. Phys. J. C **70**, 823 (2010). arXiv:1005.4568 [physics.ins-det]
83. GEANT4 Collaboration, Nucl. Instrum. Methods A **506**, 250 (2003)
84. G. D'Agostini, Nucl. Instrum. Methods A **362**, 487 (1995)
85. A. Höcker, V. Kartvelishvili, Nucl. Instrum. Methods A **372**, 469 (1996). arXiv:hep-ph/9509307
86. A. Kiryunic, P. Strizenec, In: *Proceedings of the 13th ICATPP Conference*, Como, Italy, 2011
87. V.A. Khoze et al., Eur. Phys. J. C **69**, 85 (2010). arXiv:1005.4839 [hep-ph]
88. A. Martin, M. Ryskin, V. Khoze, From hard to soft high-energy pp interactions. arXiv:1110.1973 [hep-ph]
89. M. Ryskin, private communication
90. The Durham HepData reaction database. URL: http://durpdg.dur.ac.uk/
91. B. Waugh et al., HZTool and rivet: toolkit and framework for the comparison of simulated final states and data at colliders. arXiv:hep-ph/0605034

The ATLAS Collaboration

G. Aad[48], B. Abbott[111], J. Abdallah[11], A.A. Abdelalim[49], A. Abdesselam[118], O. Abdinov[10], B. Abi[112], M. Abolins[88], O.S. AbouZeid[158], H. Abramowicz[153], H. Abreu[115], E. Acerbi[89a,89b], B.S. Acharya[164a,164b], L. Adamczyk[37], D.L. Adams[24], T.N. Addy[56], J. Adelman[175], M. Aderholz[99], S. Adomeit[98], P. Adragna[75], T. Adye[129], S. Aefsky[22], J.A. Aguilar-Saavedra[124b,a], M. Aharrouche[81], S.P. Ahlen[21], F. Ahles[48], A. Ahmad[148], M. Ahsan[40], G. Aielli[133a,133b], T. Akdogan[18a], T.P.A. Åkesson[79], G. Akimoto[155], A.V. Akimov[94], A. Akiyama[67], M.S. Alam[1], M.A. Alam[76], J. Albert[169], S. Albrand[55], M. Aleksa[29], I.N. Aleksandrov[65], F. Alessandria[89a], C. Alexa[25a], G. Alexander[153], G. Alexandre[49], T. Alexopoulos[9], M. Alhroob[20], M. Aliev[15], G. Alimonti[89a], J. Alison[120], M. Aliyev[10], P.P. Allport[73], S.E. Allwood-Spiers[53], J. Almond[82], A. Aloisio[102a,102b], R. Alon[171], A. Alonso[79], B. Alvarez Gonzalez[88], M.G. Alviggi[102a,102b], K. Amako[66], P. Amaral[29], C. Amelung[22], V.V. Ammosov[128], A. Amorim[124a,b], G. Amorós[167], N. Amram[153], C. Anastopoulos[29], L.S. Ancu[16], N. Andari[115], T. Andeen[34], C.F. Anders[20], G. Anders[58a], K.J. Anderson[30], A. Andreazza[89a,89b], V. Andrei[58a], M-L. Andrieux[55], X.S. Anduaga[70], A. Angerami[34], F. Anghinolfi[29], A. Anisenkov[107], N. Anjos[124a], A. Annovi[47], A. Antonaki[8], M. Antonelli[47], A. Antonov[96], J. Antos[144b], F. Anulli[132a], S. Aoun[83], L. Aperio Bella[4], R. Apolle[118,c], G. Arabidze[88], I. Aracena[143], Y. Arai[66], A.T.H. Arce[44], J.P. Archambault[28], S. Arfaoui[148], J-F. Arguin[14], E. Arik[18a,*], M. Arik[18a], A.J. Armbruster[87], O. Arnaez[81], C. Arnault[115], A. Artamonov[95], G. Artoni[132a,132b], D. Arutinov[20], S. Asai[155], R. Asfandiyarov[172], S. Ask[27], B. Åsman[146a,146b], L. Asquith[5], K. Assamagan[24], A. Astbury[169], A. Astvatsatourov[52], B. Aubert[4], E. Auge[115], K. Augsten[127], M. Aurousseau[145a], G. Avolio[163], R. Avramidou[9], D. Axen[168], C. Ay[54], G. Azuelos[93,d], Y. Azuma[155], M.A. Baak[29], G. Baccaglioni[89a], C. Bacci[134a,134b], A.M. Bach[14], H. Bachacou[136], K. Bachas[29], G. Bachy[29], M. Backes[49], M. Backhaus[20], E. Badescu[25a], P. Bagnaia[132a,132b], S. Bahinipati[2], Y. Bai[32a], D.C. Bailey[158], T. Bain[158], J.T. Baines[129], O.K. Baker[175], M.D. Baker[24], S. Baker[77], E. Banas[38], P. Banerjee[93], Sw. Banerjee[172], D. Banfi[29], A. Bangert[150], V. Bansal[169], H.S. Bansil[17], L. Barak[171], S.P. Baranov[94], A. Barashkou[65], A. Barbaro

Galtieri[14], T. Barber[48], E.L. Barberio[86], D. Barberis[50a,50b], M. Barbero[20], D.Y. Bardin[65], T. Barillari[99], M. Barisonzi[174], T. Barklow[143], N. Barlow[27], B.M. Barnett[129], R.M. Barnett[14], A. Baroncelli[134a], G. Barone[49], A.J. Barr[118], F. Barreiro[80], J. Barreiro Guimarães da Costa[57], P. Barrillon[115], R. Bartoldus[143], A.E. Barton[71], V. Bartsch[149], R.L. Bates[53], L. Batkova[144a], J.R. Batley[27], A. Battaglia[16], M. Battistin[29], F. Bauer[136], H.S. Bawa[143,e], S. Beale[98], B. Beare[158], T. Beau[78], P.H. Beauchemin[161], R. Beccherle[50a], P. Bechtle[20], H.P. Beck[16], S. Becker[98], M. Beckingham[138], K.H. Becks[174], A.J. Beddall[18c], A. Beddall[18c], S. Bedikian[175], V.A. Bednyakov[65], C.P. Bee[83], M. Begel[24], S. Behar Harpaz[152], P.K. Behera[63], M. Beimforde[99], C. Belanger-Champagne[85], P.J. Bell[49], W.H. Bell[49], G. Bella[153], L. Bellagamba[19a], F. Bellina[29], M. Bellomo[29], A. Belloni[57], O. Beloborodova[107,f], K. Belotskiy[96], O. Beltramello[29], S. Ben Ami[152], O. Benary[153], D. Benchekroun[135a], C. Benchouk[83], M. Bendel[81], N. Benekos[165], Y. Benhammou[153], E. Benhar Noccioli[49], J.A. Benitez Garcia[159b], D.P. Benjamin[44], M. Benoit[115], J.R. Bensinger[22], K. Benslama[130], S. Bentvelsen[105], D. Berge[29], E. Bergeaas Kuutmann[41], N. Berger[4], F. Berghaus[169], E. Berglund[105], J. Beringer[14], P. Bernat[77], R. Bernhard[48], C. Bernius[24], T. Berry[76], C. Bertella[83], A. Bertin[19a,19b], F. Bertinelli[29], F. Bertolucci[122a,122b], M.I. Besana[89a,89b], N. Besson[136], S. Bethke[99], W. Bhimji[45], R.M. Bianchi[29], M. Bianco[72a,72b], O. Biebel[98], S.P. Bieniek[77], K. Bierwagen[54], J. Biesiada[14], M. Biglietti[134a], H. Bilokon[47], M. Bindi[19a,19b], S. Binet[115], A. Bingul[18c], C. Bini[132a,132b], C. Biscarat[177], U. Bitenc[48], K.M. Black[21], R.E. Blair[5], J.-B. Blanchard[136], G. Blanchot[29], T. Blazek[144a], C. Blocker[22], J. Blocki[38], A. Blondel[49], W. Blum[81], U. Blumenschein[54], G.J. Bobbink[105], V.B. Bobrovnikov[107], S.S. Bocchetta[79], A. Bocci[44], C.R. Boddy[118], M. Boehler[41], J. Boek[174], N. Boelaert[35], S. Böser[77], J.A. Bogaerts[29], A. Bogdanchikov[107], A. Bogouch[90,*], C. Bohm[146a], V. Boisvert[76], T. Bold[37], V. Boldea[25a], N.M. Bolnet[136], M. Bona[75], V.G. Bondarenko[96], M. Bondioli[163], M. Boonekamp[136], G. Boorman[76], C.N. Booth[139], S. Bordoni[78], C. Borer[16], A. Borisov[128], G. Borissov[71], I. Borjanovic[12a], M. Borri[82], S. Borroni[87], K. Bos[105], D. Boscherini[19a], M. Bosman[11], H. Boterenbrood[105], D. Botterill[129], J. Bouchami[93], J. Boudreau[123], E.V. Bouhova-Thacker[71], D. Boumediene[33], C. Bourdarios[115], N. Bousson[83], A. Boveia[30], J. Boyd[29], I.R. Boyko[65], N.I. Bozhko[128], I. Bozovic-Jelisavcic[12b], J. Bracinik[17], A. Braem[29], P. Branchini[134a], G.W. Brandenburg[57], A. Brandt[7], G. Brandt[118], O. Brandt[54], U. Bratzler[156], B. Brau[84], J.E. Brau[114], H.M. Braun[174], B. Brelier[158], J. Bremer[29], R. Brenner[166], S. Bressler[171], D. Breton[115], D. Britton[53], F.M. Brochu[27], I. Brock[20], R. Brock[88], T.J. Brodbeck[71], E. Brodet[153], F. Broggi[89a], C. Bromberg[88], J. Bronner[99], G. Brooijmans[34], W.K. Brooks[31b], G. Brown[82], H. Brown[7], P.A. Bruckman de Renstrom[38], D. Bruncko[144b], R. Bruneliere[48], S. Brunet[61], A. Bruni[19a], G. Bruni[19a], M. Bruschi[19a], T. Buanes[13], Q. Buat[55], F. Bucci[49], J. Buchanan[118], N.J. Buchanan[2], P. Buchholz[141], R.M. Buckingham[118], A.G. Buckley[45], S.I. Buda[25a], I.A. Budagov[65], B. Budick[108], V. Büscher[81], L. Bugge[117], O. Bulekov[96], M. Bunse[42], T. Buran[117], H. Burckhart[29], S. Burdin[73], T. Burgess[13], S. Burke[129], E. Busato[33], P. Bussey[53], C.P. Buszello[166], F. Butin[29], B. Butler[143], J.M. Butler[21], C.M. Buttar[53], J.M. Butterworth[77], W. Buttinger[27], S. Cabrera Urbán[167], D. Caforio[19a,19b], O. Cakir[3a], P. Calafiura[14], G. Calderini[78], P. Calfayan[98], R. Calkins[106], L.P. Caloba[23a], R. Caloi[132a,132b], D. Calvet[33], S. Calvet[33], R. Camacho Toro[33], P. Camarri[133a,133b], M. Cambiaghi[119a,119b], D. Cameron[117], L.M. Caminada[14], S. Campana[29], M. Campanelli[77], V. Canale[102a,102b], F. Canelli[30,g], A. Canepa[159a], J. Cantero[80], L. Capasso[102a,102b], M.D.M. Capeans Garrido[29], I. Caprini[25a], M. Caprini[25a], D. Capriotti[99], M. Capua[36a,36b], R. Caputo[81], C. Caramarcu[24], R. Cardarelli[133a], T. Carli[29], G. Carlino[102a], L. Carminati[89a,89b], B. Caron[85], S. Caron[104], G.D. Carrillo Montoya[172], A.A. Carter[75], J.R. Carter[27], J. Carvalho[124a,h], D. Casadei[108], M.P. Casado[11], M. Cascella[122a,122b], C. Caso[50a,50b,*], A.M. Castaneda Hernandez[172], E. Castaneda-Miranda[172], V. Castillo Gimenez[167], N.F. Castro[124a], G. Cataldi[72a], F. Cataneo[29], A. Catinaccio[29], J.R. Catmore[71], A. Cattai[29], G. Cattani[133a,133b], S. Caughron[88], D. Cauz[164a,164c], P. Cavalleri[78], D. Cavalli[89a], M. Cavalli-Sforza[11], V. Cavasinni[122a,122b], F. Ceradini[134a,134b], A.S. Cerqueira[23b], A. Cerri[29], L. Cerrito[75], F. Cerutti[47], S.A. Cetin[18b], F. Cevenini[102a,102b], A. Chafaq[135a], D. Chakraborty[106], K. Chan[2], B. Chapleau[85], J.D. Chapman[27], J.W. Chapman[87], E. Chareyre[78], D.G. Charlton[17], V. Chavda[82], C.A. Chavez Barajas[29], S. Cheatham[85], S. Chekanov[5], S.V. Chekulaev[159a], G.A. Chelkov[65], M.A. Chelstowska[104], C. Chen[64], H. Chen[24], S. Chen[32c], T. Chen[32c], X. Chen[172], S. Cheng[32a], A. Cheplakov[65], V.F. Chepurnov[65], R. Cherkaoui El Moursli[135e], V. Chernyatin[24], E. Cheu[6], S.L. Cheung[158], L. Chevalier[136], G. Chiefari[102a,102b], L. Chikovani[51a], J.T. Childers[29], A. Chilingarov[71], G. Chiodini[72a], M.V. Chizhov[65], G. Choudalakis[30], S. Chouridou[137], I.A. Christidi[77], A. Christov[48], D. Chromek-Burckhart[29], M.L. Chu[151], J. Chudoba[125], G. Ciapetti[132a,132b], K. Ciba[37], A.K. Ciftci[3a], R. Ciftci[3a], D. Cinca[33], V. Cindro[74], M.D. Ciobotaru[163], C. Ciocca[19a], A. Ciocio[14], M. Cirilli[87], M. Citterio[89a], M. Ciubancan[25a], A. Clark[49], P.J. Clark[45], W. Cleland[123], J.C. Clemens[83], B. Clement[55], C. Clement[146a,146b], R.W. Clifft[129], Y. Coadou[83], M. Cobal[164a,164c], A. Coccaro[172], J. Cochran[64], P. Coe[118], J.G. Cogan[143], J. Coggeshall[165], E. Cogneras[177], J. Colas[4], A.P. Colijn[105], N.J. Collins[17], C. Collins-Tooth[53], J. Collot[55], G. Colon[84], P. Conde Muiño[124a], E. Coniavitis[118], M.C. Conidi[11], M. Consonni[104], V. Consorti[48], S. Constantinescu[25a], C. Conta[119a,119b], F. Conventi[102a,i], J. Cook[29], M. Cooke[14], B.D. Cooper[77], A.M. Cooper-Sarkar[118], K. Copic[14], T. Cornelissen[174], M. Corradi[19a], F. Corriveau[85,j], A. Cortes-Gonzalez[165], G. Cortiana[99], G. Costa[89a], M.J. Costa[167], D. Costanzo[139], T. Costin[30], D. Côté[29], R. Coura Torres[23a], L. Courneyea[169], G. Cowan[76], C. Cowden[27], B.E. Cox[82], K. Cranmer[108], F. Crescioli[122a,122b],

M. Cristinziani[20], G. Crosetti[36a,36b], R. Crupi[72a,72b], S. Crépé-Renaudin[55], C.-M. Cuciuc[25a], C. Cuenca Almenar[175], T. Cuhadar Donszelmann[139], M. Curatolo[47], C.J. Curtis[17], C. Cuthbert[150], P. Cwetanski[61], H. Czirr[141], P. Czodrowski[43], Z. Czyczula[175], S. D'Auria[53], M. D'Onofrio[73], A. D'Orazio[132a,132b], P.V.M. Da Silva[23a,b], C. Da Via[82], W. Dabrowski[37], T. Dai[87], C. Dallapiccola[84], M. Dam[35], M. Dameri[50a,50b], D.S. Damiani[137], H.O. Danielsson[29], D. Dannheim[99], V. Dao[49], G. Darbo[50a], G.L. Darlea[25b], C. Daum[105], W. Davey[20], T. Davidek[126], N. Davidson[86], R. Davidson[71], E. Davies[118,c], M. Davies[93], A.R. Davison[77], Y. Davygora[58a], E. Dawe[142], I. Dawson[139], J.W. Dawson[5,*], R.K. Daya-Ishmukhametova[22], K. De[7], R. de Asmundis[102a], S. De Castro[19a,19b], P.E. De Castro Faria Salgado[24], S. De Cecco[78], J. de Graat[98], N. De Groot[104], P. de Jong[105], C. De La Taille[115], H. De la Torre[80], B. De Lotto[164a,164c], L. de Mora[71], L. De Nooij[105], D. De Pedis[132a], A. De Salvo[132a], U. De Sanctis[164a,164c], A. De Santo[149], J.B. De Vivie De Regie[115], S. Dean[77], W.J. Dearnaley[71], R. Debbe[24], C. Debenedetti[45], D.V. Dedovich[65], J. Degenhardt[120], M. Dehchar[118], C. Del Papa[164a,164c], J. Del Peso[80], T. Del Prete[122a,122b], T. Delemontex[55], M. Deliyergiyev[74], A. Dell'Acqua[29], L. Dell'Asta[21], M. Della Pietra[102a,i], D. della Volpe[102a,102b], M. Delmastro[4], N. Delruelle[29], P.A. Delsart[55], C. Deluca[148], S. Demers[175], M. Demichev[65], B. Demirkoz[11,k], J. Deng[163], S.P. Denisov[128], D. Derendarz[38], J.E. Derkaoui[135d], F. Derue[78], P. Dervan[73], K. Desch[20], E. Devetak[148], P.O. Deviveiros[105], A. Dewhurst[129], B. DeWilde[148], S. Dhaliwal[158], R. Dhullipudi[24,l], A. Di Ciaccio[133a,133b], L. Di Ciaccio[4], A. Di Girolamo[29], B. Di Girolamo[29], S. Di Luise[134a,134b], A. Di Mattia[172], B. Di Micco[29], R. Di Nardo[47], A. Di Simone[133a,133b], R. Di Sipio[19a,19b], M.A. Diaz[31a], F. Diblen[18c], E.B. Diehl[87], J. Dietrich[41], T.A. Dietzsch[58a], S. Diglio[86], K. Dindar Yagci[39], J. Dingfelder[20], C. Dionisi[132a,132b], P. Dita[25a], S. Dita[25a], F. Dittus[29], F. Djama[83], T. Djobava[51b], M.A.B. do Vale[23c], A. Do Valle Wemans[124a], T.K.O. Doan[4], M. Dobbs[85], R. Dobinson[29,*], D. Dobos[29], E. Dobson[29,m], J. Dodd[34], C. Doglioni[49], T. Doherty[53], Y. Doi[66,*], J. Dolejsi[126], I. Dolenc[74], Z. Dolezal[126], B.A. Dolgoshein[96,*], T. Dohmae[155], M. Donadelli[23d], M. Donega[120], J. Donini[33], J. Dopke[29], A. Doria[102a], A. Dos Anjos[172], M. Dosil[11], A. Dotti[122a,122b], M.T. Dova[70], J.D. Dowell[17], A.D. Doxiadis[105], A.T. Doyle[53], Z. Drasal[126], J. Drees[174], N. Dressnandt[120], H. Drevermann[29], C. Driouichi[35], M. Dris[9], J. Dubbert[99], S. Dube[14], E. Duchovni[171], G. Duckeck[98], A. Dudarev[29], F. Dudziak[64], M. Dührssen[29], I.P. Duerdoth[82], L. Duflot[115], M-A. Dufour[85], M. Dunford[29], H. Duran Yildiz[3b], R. Duxfield[139], M. Dwuznik[37], F. Dydak[29], M. Düren[52], W.L. Ebenstein[44], J. Ebke[98], S. Eckweiler[81], K. Edmonds[81], C.A. Edwards[76], N.C. Edwards[53], W. Ehrenfeld[41], T. Ehrich[99], T. Eifert[143], G. Eigen[13], K. Einsweiler[14], E. Eisenhandler[75], T. Ekelof[166], M. El Kacimi[135c], M. Ellert[166], S. Elles[4], F. Ellinghaus[81], K. Ellis[75], N. Ellis[29], J. Elmsheuser[98], M. Elsing[29], D. Emeliyanov[129], R. Engelmann[148], A. Engl[98], B. Epp[62], A. Eppig[87], J. Erdmann[54], A. Ereditato[16], D. Eriksson[146a], J. Ernst[1], M. Ernst[24], J. Ernwein[136], D. Errede[165], S. Errede[165], E. Ertel[81], M. Escalier[115], C. Escobar[123], X. Espinal Curull[11], B. Esposito[47], F. Etienne[83], A.I. Etienvre[136], E. Etzion[153], D. Evangelakou[54], H. Evans[61], L. Fabbri[19a,19b], C. Fabre[29], R.M. Fakhrutdinov[128], S. Falciano[132a], Y. Fang[172], M. Fanti[89a,89b], A. Farbin[7], A. Farilla[134a], J. Farley[148], T. Farooque[158], S.M. Farrington[118], P. Farthouat[29], P. Fassnacht[29], D. Fassouliotis[8], B. Fatholahzadeh[158], A. Favareto[89a,89b], L. Fayard[115], S. Fazio[36a,36b], R. Febbraro[33], P. Federic[144a], O.L. Fedin[121], W. Fedorko[88], M. Fehling-Kaschek[48], L. Feligioni[83], D. Fellmann[5], C. Feng[32d], E.J. Feng[30], A.B. Fenyuk[128], J. Ferencei[144b], J. Ferland[93], W. Fernando[109], S. Ferrag[53], J. Ferrando[53], V. Ferrara[41], A. Ferrari[166], P. Ferrari[105], R. Ferrari[119a], A. Ferrer[167], M.L. Ferrer[47], D. Ferrere[49], C. Ferretti[87], A. Ferretto Parodi[50a,50b], M. Fiascaris[30], F. Fiedler[81], A. Filipčič[74], A. Filippas[9], F. Filthaut[104], M. Fincke-Keeler[169], M.C.N. Fiolhais[124a,h], L. Fiorini[167], A. Firan[39], G. Fischer[41], P. Fischer[20], M.J. Fisher[109], M. Flechl[48], I. Fleck[141], J. Fleckner[81], P. Fleischmann[173], S. Fleischmann[174], T. Flick[174], L.R. Flores Castillo[172], M.J. Flowerdew[99], M. Fokitis[9], T. Fonseca Martin[16], D.A. Forbush[138], A. Formica[136], A. Forti[82], D. Fortin[159a], J.M. Foster[82], D. Fournier[115], A. Foussat[29], A.J. Fowler[44], K. Fowler[137], H. Fox[71], P. Francavilla[11], S. Franchino[119a,119b], D. Francis[29], T. Frank[171], M. Franklin[57], S. Franz[29], M. Fraternali[119a,119b], S. Fratina[120], S.T. French[27], F. Friedrich[43], R. Froeschl[29], D. Froidevaux[29], J.A. Frost[27], C. Fukunaga[156], E. Fullana Torregrosa[29], J. Fuster[167], C. Gabaldon[29], O. Gabizon[171], T. Gadfort[24], S. Gadomski[49], G. Gagliardi[50a,50b], P. Gagnon[61], C. Galea[98], E.J. Gallas[118], V. Gallo[16], B.J. Gallop[129], P. Gallus[125], K.K. Gan[109], Y.S. Gao[143,e], V.A. Gapienko[128], A. Gaponenko[14], F. Garberson[175], M. Garcia-Sciveres[14], C. García[167], J.E. García Navarro[167], R.W. Gardner[30], N. Garelli[29], H. Garitaonandia[105], V. Garonne[29], J. Garvey[17], C. Gatti[47], G. Gaudio[119a], O. Gaumer[49], B. Gaur[141], L. Gauthier[136], I.L. Gavrilenko[94], C. Gay[168], G. Gaycken[20], J-C. Gayde[29], E.N. Gazis[9], P. Ge[32d], C.N.P. Gee[129], D.A.A. Geerts[105], Ch. Geich-Gimbel[20], K. Gellerstedt[146a,146b], C. Gemme[50a], A. Gemmell[53], M.H. Genest[55], S. Gentile[132a,132b], M. George[54], S. George[76], P. Gerlach[174], A. Gershon[153], C. Geweniger[58a], H. Ghazlane[135b], N. Ghodbane[33], B. Giacobbe[19a], S. Giagu[132a,132b], V. Giakoumopoulou[8], V. Giangiobbe[11], F. Gianotti[29], B. Gibbard[24], A. Gibson[158], S.M. Gibson[29], L.M. Gilbert[118], V. Gilewsky[91], D. Gillberg[28], A.R. Gillman[129], D.M. Gingrich[2,d], J. Ginzburg[153], N. Giokaris[8], M.P. Giordani[164c], R. Giordano[102a,102b], F.M. Giorgi[15], P. Giovannini[99], P.F. Giraud[136], D. Giugni[89a], M. Giunta[93], P. Giusti[19a], B.K. Gjelsten[117], L.K. Gladilin[97], C. Glasman[80], J. Glatzer[48], A. Glazov[41], K.W. Glitza[174], G.L. Glonti[65], J.R. Goddard[75], J. Godfrey[142], J. Godlewski[29], M. Goebel[41], T. Göpfert[43], C. Goeringer[81], C. Gössling[42], T. Göttfert[99], S. Goldfarb[87], T. Golling[175], S.N. Golovnia[128], A. Gomes[124a,b], L.S. Gomez Fajardo[41],

R. Gonçalo[76], J. Goncalves Pinto Firmino Da Costa[41], L. Gonella[20], A. Gonidec[29], S. Gonzalez[172], S. González de la Hoz[167], G. Gonzalez Parra[11], M.L. Gonzalez Silva[26], S. Gonzalez-Sevilla[49], J.J. Goodson[148], L. Goossens[29], P.A. Gorbounov[95], H.A. Gordon[24], I. Gorelov[103], G. Gorfine[174], B. Gorini[29], E. Gorini[72a,72b], A. Gorišek[74], E. Gornicki[38], S.A. Gorokhov[128], V.N. Goryachev[128], B. Gosdzik[41], M. Gosselink[105], M.I. Gostkin[65], I. Gough Eschrich[163], M. Gouighri[135a], D. Goujdami[135c], M.P. Goulette[49], A.G. Goussiou[138], C. Goy[4], S. Gozpinar[22], I. Grabowska-Bold[37], P. Grafström[29], K-J. Grahn[41], F. Grancagnolo[72a], S. Grancagnolo[15], V. Grassi[148], V. Gratchev[121], N. Grau[34], H.M. Gray[29], J.A. Gray[148], E. Graziani[134a], O.G. Grebenyuk[121], T. Greenshaw[73], Z.D. Greenwood[24,n], K. Gregersen[35], I.M. Gregor[41], P. Grenier[143], J. Griffiths[138], N. Grigalashvili[65], A.A. Grillo[137], S. Grinstein[11], Y.V. Grishkevich[97], J.-F. Grivaz[115], M. Groh[99], E. Gross[171], J. Grosse-Knetter[54], J. Groth-Jensen[171], K. Grybel[141], V.J. Guarino[5], D. Guest[175], C. Guicheney[33], A. Guida[72a,72b], S. Guindon[54], H. Guler[85,o], J. Gunther[125], B. Guo[158], J. Guo[34], A. Gupta[30], Y. Gusakov[65], V.N. Gushchin[128], A. Gutierrez[93], P. Gutierrez[111], N. Guttman[153], O. Gutzwiller[172], C. Guyot[136], C. Gwenlan[118], C.B. Gwilliam[73], A. Haas[143], S. Haas[29], C. Haber[14], R. Hackenburg[24], H.K. Hadavand[39], D.R. Hadley[17], P. Haefner[99], F. Hahn[29], S. Haider[29], Z. Hajduk[38], H. Hakobyan[176], D. Hall[118], J. Haller[54], K. Hamacher[174], P. Hamal[113], M. Hamer[54], A. Hamilton[145b], S. Hamilton[161], H. Han[32a], L. Han[32b], K. Hanagaki[116], K. Hanawa[160], M. Hance[14], C. Handel[81], P. Hanke[58a], J.R. Hansen[35], J.B. Hansen[35], J.D. Hansen[35], P.H. Hansen[35], P. Hansson[143], K. Hara[160], G.A. Hare[137], T. Harenberg[174], S. Harkusha[90], D. Harper[87], R.D. Harrington[45], O.M. Harris[138], K. Harrison[17], J. Hartert[48], F. Hartjes[105], T. Haruyama[66], A. Harvey[56], S. Hasegawa[101], Y. Hasegawa[140], S. Hassani[136], M. Hatch[29], D. Hauff[99], S. Haug[16], M. Hauschild[29], R. Hauser[88], M. Havranek[20], B.M. Hawes[118], C.M. Hawkes[17], R.J. Hawkings[29], A.D. Hawkins[79], D. Hawkins[163], T. Hayakawa[67], T. Hayashi[160], D. Hayden[76], H.S. Hayward[73], S.J. Haywood[129], E. Hazen[21], M. He[32d], S.J. Head[17], V. Hedberg[79], L. Heelan[7], S. Heim[88], B. Heinemann[14], S. Heisterkamp[35], L. Helary[4], C. Heller[98], M. Heller[29], S. Hellman[146a,146b], D. Hellmich[20], C. Helsens[11], R.C.W. Henderson[71], M. Henke[58a], A. Henrichs[54], A.M. Henriques Correia[29], S. Henrot-Versille[115], F. Henry-Couannier[83], C. Hensel[54], T. Henß[174], C.M. Hernandez[7], Y. Hernández Jiménez[167], R. Herrberg[15], A.D. Hershenhorn[152], G. Herten[48], R. Hertenberger[98], L. Hervas[29], N.P. Hessey[105], E. Higón-Rodriguez[167], D. Hill[5,*], J.C. Hill[27], N. Hill[5], K.H. Hiller[41], S. Hillert[20], S.J. Hillier[17], I. Hinchliffe[14], E. Hines[120], M. Hirose[116], F. Hirsch[42], D. Hirschbuehl[174], J. Hobbs[148], N. Hod[153], M.C. Hodgkinson[139], P. Hodgson[139], A. Hoecker[29], M.R. Hoeferkamp[103], J. Hoffman[39], D. Hoffmann[83], M. Hohlfeld[81], M. Holder[141], S.O. Holmgren[146a], T. Holy[127], J.L. Holzbauer[88], Y. Homma[67], T.M. Hong[120], L. Hooft van Huysduynen[108], T. Horazdovsky[127], C. Horn[143], S. Horner[48], J-Y. Hostachy[55], S. Hou[151], M.A. Houlden[73], A. Hoummada[135a], J. Howarth[82], D.F. Howell[118], I. Hristova[15], J. Hrivnac[115], I. Hruska[125], T. Hryn'ova[4], P.J. Hsu[81], S.-C. Hsu[14], G.S. Huang[111], Z. Hubacek[127], F. Hubaut[83], F. Huegging[20], A. Huettmann[41], T.B. Huffman[118], E.W. Hughes[34], G. Hughes[71], R.E. Hughes-Jones[82], M. Huhtinen[29], P. Hurst[57], M. Hurwitz[14], U. Husemann[41], N. Huseynov[65,p], J. Huston[88], J. Huth[57], G. Iacobucci[49], G. Iakovidis[9], M. Ibbotson[82], I. Ibragimov[141], R. Ichimiya[67], L. Iconomidou-Fayard[115], J. Idarraga[115], P. Iengo[102a], O. Igonkina[105], Y. Ikegami[66], M. Ikeno[66], Y. Ilchenko[39], D. Iliadis[154], N. Ilic[158], D. Imbault[78], M. Imori[155], T. Ince[20], J. Inigo-Golfin[29], P. Ioannou[8], M. Iodice[134a], V. Ippolito[132a,132b], A. Irles Quiles[167], C. Isaksson[166], A. Ishikawa[67], M. Ishino[68], R. Ishmukhametov[39], C. Issever[118], S. Istin[18a], A.V. Ivashin[128], W. Iwanski[38], H. Iwasaki[66], J.M. Izen[40], V. Izzo[102a], B. Jackson[120], J.N. Jackson[73], P. Jackson[143], M.R. Jaekel[29], V. Jain[61], K. Jakobs[48], S. Jakobsen[35], J. Jakubek[127], D.K. Jana[111], E. Jankowski[158], E. Jansen[77], H. Jansen[29], A. Jantsch[99], M. Janus[20], G. Jarlskog[79], L. Jeanty[57], K. Jelen[37], I. Jen-La Plante[30], P. Jenni[29], A. Jeremie[4], P. Ježˇ[35], S. Jézéquel[4], M.K. Jha[19a], H. Ji[172], W. Ji[81], J. Jia[148], Y. Jiang[32b], M. Jimenez Belenguer[41], G. Jin[32b], S. Jin[32a], O. Jinnouchi[157], M.D. Joergensen[35], D. Joffe[39], L.G. Johansen[13], M. Johansen[146a,146b], K.E. Johansson[146a], P. Johansson[139], S. Johnert[41], K.A. Johns[6], K. Jon-And[146a,146b], G. Jones[82], R.W.L. Jones[71], T.W. Jones[77], T.J. Jones[73], O. Jonsson[29], C. Joram[29], P.M. Jorge[124a], J. Joseph[14], T. Jovin[12b], X. Ju[172], C.A. Jung[42], R.M. Jungst[29], V. Juranek[125], P. Jussel[62], A. Juste Rozas[11], V.V. Kabachenko[128], S. Kabana[16], M. Kaci[167], A. Kaczmarska[38], P. Kadlecik[35], M. Kado[115], H. Kagan[109], M. Kagan[57], S. Kaiser[99], E. Kajomovitz[152], S. Kalinin[174], L.V. Kalinovskaya[65], S. Kama[39], N. Kanaya[155], M. Kaneda[29], S. Kaneti[27], T. Kanno[157], V.A. Kantserov[96], J. Kanzaki[66], B. Kaplan[175], A. Kapliy[30], J. Kaplon[29], D. Kar[43], M. Karagounis[20], M. Karagoz[118], M. Karnevskiy[41], K. Karr[5], V. Kartvelishvili[71], A.N. Karyukhin[128], L. Kashif[172], G. Kasieczka[58b], R.D. Kass[109], A. Kastanas[13], M. Kataoka[4], Y. Kataoka[155], E. Katsoufis[9], J. Katzy[41], V. Kaushik[6], K. Kawagoe[67], T. Kawamoto[155], G. Kawamura[81], M.S. Kayl[105], V.A. Kazanin[107], M.Y. Kazarinov[65], R. Keeler[169], R. Kehoe[39], M. Keil[54], G.D. Kekelidze[65], J. Kennedy[98], C.J. Kenney[143], M. Kenyon[53], O. Kepka[125], N. Kerschen[29], B.P. Kerševan[74], S. Kersten[174], K. Kessoku[155], J. Keung[158], F. Khalil-zada[10], H. Khandanyan[165], A. Khanov[112], D. Kharchenko[65], A. Khodinov[96], A.G. Kholodenko[128], A. Khomich[58a], T.J. Khoo[27], G. Khoriauli[20], A. Khoroshilov[174], N. Khovanskiy[65], V. Khovanskiy[95], E. Khramov[65], J. Khubua[51b], H. Kim[146a,146b], M.S. Kim[2], P.C. Kim[143], S.H. Kim[160], N. Kimura[170], O. Kind[15], B.T. King[73], M. King[67], R.S.B. King[118], J. Kirk[129], L.E. Kirsch[22], A.E. Kiryunin[99], T. Kishimoto[67], D. Kisielewska[37], T. Kittelmann[123], A.M. Kiver[128], E. Kladiva[144b], J. Klaiber-Lodewigs[42], M. Klein[73], U. Klein[73], K. Kleinknecht[81], M. Klemetti[85], A. Klier[171], P. Klimek[146a,146b], A. Klimentov[24], R. Klingenberg[42],

J.A. Klinger[82], E.B. Klinkby[35], T. Klioutchnikova[29], P.F. Klok[104], S. Klous[105], E.-E. Kluge[58a], T. Kluge[73], P. Kluit[105], S. Kluth[99], N.S. Knecht[158], E. Kneringer[62], J. Knobloch[29], E.B.F.G. Knoops[83], A. Knue[54], B.R. Ko[44], T. Kobayashi[155], M. Kobel[43], M. Kocian[143], P. Kodys[126], K. Köneke[29], A.C. König[104], S. Koenig[81], L. Köpke[81], F. Koetsveld[104], P. Koevesarki[20], T. Koffas[28], E. Koffeman[105], L.A. Kogan[118], F. Kohn[54], Z. Kohout[127], T. Kohriki[66], T. Koi[143], T. Kokott[20], G.M. Kolachev[107], H. Kolanoski[15], V. Kolesnikov[65], I. Koletsou[89a], J. Koll[88], D. Kollar[29], M. Kollefrath[48], S.D. Kolya[82], A.A. Komar[94], Y. Komori[155], T. Kondo[66], T. Kono[41,q], A.I. Kononov[48], R. Konoplich[108,r], N. Konstantinidis[77], A. Kootz[174], S. Koperny[37], K. Korcyl[38], K. Kordas[154], V. Koreshev[128], A. Korn[118], A. Korol[107], I. Korolkov[11], E.V. Korolkova[139], V.A. Korotkov[128], O. Kortner[99], S. Kortner[99], V.V. Kostyukhin[20], M.J. Kotamäki[29], S. Kotov[99], V.M. Kotov[65], A. Kotwal[44], C. Kourkoumelis[8], V. Kouskoura[154], A. Koutsman[159a], R. Kowalewski[169], T.Z. Kowalski[37], W. Kozanecki[136], A.S. Kozhin[128], V. Kral[127], V.A. Kramarenko[97], G. Kramberger[74], M.W. Krasny[78], A. Krasznahorkay[108], J. Kraus[88], J.K. Kraus[20], A. Kreisel[153], F. Krejci[127], J. Kretzschmar[73], N. Krieger[54], P. Krieger[158], K. Kroeninger[54], H. Kroha[99], J. Kroll[120], J. Kroseberg[20], J. Krstic[12a], U. Kruchonak[65], H. Krüger[20], T. Kruker[16], N. Krumnack[64], Z.V. Krumshteyn[65], A. Kruth[20], T. Kubota[86], S. Kuehn[48], A. Kugel[58c], T. Kuhl[41], D. Kuhn[62], V. Kukhtin[65], Y. Kulchitsky[90], S. Kuleshov[31b], C. Kummer[98], M. Kuna[78], N. Kundu[118], J. Kunkle[120], A. Kupco[125], H. Kurashige[67], M. Kurata[160], Y.A. Kurochkin[90], V. Kus[125], E.S. Kuwertz[147], M. Kuze[157], J. Kvita[142], R. Kwee[15], A. La Rosa[49], L. La Rotonda[36a,36b], L. Labarga[80], J. Labbe[4], S. Lablak[135a], C. Lacasta[167], F. Lacava[132a,132b], H. Lacker[15], D. Lacour[78], V.R. Lacuesta[167], E. Ladygin[65], R. Lafaye[4], B. Laforge[78], T. Lagouri[80], S. Lai[48], E. Laisne[55], M. Lamanna[29], C.L. Lampen[6], W. Lampl[6], E. Lancon[136], U. Landgraf[48], M.P.J. Landon[75], H. Landsman[152], J.L. Lane[82], C. Lange[41], A.J. Lankford[163], F. Lanni[24], K. Lantzsch[174], S. Laplace[78], C. Lapoire[20], J.F. Laporte[136], T. Lari[89a], A.V. Larionov[128], A. Larner[118], C. Lasseur[29], M. Lassnig[29], P. Laurelli[47], W. Lavrijsen[14], P. Laycock[73], A.B. Lazarev[65], O. Le Dortz[78], E. Le Guirriec[83], C. Le Maner[158], E. Le Menedeu[9], C. Lebel[93], T. LeCompte[5], F. Ledroit-Guillon[55], H. Lee[105], J.S.H. Lee[116], S.C. Lee[151], L. Lee[175], M. Lefebvre[169], M. Legendre[136], A. Leger[49], B.C. LeGeyt[120], F. Legger[98], C. Leggett[14], M. Lehmacher[20], G. Lehmann Miotto[29], X. Lei[6], M.A.L. Leite[23d], R. Leitner[126], D. Lellouch[171], M. Leltchouk[34], B. Lemmer[54], V. Lendermann[58a], K.J.C. Leney[145b], T. Lenz[105], G. Lenzen[174], B. Lenzi[29], K. Leonhardt[43], S. Leontsinis[9], C. Leroy[93], J-R. Lessard[169], J. Lesser[146a], C.G. Lester[27], A. Leung Fook Cheong[172], J. Levêque[4], D. Levin[87], L.J. Levinson[171], M.S. Levitski[128], A. Lewis[118], G.H. Lewis[108], A.M. Leyko[20], M. Leyton[15], B. Li[83], H. Li[172,s], S. Li[32b,t], X. Li[87], Z. Liang[118,u], H. Liao[33], B. Liberti[133a], P. Lichard[29], M. Lichtnecker[98], K. Lie[165], W. Liebig[13], R. Lifshitz[152], J.N. Lilley[17], C. Limbach[20], A. Limosani[86], M. Limper[63], S.C. Lin[151,v], F. Linde[105], J.T. Linnemann[88], E. Lipeles[120], L. Lipinsky[125], A. Lipniacka[13], T.M. Liss[165], D. Lissauer[24], A. Lister[49], A.M. Litke[137], C. Liu[28], D. Liu[151], H. Liu[87], J.B. Liu[87], M. Liu[32b], S. Liu[2], Y. Liu[32b], M. Livan[119a,119b], S.S.A. Livermore[118], A. Lleres[55], J. Llorente Merino[80], S.L. Lloyd[75], E. Lobodzinska[41], P. Loch[6], W.S. Lockman[137], T. Loddenkoetter[20], F.K. Loebinger[82], A. Loginov[175], C.W. Loh[168], T. Lohse[15], K. Lohwasser[48], M. Lokajicek[125], J. Loken[118], V.P. Lombardo[4], R.E. Long[71], L. Lopes[124a,b], D. Lopez Mateos[57], J. Lorenz[98], M. Losada[162], P. Loscutoff[14], F. Lo Sterzo[132a,132b], M.J. Losty[159a], X. Lou[40], A. Lounis[115], K.F. Loureiro[162], J. Love[21], P.A. Love[71], A.J. Lowe[143,e], F. Lu[32a], H.J. Lubatti[138], C. Luci[132a,132b], A. Lucotte[55], A. Ludwig[43], D. Ludwig[41], I. Ludwig[48], J. Ludwig[48], F. Luehring[61], G. Luijckx[105], D. Lumb[48], L. Luminari[132a], E. Lund[117], B. Lund-Jensen[147], B. Lundberg[79], J. Lundberg[146a,146b], J. Lundquist[35], M. Lungwitz[81], G. Lutz[99], D. Lynn[24], J. Lys[14], E. Lytken[79], H. Ma[24], L.L. Ma[172], J.A. Macana Goia[93], G. Maccarrone[47], A. Macchiolo[99], B. Maček[74], J. Machado Miguens[124a], R. Mackeprang[35], R.J. Madaras[14], W.F. Mader[43], R. Maenner[58c], T. Maeno[24], P. Mättig[174], S. Mättig[41], L. Magnoni[29], E. Magradze[54], Y. Mahalalel[153], K. Mahboubi[48], G. Mahout[17], C. Maiani[132a,132b], C. Maidantchik[23a], A. Maio[124a,b], S. Majewski[24], Y. Makida[66], N. Makovec[115], P. Mal[136], B. Malaescu[29], Pa. Malecki[38], P. Malecki[38], V.P. Maleev[121], F. Malek[55], U. Mallik[63], D. Malon[5], C. Malone[143], S. Maltezos[9], V. Malyshev[107], S. Malyukov[29], R. Mameghani[98], J. Mamuzic[12b], A. Manabe[66], L. Mandelli[89a], I. Mandić[74], R. Mandrysch[15], J. Maneira[124a], P.S. Mangeard[88], L. Manhaes de Andrade Filho[23a], I.D. Manjavidze[65], A. Mann[54], P.M. Manning[137], A. Manousakis-Katsikakis[8], B. Mansoulie[136], A. Manz[99], A. Mapelli[29], L. Mapelli[29], L. March[80], J.F. Marchand[28], F. Marchese[133a,133b], G. Marchiori[78], M. Marcisovsky[125], A. Marin[21,*], C.P. Marino[169], F. Marroquim[23a], R. Marshall[82], Z. Marshall[29], F.K. Martens[158], S. Marti-Garcia[167], A.J. Martin[175], B. Martin[29], B. Martin[88], F.F. Martin[120], J.P. Martin[93], Ph. Martin[55], T.A. Martin[17], V.J. Martin[45], B. Martin dit Latour[49], S. Martin-Haugh[149], M. Martinez[11], V. Martinez Outschoorn[57], A.C. Martyniuk[169], M. Marx[82], F. Marzano[132a], A. Marzin[111], L. Masetti[81], T. Mashimo[155], R. Mashinistov[94], J. Masik[82], A.L. Maslennikov[107], I. Massa[19a,19b], G. Massaro[105], N. Massol[4], P. Mastrandrea[132a,132b], A. Mastroberardino[36a,36b], T. Masubuchi[155], M. Mathes[20], P. Matricon[115], H. Matsumoto[155], H. Matsunaga[155], T. Matsushita[67], C. Mattravers[118,c], J.M. Maugain[29], J. Maurer[83], S.J. Maxfield[73], D.A. Maximov[107,f], E.N. May[5], A. Mayne[139], R. Mazini[151], M. Mazur[20], M. Mazzanti[89a], E. Mazzoni[122a,122b], S.P. Mc Kee[87], A. McCarn[165], R.L. McCarthy[148], T.G. McCarthy[28], N.A. McCubbin[129], K.W. McFarlane[56], J.A. Mcfayden[139], H. McGlone[53], G. Mchedlidze[51b], R.A. McLaren[29], T. Mclaughlan[17], S.J. McMahon[129], R.A. McPherson[169,j], A. Meade[84], J. Mechnich[105], M. Mechtel[174], M. Medinnis[41],

R. Meera-Lebbai[111], T. Meguro[116], R. Mehdiyev[93], S. Mehlhase[35], A. Mehta[73], K. Meier[58a], B. Meirose[79], C. Melachrinos[30], B.R. Mellado Garcia[172], L. Mendoza Navas[162], Z. Meng[151,s], A. Mengarelli[19a,19b], S. Menke[99], C. Menot[29], E. Meoni[11], K.M. Mercurio[57], P. Mermod[49], L. Merola[102a,102b], C. Meroni[89a], F.S. Merritt[30], A. Messina[29], J. Metcalfe[103], A.S. Mete[64], C. Meyer[81], C. Meyer[30], J-P. Meyer[136], J. Meyer[173], J. Meyer[54], T.C. Meyer[29], W.T. Meyer[64], J. Miao[32d], S. Michal[29], L. Micu[25a], R.P. Middleton[129], S. Migas[73], L. Mijović[41], G. Mikenberg[171], M. Mikestikova[125], M. Mikuž[74], D.W. Miller[30], R.J. Miller[88], W.J. Mills[168], C. Mills[57], A. Milov[171], D.A. Milstead[146a,146b], D. Milstein[171], A.A. Minaenko[128], M. Miñano Moya[167], I.A. Minashvili[65], A.I. Mincer[108], B. Mindur[37], M. Mineev[65], Y. Ming[172], L.M. Mir[11], G. Mirabelli[132a], L. Miralles Verge[11], A. Misiejuk[76], J. Mitrevski[137], G.Y. Mitrofanov[128], V.A. Mitsou[167], S. Mitsui[66], P.S. Miyagawa[139], K. Miyazaki[67], J.U. Mjörnmark[79], T. Moa[146a,146b], P. Mockett[138], S. Moed[57], V. Moeller[27], K. Mönig[41], N. Möser[20], S. Mohapatra[148], W. Mohr[48], S. Mohrdieck-Möck[99], A.M. Moisseev[128,*], R. Moles-Valls[167], J. Molina-Perez[29], J. Monk[77], E. Monnier[83], S. Montesano[89a,89b], F. Monticelli[70], S. Monzani[19a,19b], R.W. Moore[2], G.F. Moorhead[86], C. Mora Herrera[49], A. Moraes[53], N. Morange[136], J. Morel[54], G. Morello[36a,36b], D. Moreno[81], M. Moreno Llácer[167], P. Morettini[50a], M. Morii[57], J. Morin[75], A.K. Morley[29], G. Mornacchi[29], S.V. Morozov[96], J.D. Morris[75], L. Morvaj[101], H.G. Moser[99], M. Mosidze[51b], J. Moss[109], R. Mount[143], E. Mountricha[9,w], S.V. Mouraviev[94], E.J.W. Moyse[84], M. Mudrinic[12b], F. Mueller[58a], J. Mueller[123], K. Mueller[20], T.A. Müller[98], T. Mueller[81], D. Muenstermann[29], A. Muir[168], Y. Munwes[153], W.J. Murray[129], I. Mussche[105], E. Musto[102a,102b], A.G. Myagkov[128], J. Nadal[11], K. Nagai[160], K. Nagano[66], Y. Nagasaka[60], M. Nagel[99], A.M. Nairz[29], Y. Nakahama[29], K. Nakamura[155], T. Nakamura[155], I. Nakano[110], G. Nanava[20], A. Napier[161], R. Narayan[58b], M. Nash[77,c], N.R. Nation[21], T. Nattermann[20], T. Naumann[41], G. Navarro[162], H.A. Neal[87], E. Nebot[80], P.Yu. Nechaeva[94], T.J. Neep[82], A. Negri[119a,119b], G. Negri[29], S. Nektarijevic[49], A. Nelson[163], S. Nelson[143], T.K. Nelson[143], S. Nemecek[125], P. Nemethy[108], A.A. Nepomuceno[23a], M. Nessi[29,x], M.S. Neubauer[165], A. Neusiedl[81], R.M. Neves[108], P. Nevski[24], P.R. Newman[17], V. Nguyen Thi Hong[136], R.B. Nickerson[118], R. Nicolaidou[136], L. Nicolas[139], B. Nicquevert[29], F. Niedercorn[115], J. Nielsen[137], T. Niinikoski[29], N. Nikiforou[34], A. Nikiforov[15], V. Nikolaenko[128], K. Nikolaev[65], I. Nikolic-Audit[78], K. Nikolics[49], K. Nikolopoulos[24], H. Nilsen[48], P. Nilsson[7], Y. Ninomiya[155], A. Nisati[132a], T. Nishiyama[67], R. Nisius[99], L. Nodulman[5], M. Nomachi[116], I. Nomidis[154], M. Nordberg[29], B. Nordkvist[146a,146b], P.R. Norton[129], J. Novakova[126], M. Nozaki[66], L. Nozka[113], I.M. Nugent[159a], A.-E. Nuncio-Quiroz[20], G. Nunes Hanninger[86], T. Nunnemann[98], E. Nurse[77], T. Nyman[29], B.J. O'Brien[45], S.W. O'Neale[17,*], D.C. O'Neil[142], V. O'Shea[53], L.B. Oakes[98], F.G. Oakham[28,d], H. Oberlack[99], J. Ocariz[78], A. Ochi[67], S. Oda[155], S. Odaka[66], J. Odier[83], H. Ogren[61], A. Oh[82], S.H. Oh[44], C.C. Ohm[146a,146b], T. Ohshima[101], H. Ohshita[140], T. Ohsugi[59], S. Okada[67], H. Okawa[163], Y. Okumura[101], T. Okuyama[155], A. Olariu[25a], M. Olcese[50a], A.G. Olchevski[65], M. Oliveira[124a,h], D. Oliveira Damazio[24], E. Oliver Garcia[167], D. Olivito[120], A. Olszewski[38], J. Olszowska[38], C. Omachi[67], A. Onofre[124a,y], P.U.E. Onyisi[30], C.J. Oram[159a], M.J. Oreglia[30], Y. Oren[153], D. Orestano[134a,134b], I. Orlov[107], C. Oropeza Barrera[53], R.S. Orr[158], B. Osculati[50a,50b], R. Ospanov[120], C. Osuna[11], G. Otero y Garzon[26], J.P. Ottersbach[105], M. Ouchrif[135d], E.A. Ouellette[169], F. Ould-Saada[117], A. Ouraou[136], Q. Ouyang[32a], A. Ovcharova[14], M. Owen[82], S. Owen[139], V.E. Ozcan[18a], N. Ozturk[7], A. Pacheco Pages[11], C. Padilla Aranda[11], S. Pagan Griso[14], E. Paganis[139], F. Paige[24], P. Pais[84], K. Pajchel[117], G. Palacino[159b], C.P. Paleari[6], S. Palestini[29], D. Pallin[33], A. Palma[124a], J.D. Palmer[17], Y.B. Pan[172], E. Panagiotopoulou[9], B. Panes[31a], N. Panikashvili[87], S. Panitkin[24], D. Pantea[25a], M. Panuskova[125], V. Paolone[123], A. Papadelis[146a], Th.D. Papadopoulou[9], A. Paramonov[5], W. Park[24,z], M.A. Parker[27], F. Parodi[50a,50b], J.A. Parsons[34], U. Parzefall[48], E. Pasqualucci[132a], S. Passaggio[50a], A. Passeri[134a], F. Pastore[134a,134b], Fr. Pastore[76], G. Pásztor[49,aa], S. Pataraia[174], N. Patel[150], J.R. Pater[82], S. Patricelli[102a,102b], T. Pauly[29], M. Pecsy[144a], M.I. Pedraza Morales[172], S.V. Peleganchuk[107], H. Peng[32b], R. Pengo[29], A. Penson[34], J. Penwell[61], M. Perantoni[23a], K. Perez[34,ab], T. Perez Cavalcanti[41], E. Perez Codina[11], M.T. Pérez García-Estañ[167], V. Perez Reale[34], L. Perini[89a,89b], H. Pernegger[29], R. Perrino[72a], P. Perrodo[4], S. Persembe[3a], A. Perus[115], V.D. Peshekhonov[65], K. Peters[29], B.A. Petersen[29], J. Petersen[29], T.C. Petersen[35], E. Petit[4], A. Petridis[154], C. Petridou[154], E. Petrolo[132a], F. Petrucci[134a,134b], D. Petschull[41], M. Petteni[142], R. Pezoa[31b], A. Phan[86], P.W. Phillips[129], G. Piacquadio[29], E. Piccaro[75], M. Piccinini[19a,19b], S.M. Piec[41], R. Piegaia[26], D.T. Pignotti[109], J.E. Pilcher[30], A.D. Pilkington[82], J. Pina[124a,b], M. Pinamonti[164a,164c], A. Pinder[118], J.L. Pinfold[2], J. Ping[32c], B. Pinto[124a,b], O. Pirotte[29], C. Pizio[89a,89b], R. Placakyte[41], M. Plamondon[169], M.-A. Pleier[24], A.V. Pleskach[128], A. Poblaguev[24], S. Poddar[58a], F. Podlyski[33], L. Poggioli[115], T. Poghosyan[20], M. Pohl[49], F. Polci[55], G. Polesello[119a], A. Policicchio[36a,36b], A. Polini[19a], J. Poll[75], V. Polychronakos[24], D.M. Pomarede[136], D. Pomeroy[22], K. Pommès[29], L. Pontecorvo[132a], B.G. Pope[88], G.A. Popeneciu[25a], D.S. Popovic[12a], A. Poppleton[29], X. Portell Bueso[29], C. Posch[21], G.E. Pospelov[99], S. Pospisil[127], I.N. Potrap[99], C.J. Potter[149], C.T. Potter[114], G. Poulard[29], J. Poveda[172], R. Prabhu[77], P. Pralavorio[83], A. Pranko[14], S. Prasad[57], R. Pravahan[7], S. Prell[64], K. Pretzl[16], L. Pribyl[29], D. Price[61], J. Price[73], L.E. Price[5], M.J. Price[29], D. Prieur[123], M. Primavera[72a], K. Prokofiev[108], F. Prokoshin[31b], S. Protopopescu[24], J. Proudfoot[5], X. Prudent[43], M. Przybycien[37], H. Przysiezniak[4], S. Psoroulas[20], E. Ptacek[114], E. Pueschel[84], J. Purdham[87], M. Purohit[24,z], P. Puzo[115], Y. Pylypchenko[63], J. Qian[87], Z. Qian[83], Z. Qin[41], A. Quadt[54], D.R. Quarrie[14], W.B. Quayle[172], F. Quinonez[31a], M. Raas[104],

V. Radescu[58b], B. Radics[20], P. Radloff[114], T. Rador[18a], F. Ragusa[89a,89b], G. Rahal[177], A.M. Rahimi[109], D. Rahm[24], S. Rajagopalan[24], M. Rammensee[48], M. Rammes[141], A.S. Randle-Conde[39], K. Randrianarivony[28], P.N. Ratoff[71], F. Rauscher[98], M. Raymond[29], A.L. Read[117], D.M. Rebuzzi[119a,119b], A. Redelbach[173], G. Redlinger[24], R. Reece[120], K. Reeves[40], A. Reichold[105], E. Reinherz-Aronis[153], A. Reinsch[114], I. Reisinger[42], D. Reljic[12a], C. Rembser[29], Z.L. Ren[151], A. Renaud[115], P. Renkel[39], M. Rescigno[132a], S. Resconi[89a], B. Resende[136], P. Reznicek[98], R. Rezvani[158], A. Richards[77], R. Richter[99], E. Richter-Was[4,ac], M. Ridel[78], M. Rijpstra[105], M. Rijssenbeek[148], A. Rimoldi[119a,119b], L. Rinaldi[19a], R.R. Rios[39], I. Riu[11], G. Rivoltella[89a,89b], F. Rizatdinova[112], E. Rizvi[75], S.H. Robertson[85,j], A. Robichaud-Veronneau[118], D. Robinson[27], J.E.M. Robinson[77], M. Robinson[114], A. Robson[53], J.G. Rocha de Lima[106], C. Roda[122a,122b], D. Roda Dos Santos[29], D. Rodriguez[162], A. Roe[54], S. Roe[29], O. Røhne[117], V. Rojo[1], S. Rolli[161], A. Romaniouk[96], M. Romano[19a,19b], V.M. Romanov[65], G. Romeo[26], E. Romero Adam[167], L. Roos[78], E. Ros[167], S. Rosati[132a], K. Rosbach[49], A. Rose[149], M. Rose[76], G.A. Rosenbaum[158], E.I. Rosenberg[64], P.L. Rosendahl[13], O. Rosenthal[141], L. Rosselet[49], V. Rossetti[11], E. Rossi[132a,132b], L.P. Rossi[50a], M. Rotaru[25a], I. Roth[171], J. Rothberg[138], D. Rousseau[115], C.R. Royon[136], A. Rozanov[83], Y. Rozen[152], X. Ruan[115,ad], I. Rubinskiy[41], B. Ruckert[98], N. Ruckstuhl[105], V.I. Rud[97], C. Rudolph[43], G. Rudolph[62], F. Rühr[6], F. Ruggieri[134a,134b], A. Ruiz-Martinez[64], V. Rumiantsev[91,*], L. Rumyantsev[65], K. Runge[48], Z. Rurikova[48], N.A. Rusakovich[65], D.R. Rust[61], J.P. Rutherfoord[6], C. Ruwiedel[14], P. Ruzicka[125], Y.F. Ryabov[121], V. Ryadovikov[128], P. Ryan[88], M. Rybar[126], G. Rybkin[115], N.C. Ryder[118], S. Rzaeva[10], A.F. Saavedra[150], I. Sadeh[153], H.F-W. Sadrozinski[137], R. Sadykov[65], F. Safai Tehrani[132a], H. Sakamoto[155], G. Salamanna[75], A. Salamon[133a], M. Saleem[111], D. Salihagic[99], A. Salnikov[143], J. Salt[167], B.M. Salvachua Ferrando[5], D. Salvatore[36a,36b], F. Salvatore[149], A. Salvucci[104], A. Salzburger[29], D. Sampsonidis[154], B.H. Samset[117], A. Sanchez[102a,102b], H. Sandaker[13], H.G. Sander[81], M.P. Sanders[98], M. Sandhoff[174], T. Sandoval[27], C. Sandoval[162], R. Sandstroem[99], S. Sandvoss[174], D.P.C. Sankey[129], A. Sansoni[47], C. Santamarina Rios[85], C. Santoni[33], R. Santonico[133a,133b], H. Santos[124a], J.G. Saraiva[124a], T. Sarangi[172], E. Sarkisyan-Grinbaum[7], F. Sarri[122a,122b], G. Sartisohn[174], O. Sasaki[66], T. Sasaki[66], N. Sasao[68], I. Satsounkevitch[90], G. Sauvage[4], E. Sauvan[4], J.B. Sauvan[115], P. Savard[158,d], V. Savinov[123], D.O. Savu[29], L. Sawyer[24,l], D.H. Saxon[53], L.P. Says[33], C. Sbarra[19a], A. Sbrizzi[19a,19b], O. Scallon[93], D.A. Scannicchio[163], M. Scarcella[150], J. Schaarschmidt[115], P. Schacht[99], U. Schäfer[81], S. Schaepe[20], S. Schaetzel[58b], A.C. Schaffer[115], D. Schaile[98], R.D. Schamberger[148], A.G. Schamov[107], V. Scharf[58a], V.A. Schegelsky[121], D. Scheirich[87], M. Schernau[163], M.I. Scherzer[34], C. Schiavi[50a,50b], J. Schieck[98], M. Schioppa[36a,36b], S. Schlenker[29], J.L. Schlereth[5], E. Schmidt[48], K. Schmieden[20], C. Schmitt[81], S. Schmitt[58b], M. Schmitz[20], A. Schöning[58b], M. Schott[29], D. Schouten[159a], J. Schovancova[125], M. Schram[85], C. Schroeder[81], N. Schroer[58c], S. Schuh[29], G. Schuler[29], J. Schultes[174], H.-C. Schultz-Coulon[58a], H. Schulz[15], J.W. Schumacher[20], M. Schumacher[48], B.A. Schumm[137], Ph. Schune[136], A. Schwartzman[143], Ph. Schwemling[78], R. Schwienhorst[88], R. Schwierz[43], J. Schwindling[136], T. Schwindt[20], M. Schwoerer[4], W.G. Scott[129], J. Searcy[114], G. Sedov[41], E. Sedykh[121], E. Segura[11], S.C. Seidel[103], A. Seiden[137], F. Seifert[43], J.M. Seixas[23a], G. Sekhniaidze[102a], K.E. Selbach[45], D.M. Seliverstov[121], B. Sellden[146a], G. Sellers[73], M. Seman[144b], N. Semprini-Cesari[19a,19b], C. Serfon[98], L. Serin[115], R. Seuster[99], H. Severini[111], M.E. Sevior[86], A. Sfyrla[29], E. Shabalina[54], M. Shamim[114], L.Y. Shan[32a], J.T. Shank[21], Q.T. Shao[86], M. Shapiro[14], P.B. Shatalov[95], L. Shaver[6], K. Shaw[164a,164c], D. Sherman[175], P. Sherwood[77], A. Shibata[108], H. Shichi[101], S. Shimizu[29], M. Shimojima[100], T. Shin[56], M. Shiyakova[65], A. Shmeleva[94], M.J. Shochet[30], D. Short[118], S. Shrestha[64], M.A. Shupe[6], P. Sicho[125], A. Sidoti[132a], F. Siegert[48], Dj. Sijacki[12a], O. Silbert[171], J. Silva[124a], Y. Silver[153], D. Silverstein[143], S.B. Silverstein[146a], V. Simak[127], O. Simard[136], Lj. Simic[12a], S. Simion[115], B. Simmons[77], M. Simonyan[35], P. Sinervo[158], N.B. Sinev[114], V. Sipica[141], G. Siragusa[173], A. Sircar[24], A.N. Sisakyan[65], S.Yu. Sivoklokov[97], J. Sjölin[146a,146b], T.B. Sjursen[13], L.A. Skinnari[14], H.P. Skottowe[57], K. Skovpen[107], P. Skubic[111], N. Skvorodnev[22], M. Slater[17], T. Slavicek[127], K. Sliwa[161], J. Sloper[29], V. Smakhtin[171], S.Yu. Smirnov[96], L.N. Smirnova[97], O. Smirnova[79], B.C. Smith[57], D. Smith[143], K.M. Smith[53], M. Smizanska[71], K. Smolek[127], A.A. Snesarev[94], S.W. Snow[82], J. Snow[111], J. Snuverink[105], S. Snyder[24], M. Soares[124a], R. Sobie[169,j], J. Sodomka[127], A. Soffer[153], C.A. Solans[167], M. Solar[127], J. Solc[127], E. Soldatov[96], U. Soldevila[167], E. Solfaroli Camillocci[132a,132b], A.A. Solodkov[128], O.V. Solovyanov[128], N. Soni[2], V. Sopko[127], B. Sopko[127], M. Sosebee[7], R. Soualah[164a,164c], A. Soukharev[107], S. Spagnolo[72a,72b], F. Spanò[76], R. Spighi[19a], G. Spigo[29], F. Spila[132a,132b], R. Spiwoks[29], M. Spousta[126], T. Spreitzer[158], B. Spurlock[7], R.D. St. Denis[53], T. Stahl[141], J. Stahlman[120], R. Stamen[58a], E. Stanecka[38], R.W. Stanek[5], C. Stanescu[134a], S. Stapnes[117], E.A. Starchenko[128], J. Stark[55], P. Staroba[125], P. Starovoitov[91], A. Staude[98], P. Stavina[144a], G. Stavropoulos[14], G. Steele[53], P. Steinbach[43], P. Steinberg[24], I. Stekl[127], B. Stelzer[142], H.J. Stelzer[88], O. Stelzer-Chilton[159a], H. Stenzel[52], S. Stern[99], K. Stevenson[75], G.A. Stewart[29], J.A. Stillings[20], M.C. Stockton[85], K. Stoerig[48], G. Stoicea[25a], S. Stonjek[99], P. Strachota[126], A.R. Stradling[7], A. Straessner[43], J. Strandberg[147], S. Strandberg[146a,146b], A. Strandlie[117], M. Strang[109], E. Strauss[143], M. Strauss[111], P. Strizenec[144b], R. Ströhmer[173], D.M. Strom[114], J.A. Strong[76,*], R. Stroynowski[39], J. Strube[129], B. Stugu[13], I. Stumer[24,*], J. Stupak[148], P. Sturm[174], N.A. Styles[41], D.A. Soh[151,u], D. Su[143], HS. Subramania[2], A. Succurro[11], Y. Sugaya[116], T. Sugimoto[101], C. Suhr[106], K. Suita[67], M. Suk[126], V.V. Sulin[94], S. Sultansoy[3d], T. Sumida[68], X. Sun[55], J.E. Sundermann[48],

K. Suruliz[139], S. Sushkov[11], G. Susinno[36a,36b], M.R. Sutton[149], Y. Suzuki[66], Y. Suzuki[67], M. Svatos[125], Yu.M. Sviridov[128], S. Swedish[168], I. Sykora[144a], T. Sykora[126], B. Szeless[29], J. Sánchez[167], D. Ta[105], K. Tackmann[41], A. Taffard[163], R. Tafirout[159a], N. Taiblum[153], Y. Takahashi[101], H. Takai[24], R. Takashima[69], H. Takeda[67], T. Takeshita[140], Y. Takubo[66], M. Talby[83], A. Talyshev[107,f], M.C. Tamsett[24], J. Tanaka[155], R. Tanaka[115], S. Tanaka[131], S. Tanaka[66], Y. Tanaka[100], A.J. Tanasijczuk[142], K. Tani[67], N. Tannoury[83], G.P. Tappern[29], S. Tapprogge[81], D. Tardif[158], S. Tarem[152], F. Tarrade[28], G.F. Tartarelli[89a], P. Tas[126], M. Tasevsky[125], E. Tassi[36a,36b], M. Tatarkhanov[14], Y. Tayalati[135d], C. Taylor[77], F.E. Taylor[92], G.N. Taylor[86], W. Taylor[159b], M. Teinturier[115], M. Teixeira Dias Castanheira[75], P. Teixeira-Dias[76], K.K. Temming[48], H. Ten Kate[29], P.K. Teng[151], S. Terada[66], K. Terashi[155], J. Terron[80], M. Testa[47], R.J. Teuscher[158,j], J. Thadome[174], J. Therhaag[20], T. Theveneaux-Pelzer[78], M. Thioye[175], S. Thoma[48], J.P. Thomas[17], E.N. Thompson[34], P.D. Thompson[17], P.D. Thompson[158], A.S. Thompson[53], E. Thomson[120], M. Thomson[27], R.P. Thun[87], F. Tian[34], M.J. Tibbetts[14], T. Tic[125], V.O. Tikhomirov[94], Y.A. Tikhonov[107,f], S. Timoshenko[96], P. Tipton[175], F.J. Tique Aires Viegas[29], S. Tisserant[83], B. Toczek[37], T. Todorov[4], S. Todorova-Nova[161], B. Toggerson[163], J. Tojo[66], S. Tokár[144a], K. Tokunaga[67], K. Tokushuku[66], K. Tollefson[88], M. Tomoto[101], L. Tompkins[30], K. Toms[103], G. Tong[32a], A. Tonoyan[13], C. Topfel[16], N.D. Topilin[65], I. Torchiani[29], E. Torrence[114], H. Torres[78], E. Torró Pastor[167], J. Toth[83,aa], F. Touchard[83], D.R. Tovey[139], T. Trefzger[173], L. Tremblet[29], A. Tricoli[29], I.M. Trigger[159a], S. Trincaz-Duvoid[78], T.N. Trinh[78], M.F. Tripiana[70], W. Trischuk[158], A. Trivedi[24,z], B. Trocmé[55], C. Troncon[89a], M. Trottier-McDonald[142], M. Trzebinski[38], A. Trzupek[38], C. Tsarouchas[29], J.C-L. Tseng[118], M. Tsiakiris[105], P.V. Tsiareshka[90], D. Tsionou[4,ae], G. Tsipolitis[9], V. Tsiskaridze[48], E.G. Tskhadadze[51a], I.I. Tsukerman[95], V. Tsulaia[14], J.-W. Tsung[20], S. Tsuno[66], D. Tsybychev[148], A. Tua[139], A. Tudorache[25a], V. Tudorache[25a], J.M. Tuggle[30], M. Turala[38], D. Turecek[127], I. Turk Cakir[3e], E. Turlay[105], R. Turra[89a,89b], P.M. Tuts[34], A. Tykhonov[74], M. Tylmad[146a,146b], M. Tyndel[129], G. Tzanakos[8], K. Uchida[20], I. Ueda[155], R. Ueno[28], M. Ugland[13], M. Uhlenbrock[20], M. Uhrmacher[54], F. Ukegawa[160], G. Unal[29], D.G. Underwood[5], A. Undrus[24], G. Unel[163], Y. Unno[66], D. Urbaniec[34], G. Usai[7], M. Uslenghi[119a,119b], L. Vacavant[83], V. Vacek[127], B. Vachon[85], S. Vahsen[14], J. Valenta[125], P. Valente[132a], S. Valentinetti[19a,19b], S. Valkar[126], E. Valladolid Gallego[167], S. Vallecorsa[152], J.A. Valls Ferrer[167], H. van der Graaf[105], E. van der Kraaij[105], R. Van Der Leeuw[105], E. van der Poel[105], D. van der Ster[29], N. van Eldik[84], P. van Gemmeren[5], Z. van Kesteren[105], I. van Vulpen[105], M. Vanadia[99], W. Vandelli[29], G. Vandoni[29], A. Vaniachine[5], P. Vankov[41], F. Vannucci[78], F. Varela Rodriguez[29], R. Vari[132a], E.W. Varnes[6], D. Varouchas[14], A. Vartapetian[7], K.E. Varvell[150], V.I. Vassilakopoulos[56], F. Vazeille[33], G. Vegni[89a,89b], J.J. Veillet[115], C. Vellidis[8], F. Veloso[124a], R. Veness[29], S. Veneziano[132a], A. Ventura[72a,72b], D. Ventura[138], M. Venturi[48], N. Venturi[158], V. Vercesi[119a], M. Verducci[138], W. Verkerke[105], J.C. Vermeulen[105], A. Vest[43], M.C. Vetterli[142,d], I. Vichou[165], T. Vickey[145b,af], O.E. Vickey Boeriu[145b], G.H.A. Viehhauser[118], S. Viel[168], M. Villa[19a,19b], M. Villaplana Perez[167], E. Vilucchi[47], M.G. Vincter[28], E. Vinek[29], V.B. Vinogradov[65], M. Virchaux[136,*], J. Virzi[14], O. Vitells[171], M. Viti[41], I. Vivarelli[48], F. Vives Vaque[2], S. Vlachos[9], D. Vladoiu[98], M. Vlasak[127], N. Vlasov[20], A. Vogel[20], P. Vokac[127], G. Volpi[47], M. Volpi[86], G. Volpini[89a], H. von der Schmitt[99], J. von Loeben[99], H. von Radziewski[48], E. von Toerne[20], V. Vorobel[126], A.P. Vorobiev[128], V. Vorwerk[11], M. Vos[167], R. Voss[29], T.T. Voss[174], J.H. Vossebeld[73], N. Vranjes[12a], M. Vranjes Milosavljevic[105], V. Vrba[125], M. Vreeswijk[105], T. Vu Anh[81], R. Vuillermet[29], I. Vukotic[115], W. Wagner[174], P. Wagner[120], H. Wahlen[174], J. Wakabayashi[101], J. Walbersloh[42], S. Walch[87], J. Walder[71], R. Walker[98], W. Walkowiak[141], R. Wall[175], P. Waller[73], C. Wang[44], H. Wang[172], H. Wang[32b,ag], J. Wang[151], J. Wang[55], J.C. Wang[138], R. Wang[103], S.M. Wang[151], A. Warburton[85], C.P. Ward[27], M. Warsinsky[48], P.M. Watkins[17], A.T. Watson[17], I.J. Watson[150], M.F. Watson[17], G. Watts[138], S. Watts[82], A.T. Waugh[150], B.M. Waugh[77], M. Weber[129], M.S. Weber[16], P. Weber[54], A.R. Weidberg[118], P. Weigell[99], J. Weingarten[54], C. Weiser[48], H. Wellenstein[22], P.S. Wells[29], M. Wen[47], T. Wenaus[24], S. Wendler[123], Z. Weng[151,u], T. Wengler[29], S. Wenig[29], N. Wermes[20], M. Werner[48], P. Werner[29], M. Werth[163], M. Wessels[58a], C. Weydert[55], K. Whalen[28], S.J. Wheeler-Ellis[163], S.P. Whitaker[21], A. White[7], M.J. White[86], S.R. Whitehead[118], D. Whiteson[163], D. Whittington[61], F. Wicek[115], D. Wicke[174], F.J. Wickens[129], W. Wiedenmann[172], M. Wielers[129], P. Wienemann[20], C. Wiglesworth[75], L.A.M. Wiik-Fuchs[48], P.A. Wijeratne[77], A. Wildauer[167], M.A. Wildt[41,q], I. Wilhelm[126], H.G. Wilkens[29], J.Z. Will[98], E. Williams[34], H.H. Williams[120], W. Willis[34], S. Willocq[84], J.A. Wilson[17], M.G. Wilson[143], A. Wilson[87], I. Wingerter-Seez[4], S. Winkelmann[48], F. Winklmeier[29], M. Wittgen[143], M.W. Wolter[38], H. Wolters[124a,h], W.C. Wong[40], G. Wooden[87], B.K. Wosiek[38], J. Wotschack[29], M.J. Woudstra[84], K.W. Wozniak[38], K. Wraight[53], C. Wright[53], M. Wright[53], B. Wrona[73], S.L. Wu[172], X. Wu[49], Y. Wu[32b,ah], E. Wulf[34], R. Wunstorf[42], B.M. Wynne[45], S. Xella[35], M. Xiao[136], S. Xie[48], Y. Xie[32a], C. Xu[32b,w], D. Xu[139], G. Xu[32a], B. Yabsley[150], S. Yacoob[145b], M. Yamada[66], H. Yamaguchi[155], A. Yamamoto[66], K. Yamamoto[64], S. Yamamoto[155], T. Yamamura[155], T. Yamanaka[155], J. Yamaoka[44], T. Yamazaki[155], Y. Yamazaki[67], Z. Yan[21], H. Yang[87], U.K. Yang[82], Y. Yang[61], Y. Yang[32a], Z. Yang[146a,146b], S. Yanush[91], Y. Yao[14], Y. Yasu[66], G.V. Ybeles Smit[130], J. Ye[39], S. Ye[24], M. Yilmaz[3c], R. Yoosoofmiya[123], K. Yorita[170], R. Yoshida[5], C. Young[143], S. Youssef[21], D. Yu[24], J. Yu[7], J. Yu[112], L. Yuan[32a,ai], A. Yurkewicz[106], B. Zabinski[38], V.G. Zaets[128], R. Zaidan[63], A.M. Zaitsev[128], Z. Zajacova[29], L. Zanello[132a,132b], P. Zarzhitsky[39], A. Zaytsev[107], C. Zeitnitz[174], M. Zeller[175], M. Zeman[125], A. Zemla[38], C. Zendler[20], O. Zenin[128], T. Ženiš[144a],

Z. Zenonos[122a,122b], S. Zenz[14], D. Zerwas[115], G. Zevi della Porta[57], Z. Zhan[32d], D. Zhang[32b,ag], H. Zhang[88], J. Zhang[5], X. Zhang[32d], Z. Zhang[115], L. Zhao[108], T. Zhao[138], Z. Zhao[32b], A. Zhemchugov[65], S. Zheng[32a], J. Zhong[118], B. Zhou[87], N. Zhou[163], Y. Zhou[151], C.G. Zhu[32d], H. Zhu[41], J. Zhu[87], Y. Zhu[32b], X. Zhuang[98], V. Zhuravlov[99], D. Zieminska[61], R. Zimmermann[20], S. Zimmermann[20], S. Zimmermann[48], M. Ziolkowski[141], R. Zitoun[4], L. Živković[34], V.V. Zmouchko[128,*], G. Zobernig[172], A. Zoccoli[19a,19b], Y. Zolnierowski[4], A. Zsenei[29], M. zur Nedden[15], V. Zutshi[106], L. Zwalinski[29]

[1]University at Albany, Albany NY, United States of America
[2]Department of Physics, University of Alberta, Edmonton AB, Canada
[3(a)]Department of Physics, Ankara University, Ankara; [(b)]Department of Physics, Dumlupinar University, Kutahya; [(c)]Department of Physics, Gazi University, Ankara; [(d)]Division of Physics, TOBB University of Economics and Technology, Ankara; [(e)]Turkish Atomic Energy Authority, Ankara, Turkey
[4]LAPP, CNRS/IN2P3 and Université de Savoie, Annecy-le-Vieux, France
[5]High Energy Physics Division, Argonne National Laboratory, Argonne IL, United States of America
[6]Department of Physics, University of Arizona, Tucson AZ, United States of America
[7]Department of Physics, The University of Texas at Arlington, Arlington TX, United States of America
[8]Physics Department, University of Athens, Athens, Greece
[9]Physics Department, National Technical University of Athens, Zografou, Greece
[10]Institute of Physics, Azerbaijan Academy of Sciences, Baku, Azerbaijan
[11]Institut de Física d'Altes Energies and Departament de Física de la Universitat Autònoma de Barcelona and ICREA, Barcelona, Spain
[12(a)]Institute of Physics, University of Belgrade, Belgrade; [(b)]Vinca Institute of Nuclear Sciences, Belgrade, Serbia
[13]Department for Physics and Technology, University of Bergen, Bergen, Norway
[14]Physics Division, Lawrence Berkeley National Laboratory and University of California, Berkeley CA, United States of America
[15]Department of Physics, Humboldt University, Berlin, Germany
[16]Albert Einstein Center for Fundamental Physics and Laboratory for High Energy Physics, University of Bern, Bern, Switzerland
[17]School of Physics and Astronomy, University of Birmingham, Birmingham, United Kingdom
[18(a)]Department of Physics, Bogazici University, Istanbul; [(b)]Division of Physics, Dogus University, Istanbul; [(c)]Department of Physics Engineering, Gaziantep University, Gaziantep; [(d)]Department of Physics, Istanbul Technical University, Istanbul, Turkey
[19(a)]INFN Sezione di Bologna; [(b)]Dipartimento di Fisica, Università di Bologna, Bologna, Italy
[20]Physikalisches Institut, University of Bonn, Bonn, Germany
[21]Department of Physics, Boston University, Boston MA, United States of America
[22]Department of Physics, Brandeis University, Waltham MA, United States of America
[23(a)]Universidade Federal do Rio De Janeiro COPPE/EE/IF, Rio de Janeiro; [(b)]Federal University of Juiz de Fora (UFJF), Juiz de Fora; [(c)]Federal University of Sao Joao del Rei (UFSJ), Sao Joao del Rei; [(d)]Instituto de Fisica, Universidade de Sao Paulo, Sao Paulo, Brazil
[24]Physics Department, Brookhaven National Laboratory, Upton NY, United States of America
[25(a)]National Institute of Physics and Nuclear Engineering, Bucharest; [(b)]University Politehnica Bucharest, Bucharest; [(c)]West University in Timisoara, Timisoara, Romania
[26]Departamento de Física, Universidad de Buenos Aires, Buenos Aires, Argentina
[27]Cavendish Laboratory, University of Cambridge, Cambridge, United Kingdom
[28]Department of Physics, Carleton University, Ottawa ON, Canada
[29]CERN, Geneva, Switzerland
[30]Enrico Fermi Institute, University of Chicago, Chicago IL, United States of America
[31(a)]Departamento de Fisica, Pontificia Universidad Católica de Chile, Santiago; [(b)]Departamento de Física, Universidad Técnica Federico Santa María, Valparaíso, Chile
[32(a)]Institute of High Energy Physics, Chinese Academy of Sciences, Beijing; [(b)]Department of Modern Physics, University of Science and Technology of China, Anhui; [(c)]Department of Physics, Nanjing University, Jiangsu; [(d)]School of Physics, Shandong University, Shandong, China
[33]Laboratoire de Physique Corpusculaire, Clermont Université and Université Blaise Pascal and CNRS/IN2P3, Aubiere Cedex, France
[34]Nevis Laboratory, Columbia University, Irvington NY, United States of America

[35]Niels Bohr Institute, University of Copenhagen, Kobenhavn, Denmark
[36(a)]INFN Gruppo Collegato di Cosenza; [(b)]Dipartimento di Fisica, Università della Calabria, Arcavata di Rende, Italy
[37]AGH University of Science and Technology, Faculty of Physics and Applied Computer Science, Krakow, Poland
[38]The Henryk Niewodniczanski Institute of Nuclear Physics, Polish Academy of Sciences, Krakow, Poland
[39]Physics Department, Southern Methodist University, Dallas TX, United States of America
[40]Physics Department, University of Texas at Dallas, Richardson TX, United States of America
[41]DESY, Hamburg and Zeuthen, Germany
[42]Institut für Experimentelle Physik IV, Technische Universität Dortmund, Dortmund, Germany
[43]Institut für Kern- und Teilchenphysik, Technical University Dresden, Dresden, Germany
[44]Department of Physics, Duke University, Durham NC, United States of America
[45]SUPA - School of Physics and Astronomy, University of Edinburgh, Edinburgh, United Kingdom
[46]Fachhochschule Wiener Neustadt, Johannes Gutenbergstrasse 3, 2700 Wiener Neustadt, Austria
[47]INFN Laboratori Nazionali di Frascati, Frascati, Italy
[48]Fakultät für Mathematik und Physik, Albert-Ludwigs-Universität, Freiburg i.Br., Germany
[49]Section de Physique, Université de Genève, Geneva, Switzerland
[50(a)]INFN Sezione di Genova; [(b)]Dipartimento di Fisica, Università di Genova, Genova, Italy
[51(a)]E.Andronikashvili Institute of Physics, Georgian Academy of Sciences, Tbilisi; [(b)]High Energy Physics Institute, Tbilisi State University, Tbilisi, Georgia
[52]II Physikalisches Institut, Justus-Liebig-Universität Giessen, Giessen, Germany
[53]SUPA - School of Physics and Astronomy, University of Glasgow, Glasgow, United Kingdom
[54]II Physikalisches Institut, Georg-August-Universität, Göttingen, Germany
[55]Laboratoire de Physique Subatomique et de Cosmologie, Université Joseph Fourier and CNRS/IN2P3 and Institut National Polytechnique de Grenoble, Grenoble, France
[56]Department of Physics, Hampton University, Hampton VA, United States of America
[57]Laboratory for Particle Physics and Cosmology, Harvard University, Cambridge MA, United States of America
[58(a)]Kirchhoff-Institut für Physik, Ruprecht-Karls-Universität Heidelberg, Heidelberg; [(b)]Physikalisches Institut, Ruprecht-Karls-Universität Heidelberg, Heidelberg; [(c)]ZITI Institut für technische Informatik, Ruprecht-Karls-Universität Heidelberg, Mannheim, Germany
[59]Faculty of Science, Hiroshima University, Hiroshima, Japan
[60]Faculty of Applied Information Science, Hiroshima Institute of Technology, Hiroshima, Japan
[61]Department of Physics, Indiana University, Bloomington IN, United States of America
[62]Institut für Astro- und Teilchenphysik, Leopold-Franzens-Universität, Innsbruck, Austria
[63]University of Iowa, Iowa City IA, United States of America
[64]Department of Physics and Astronomy, Iowa State University, Ames IA, United States of America
[65]Joint Institute for Nuclear Research, JINR Dubna, Dubna, Russia
[66]KEK, High Energy Accelerator Research Organization, Tsukuba, Japan
[67]Graduate School of Science, Kobe University, Kobe, Japan
[68]Faculty of Science, Kyoto University, Kyoto, Japan
[69]Kyoto University of Education, Kyoto, Japan
[70]Instituto de Física La Plata, Universidad Nacional de La Plata and CONICET, La Plata, Argentina
[71]Physics Department, Lancaster University, Lancaster, United Kingdom
[72(a)]INFN Sezione di Lecce; [(b)]Dipartimento di Fisica, Università del Salento, Lecce, Italy
[73]Oliver Lodge Laboratory, University of Liverpool, Liverpool, United Kingdom
[74]Department of Physics, Jožef Stefan Institute and University of Ljubljana, Ljubljana, Slovenia
[75]School of Physics and Astronomy, Queen Mary University of London, London, United Kingdom
[76]Department of Physics, Royal Holloway University of London, Surrey, United Kingdom
[77]Department of Physics and Astronomy, University College London, London, United Kingdom
[78]Laboratoire de Physique Nucléaire et de Hautes Energies, UPMC and Université Paris-Diderot and CNRS/IN2P3, Paris, France
[79]Fysiska institutionen, Lunds universitet, Lund, Sweden
[80]Departamento de Fisica Teorica C-15, Universidad Autonoma de Madrid, Madrid, Spain
[81]Institut für Physik, Universität Mainz, Mainz, Germany
[82]School of Physics and Astronomy, University of Manchester, Manchester, United Kingdom

[83]CPPM, Aix-Marseille Université and CNRS/IN2P3, Marseille, France
[84]Department of Physics, University of Massachusetts, Amherst MA, United States of America
[85]Department of Physics, McGill University, Montreal QC, Canada
[86]School of Physics, University of Melbourne, Victoria, Australia
[87]Department of Physics, The University of Michigan, Ann Arbor MI, United States of America
[88]Department of Physics and Astronomy, Michigan State University, East Lansing MI, United States of America
[89(a)]INFN Sezione di Milano; [(b)]Dipartimento di Fisica, Università di Milano, Milano, Italy
[90]B.I. Stepanov Institute of Physics, National Academy of Sciences of Belarus, Minsk, Republic of Belarus
[91]National Scientific and Educational Centre for Particle and High Energy Physics, Minsk, Republic of Belarus
[92]Department of Physics, Massachusetts Institute of Technology, Cambridge MA, United States of America
[93]Group of Particle Physics, University of Montreal, Montreal QC, Canada
[94]P.N. Lebedev Institute of Physics, Academy of Sciences, Moscow, Russia
[95]Institute for Theoretical and Experimental Physics (ITEP), Moscow, Russia
[96]Moscow Engineering and Physics Institute (MEPhI), Moscow, Russia
[97]Skobeltsyn Institute of Nuclear Physics, Lomonosov Moscow State University, Moscow, Russia
[98]Fakultät für Physik, Ludwig-Maximilians-Universität München, München, Germany
[99]Max-Planck-Institut für Physik (Werner-Heisenberg-Institut), München, Germany
[100]Nagasaki Institute of Applied Science, Nagasaki, Japan
[101]Graduate School of Science, Nagoya University, Nagoya, Japan
[102(a)]INFN Sezione di Napoli; [(b)]Dipartimento di Scienze Fisiche, Università di Napoli, Napoli, Italy
[103]Department of Physics and Astronomy, University of New Mexico, Albuquerque NM, United States of America
[104]Institute for Mathematics, Astrophysics and Particle Physics, Radboud University Nijmegen/Nikhef, Nijmegen, Netherlands
[105]Nikhef National Institute for Subatomic Physics and University of Amsterdam, Amsterdam, Netherlands
[106]Department of Physics, Northern Illinois University, DeKalb IL, United States of America
[107]Budker Institute of Nuclear Physics, SB RAS, Novosibirsk, Russia
[108]Department of Physics, New York University, New York NY, United States of America
[109]Ohio State University, Columbus OH, United States of America
[110]Faculty of Science, Okayama University, Okayama, Japan
[111]Homer L. Dodge Department of Physics and Astronomy, University of Oklahoma, Norman OK, United States of America
[112]Department of Physics, Oklahoma State University, Stillwater OK, United States of America
[113]Palacký University, RCPTM, Olomouc, Czech Republic
[114]Center for High Energy Physics, University of Oregon, Eugene OR, United States of America
[115]LAL, Univ. Paris-Sud and CNRS/IN2P3, Orsay, France
[116]Graduate School of Science, Osaka University, Osaka, Japan
[117]Department of Physics, University of Oslo, Oslo, Norway
[118]Department of Physics, Oxford University, Oxford, United Kingdom
[119(a)]INFN Sezione di Pavia; [(b)]Dipartimento di Fisica Nucleare e Teorica, Università di Pavia, Pavia, Italy
[120]Department of Physics, University of Pennsylvania, Philadelphia PA, United States of America
[121]Petersburg Nuclear Physics Institute, Gatchina, Russia
[122(a)]INFN Sezione di Pisa; [(b)]Dipartimento di Fisica E. Fermi, Università di Pisa, Pisa, Italy
[123]Department of Physics and Astronomy, University of Pittsburgh, Pittsburgh PA, United States of America
[124(a)]Laboratorio de Instrumentacao e Fisica Experimental de Particulas - LIP, Lisboa, Portugal; [(b)]Departamento de Fisica Teorica y del Cosmos and CAFPE, Universidad de Granada, Granada, Spain
[125]Institute of Physics, Academy of Sciences of the Czech Republic, Praha, Czech Republic
[126]Faculty of Mathematics and Physics, Charles University in Prague, Praha, Czech Republic
[127]Czech Technical University in Prague, Praha, Czech Republic
[128]State Research Center Institute for High Energy Physics, Protvino, Russia
[129]Particle Physics Department, Rutherford Appleton Laboratory, Didcot, United Kingdom
[130]Physics Department, University of Regina, Regina SK, Canada
[131]Ritsumeikan University, Kusatsu, Shiga, Japan
[132(a)]INFN Sezione di Roma I; [(b)]Dipartimento di Fisica, Università La Sapienza, Roma, Italy

[133](a)INFN Sezione di Roma Tor Vergata; (b)Dipartimento di Fisica, Università di Roma Tor Vergata, Roma, Italy
[134](a)INFN Sezione di Roma Tre; (b)Dipartimento di Fisica, Università Roma Tre, Roma, Italy
[135](a)Faculté des Sciences Ain Chock, Réseau Universitaire de Physique des Hautes Energies - Université Hassan II, Casablanca; (b)Centre National de l'Energie des Sciences Techniques Nucleaires, Rabat; (c)Faculté des Sciences Semlalia, Université Cadi Ayyad, LPHEA-Marrakech; (d)Faculté des Sciences, Université Mohamed Premier and LPTPM, Oujda; (e)Faculté des Sciences, Université Mohammed V- Agdal, Rabat, Morocco
[136]DSM/IRFU (Institut de Recherches sur les Lois Fondamentales de l'Univers), CEA Saclay (Commissariat a l'Energie Atomique), Gif-sur-Yvette, France
[137]Santa Cruz Institute for Particle Physics, University of California Santa Cruz, Santa Cruz CA, United States of America
[138]Department of Physics, University of Washington, Seattle WA, United States of America
[139]Department of Physics and Astronomy, University of Sheffield, Sheffield, United Kingdom
[140]Department of Physics, Shinshu University, Nagano, Japan
[141]Fachbereich Physik, Universität Siegen, Siegen, Germany
[142]Department of Physics, Simon Fraser University, Burnaby BC, Canada
[143]SLAC National Accelerator Laboratory, Stanford CA, United States of America
[144](a)Faculty of Mathematics, Physics & Informatics, Comenius University, Bratislava; (b)Department of Subnuclear Physics, Institute of Experimental Physics of the Slovak Academy of Sciences, Kosice, Slovak Republic
[145](a)Department of Physics, University of Johannesburg, Johannesburg; (b)School of Physics, University of the Witwatersrand, Johannesburg, South Africa
[146](a)Department of Physics, Stockholm University; (b)The Oskar Klein Centre, Stockholm, Sweden
[147]Physics Department, Royal Institute of Technology, Stockholm, Sweden
[148]Departments of Physics & Astronomy and Chemistry, Stony Brook University, Stony Brook NY, United States of America
[149]Department of Physics and Astronomy, University of Sussex, Brighton, United Kingdom
[150]School of Physics, University of Sydney, Sydney, Australia
[151]Institute of Physics, Academia Sinica, Taipei, Taiwan
[152]Department of Physics, Technion: Israel Inst. of Technology, Haifa, Israel
[153]Raymond and Beverly Sackler School of Physics and Astronomy, Tel Aviv University, Tel Aviv, Israel
[154]Department of Physics, Aristotle University of Thessaloniki, Thessaloniki, Greece
[155]International Center for Elementary Particle Physics and Department of Physics, The University of Tokyo, Tokyo, Japan
[156]Graduate School of Science and Technology, Tokyo Metropolitan University, Tokyo, Japan
[157]Department of Physics, Tokyo Institute of Technology, Tokyo, Japan
[158]Department of Physics, University of Toronto, Toronto ON, Canada
[159](a)TRIUMF, Vancouver BC; (b)Department of Physics and Astronomy, York University, Toronto ON, Canada
[160]Institute of Pure and Applied Sciences, University of Tsukuba, 1-1-1 Tennodai, Tsukuba, Ibaraki 305-8571, Japan
[161]Science and Technology Center, Tufts University, Medford MA, United States of America
[162]Centro de Investigaciones, Universidad Antonio Narino, Bogota, Colombia
[163]Department of Physics and Astronomy, University of California Irvine, Irvine CA, United States of America
[164](a)INFN Gruppo Collegato di Udine, Udine; (b)ICTP, Trieste; (c)Dipartimento di Chimica, Fisica e Ambiente, Università di Udine, Udine, Italy
[165]Department of Physics, University of Illinois, Urbana IL, United States of America
[166]Department of Physics and Astronomy, University of Uppsala, Uppsala, Sweden
[167]Instituto de Física Corpuscular (IFIC) and Departamento de Física Atómica, Molecular y Nuclear and Departamento de Ingeniería Electrónica and Instituto de Microelectrónica de Barcelona (IMB-CNM), University of Valencia and CSIC, Valencia, Spain
[168]Department of Physics, University of British Columbia, Vancouver BC, Canada
[169]Department of Physics and Astronomy, University of Victoria, Victoria BC, Canada
[170]Waseda University, Tokyo, Japan
[171]Department of Particle Physics, The Weizmann Institute of Science, Rehovot, Israel
[172]Department of Physics, University of Wisconsin, Madison WI, United States of America
[173]Fakultät für Physik und Astronomie, Julius-Maximilians-Universität, Würzburg, Germany
[174]Fachbereich C Physik, Bergische Universität Wuppertal, Wuppertal, Germany
[175]Department of Physics, Yale University, New Haven CT, United States of America

[176]Yerevan Physics Institute, Yerevan, Armenia
[177]Domaine scientifique de la Doua, Centre de Calcul CNRS/IN2P3, Villeurbanne Cedex, France
[a]Also at Laboratorio de Instrumentacao e Fisica Experimental de Particulas - LIP, Lisboa, Portugal
[b]Also at Faculdade de Ciencias and CFNUL, Universidade de Lisboa, Lisboa, Portugal
[c]Also at Particle Physics Department, Rutherford Appleton Laboratory, Didcot, United Kingdom
[d]Also at TRIUMF, Vancouver BC, Canada
[e]Also at Department of Physics, California State University, Fresno CA, United States of America
[f]Also at Novosibirsk State University, Novosibirsk, Russia
[g]Also at Fermilab, Batavia IL, United States of America
[h]Also at Department of Physics, University of Coimbra, Coimbra, Portugal
[i]Also at Università di Napoli Parthenope, Napoli, Italy
[j]Also at Institute of Particle Physics (IPP), Canada
[k]Also at Department of Physics, Middle East Technical University, Ankara, Turkey
[l]Also at Louisiana Tech University, Ruston LA, United States of America
[m]Also at Department of Physics and Astronomy, University College London, London, United Kingdom
[n]Also at Louisiana Tech University, Ruston LA, Unites States of America
[o]Also at Group of Particle Physics, University of Montreal, Montreal QC, Canada
[p]Also at Institute of Physics, Azerbaijan Academy of Sciences, Baku, Azerbaijan
[q]Also at Institut für Experimentalphysik, Universität Hamburg, Hamburg, Germany
[r]Also at Manhattan College, New York NY, United States of America
[s]Also at School of Physics, Shandong University, Shandong, China
[t]Also at CPPM, Aix-Marseille Université and CNRS/IN2P3, Marseille, France
[u]Also at School of Physics and Engineering, Sun Yat-sen University, Guangzhou, China
[v]Also at Academia Sinica Grid Computing, Institute of Physics, Academia Sinica, Taipei, Taiwan
[w]Also at DSM/IRFU (Institut de Recherches sur les Lois Fondamentales de l'Univers), CEA Saclay (Commissariat a l'Energie Atomique), Gif-sur-Yvette, France
[x]Also at Section de Physique, Universite de Geneve, Geneva, Switzerland
[y]Also at Departamento de Fisica, Universidade de Minho, Braga, Portugal
[z]Also at Department of Physics and Astronomy, University of South Carolina, Columbia SC, United States of America
[aa]Also at Institute for Particle and Nuclear Physics, Wigner Research Centre for Physics, Budapest, Hungary
[ab]Also at California Institute of Technology, Pasadena CA, United States of America
[ac]Also at Institute of Physics, Jagiellonian University, Krakow, Poland
[ad]Also at Institute of High Energy Physics, Chinese Academy of Sciences, Beijing, China
[ae]Also at Department of Physics and Astronomy, University of Sheffield, Sheffield, United Kingdom
[af]Also at Department of Physics, Oxford University, Oxford, United Kingdom
[ag]Also at Institute of Physics, Academia Sinica, Taipei, Taiwan
[ah]Also at Department of Physics, The University of Michigan, Ann Arbor MI, United States of America
[ai]Also at Laboratoire de Physique Nucléaire et de Hautes Energies, UPMC and Université Paris-Diderot and CNRS/IN2P3, Paris, France
[*]Deceased